Progress in Materials Science 58 (2013) 636–704

Contents lists available at SciVerse ScienceDirect

Progress in Materials Science

journal homepage: www.elsevier.com/locate/pmatsci

Nanoporous anodic aluminium oxide: Advances in surface engineering and emerging applications

Abdul Mutalib Md Jani [a,b,*], Dusan Losic [c], Nicolas H. Voelcker [d,*]

[a] Faculty of Applied Sciences, Universiti Teknologi MARA, 40450 Shah Alam, Selangor, Malaysia
[b] Chemistry Department, Faculty of Applied Sciences, Universiti Teknologi MARA, Arau 02600, Perlis, Malaysia
[c] School of Chemical Engineering, University of Adelaide, Adelaide, SA 5005, Australia
[d] Mawson Institute, University of South Australia, Mawson Lakes, SA 5095, Australia

ARTICLE INFO

Article history:
Received 14 September 2012
Accepted 15 January 2013
Available online 26 January 2013

ABSTRACT

Anodic aluminium oxide (AAO) has been investigated and utilized in numerous products for almost a century. But the rapidly increasing interest in nanoscale materials and their outstanding properties has propelled nanoporous AAO to the fore as one of the most popular nanomaterial with applications across a gamut of areas including molecular separation, catalysis, energy generation and storage, electronics and photonics, sensors and biosensors, drug delivery and template synthesis. Material fabrication of AAO is based on facile and inexpensive electrochemical anodization with the self-ordering process of nanopores not requiring any lithography or templating, and the outcome of the process are perfectly ordered and size controlled nanopores with distinctive pore geometries. Recent research on AAO is characterized by a remarkable trajectory of innovation, in particular with regards to control of surface functionality and, concomitantly, to the design of intricate structural features such as modulated, branched, and multilayered pore architectures. This review illuminates research on recent development of AAO focussing on surface and structural engineering, and on emerging applications. Key examples and critical preparative issues and resulting improvements sparking opportunities for further applications in AAO properties are discussed. We conclude this review with an outlook providing a critical perspective on future trends on surface and structural engineering of AAO.

* Corresponding authors.
E-mail addresses: abdmutalib@perlis.uitm.edu.my (A.M. Md Jani), Nico.Voelcker@unisa.edu.au (N.H. Voelcker).

0079-6425/$ - see front matter © 2013 Elsevier Ltd. All rights reserved.
http://dx.doi.org/10.1016/j.pmatsci.2013.01.002

Contents

1. Introduction

Ordered porous structures from the molecular to the macro-level are widely used in nature [1–3]. Indeed, these pore structures with their elegant and intricate designs have played pivotal roles in many biological processes [4]. These processes include transport of nutrients through the cell wall, selective transport of small or specific molecules or solutes, energy or charge transport, gas adsorption, ion exchange, signalling, and many other activities [5–7]. Arguably, the most significant feature of these nature-designed structures is their multifunctional properties and creation through unique genetically guided self-assembled processes. Indeed, self-assembly, or the spontaneous organization of small individual subunits into larger scale ordered and stable structures, is ubiquitous in nature [8]. It is therefore not surprising that the concept of mimicking these processes through the development of man-made periodically ordered porous materials that resemble nature's structural design has attracted a considerable amount of attention in materials science.

Self-assembly and self-organized (or self-ordered) fabrication processes are recognized as cost effective, and the most elegant route in nanotechnology leading to the generation of complex and

functional nanostructured materials [9,10]. Several synthetic approaches based on chemical, electrochemical, sol–gel and hydrothermal methods involving self-organization have been explored for their synthesis using both top-down and bottom-up approaches [10,11]. For example, exploiting the phenomenon of self-ordering during electrochemical anodization of metals has resulted in successful fabrication of highly ordered nanoporous metal oxide structures including anodic alumina oxide (AAO), nanotubular titania oxide (TNT) and porous silicon (pSi) [12–16]. There are numerous advantages of this method of fabrication in comparison to conventional lithography-based fabrication methods including cost effectiveness, wide accessibility, the capability of top–bottom fabrication with nanoscale precision and access to high aspect ratio structures [17,18].

AAO prepared by anodization of aluminium (Al) is a prime example of the self-ordered electrochemical process. Ordered AAO stands out due to its remarkable properties such as chemical, thermal stability, hardness and high surface area [14,18,19]. Over the past decade, we have witnessed the emergence of various applications based on AAO membranes such as molecular separation, separation, chemical/biological sensing devices, cell adhesion, catalysis, energy storage and drug delivery vehicles. More than 2000 papers were published on this topic in last decade (Thomas Reuters, Web of Knowledge, September 2012). All these applications require AAO with appropriate structural properties, which can be achieved through judicious choice of chemical and structural modification steps.

This review presents recent developments on AAO primarily focussing on surface and structural engineering and emerging applications. Firstly, the basic properties and fabrication of AAO including the current stage of development is described, followed by a brief description of the self-ordering process for nanopore formation. Regarding structural modifications, recent advances in fabrication procedures toward structural modification and generation of AAO with complex pore geometries of AAO structures, resulting in branched, multilayered, modulated and hierarchically complex pores architectures are presented. Then, recent progress on surface modification of AAO using both wet chemical synthesis and gas-phase methods is highlighted. Several key examples of wet chemical synthesis are given based on self-assembly (self-assembled monolayers (SAMs)), organic acids, lipid bilayers, layer-by-layer deposition), polymer grafting, sol–gel deposition as well as electrochemical and electroless deposition. The gas-phase surface modification methods of AAO including physical vapor depo-

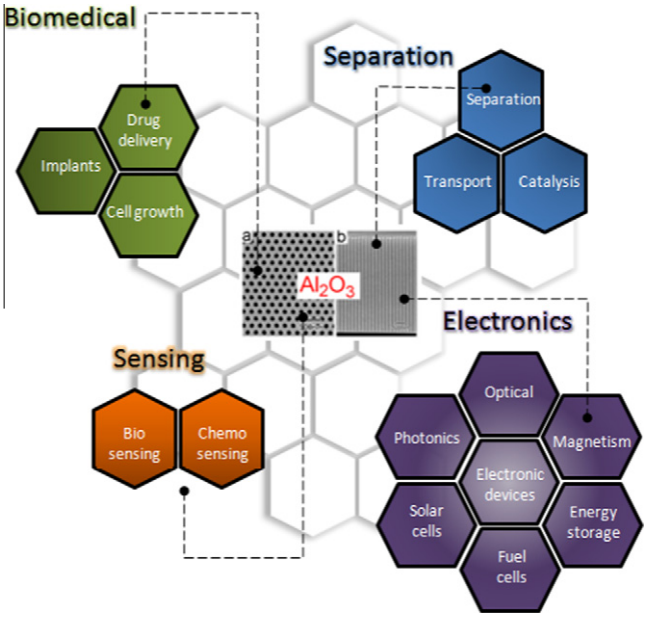

Fig. 1. Scheme showing the typical AAO structure and the major applications for this nanostructured material.

sition (PVD), chemical vapor deposition (CVD), atomic layer deposition (ADL) and plasma polymerization are discussed. Finally, to show how surface and structural modifications are being implemented into advanced applications, AAO-enabled progress in technologies including sensing (chemo- and biosensing), molecular separation, catalysis, biomedical applications for local drug delivery, implants and cell growth, molecular electronics, optics, photonics, solar cells, fuel cells, and energy storage are highlighted (Fig. 1).

2. Basic properties of AAO

The structure of AAO can be described as a close-packed hexagonal array of parallel cylindrical nanopores perpendicular to the surface on top of the underlying Al substrates (Fig. 2a). The pore structures are characterized by parameters such as: pore organization (hexagonal), pore diameter, interpore distance (cell diameter), wall thickness, pore length and barrier layer thickness. By controlling anodization conditions, these parameters can be precisely tuned in the range of about 10–400 nm for pore diameter, 50–600 nm for interpore distance, pore aspect ratio from 10 to 5000, a thickness of the porous layer from 10 nm to 150 μm, a pore density from 10^9 to 10^{11} cm^{-2} and porosity from 5% to 50% [20–22].

Numerous studies over the last decades have explored the anodization conditions of Al metal, such as the applied potential [23–25], current [26,27], pH and electrolyte type [28–30], electrolyte composition and concentration [30], temperature [31], and pre-patterning of the surface [32–34] in order to

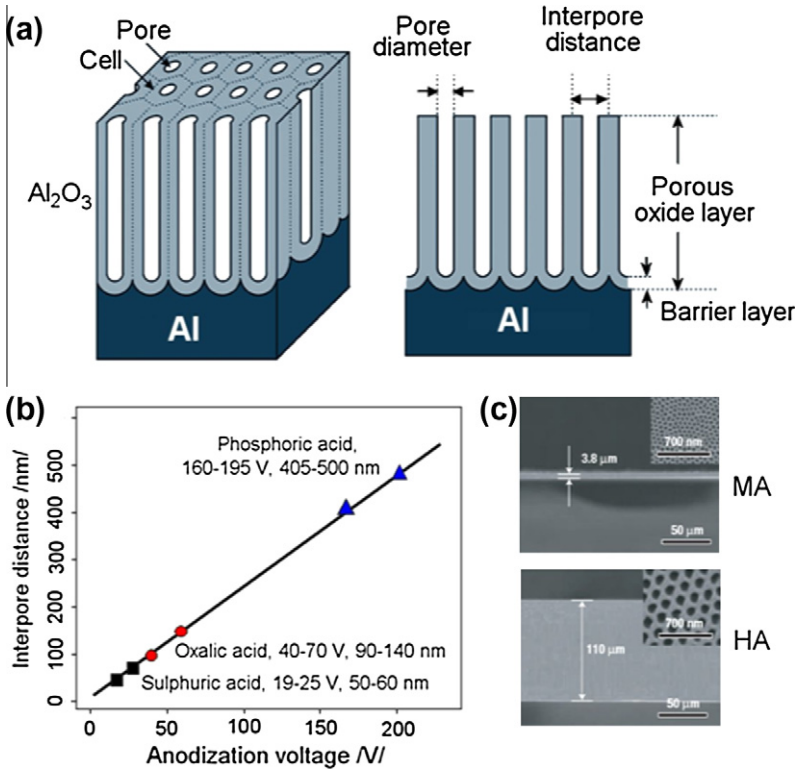

Fig. 2. (a) Schematic drawing of AAO structure prepared by electrochemical anodization of Al. (b) Summary of self-ordering voltage and corresponding interpore distance of AAO produced within three well-known regimes of electrolytes (sulfuric, oxalic and phosphoric). (c) (Top) SEM cross-sectional view of AAO membrane formed by MA (0.3 M $H_2C_2O_4$, 1 °C, 40 V) and (bottom) by HA (at 140 V) for 2 h (insets: SEM top view of pore structures). Adapted and permission from Refs. [41,45].

achieve improved control of the self-ordering process and hence highly ordered AAO pore structures with desired and tunable pore diameters and interpore spacing. As depicted in Fig. 2b, three different electrolytes including sulfuric, oxalic and phosphoric acids are commonly used for anodization processes. Under conventional anodization conditions, also called "mild" anodization (MA), ordered arrays of alumina nanopores can be obtained within three well-known growth regimes: with sulfuric acid as electrolyte at 25 V for an interpore distance (D_{int}) = 63 nm, with oxalic acid at 40 V for D_{int} = 100 nm, and with phosphoric acid at 195 V for D_{int} = 500 nm (Fig. 2c) [35–38]. Several studies have shown that other acids such as chromic, boric, citric and tartaric acid can also be used for preparation of AAO, but with inferior pore ordering in comparison with the three common electrolytes. The fabrication procedure for AAO with controlled pore diameters and their characterization have been described in several reviews [39,40].

Arguably, the most significant progress toward fabrication of AAO with a high degree of pore order has been made by Masuda and Fukuda by introducing a two-step anodization approach [33]. A first anodization step is followed by removal of the first generated porous layer, which results in pre-structuring of Al and facilitates the propagation of pores with long-range order over the entire surface in a subsequent anodization step. However, the main disadvantage of this process is the tediously slow fabrication speed (1–2 $\mu m\, h^{-1}$), which requires almost two working days to prepare an AAO membrane. To solve this problem of throughput, a new method called hard (HA) or high-field anodization has recently been introduced by the Gösele group. This method achieves considerably higher anodization speeds of 50–100 $\mu m\, h^{-1}$ [41]. The HA process has been implemented with all three common electrolytes (sulfuric, oxalic and phosphoric acid) and provides more options for controlling pore diameters and interpore distance. The combination of anodization with additional chemical wet chemical etching further expands the opportunities for controlling the structural parameters in AAO [41,42].

3. Self-ordering electrochemistry for nanopore formation

Self-ordering pore formation during anodization is reported for selected metals including Al, Ti Ta, Hf, W, Zr, Nb (frequently called valve metals) and their alloys, under appropriate experimental conditions (Fig. 3) [14,30,43–46]. The process is influenced by the type of electrolyte, the electrolyte concentration, pH, temperature, applied voltage and current, as well as the surface pre-texturing. Tuning the pore to nanotube morphology has been demonstrated for some metals (Ti, Zr, Ta, Hf) by changing these anodization parameters.

At the beginning of the anodization process under constant voltage conditions, the metal surface is covered entirely with a compact and uniform oxide layer. Once this layer has formed, the current density drops rapidly (Stage I). The distribution of the electric field (E) strongly depends on inhomogeneities and surface roughness of the oxide layer, leading to a locally focused electric field and depressions at the oxide–electrolyte interface (Stage II). As a result, electric-field-assisted dissolution of the oxide layer takes place and the first localized pores are formed and become sites for further pore growth (Stage III). Consequently, an increase in ionic migration will lead to an increase in current density until pores completely cover the entire surface. Further anodization process increases propagation of individual pores through the oxide layer where maximum electric field is concentrated at the pore tip and decreases towards pore walls. The pores are not uniform at this stage, although prolonged anodization improves pore order to some extent. At this stage, there is a competition between oxide growth at the pore bottom and at the same time oxide dissolution processes at barrier oxide layer interfaces. Finally, the pore growth process reaches a steady state and uniformly distributed pores are formed (Stage IV) [14,44–47].

Whilst the mechanism of pore formation is still not fully resolved, it is generally accepted that the driving force for the self-ordering process can be attributed to a stress-driven interface caused by the repulsive forces between neighboring pores that lead to ideal self-organization. In the case of the AAO self-assembly process, the elastic stress caused by volume expansion regulates the degree of uniformity and drives the perfect cylindrical and hexagonal arrangement of pores [48]. In contrast to Al, other metals such as Ti, Zr, Ta, Hf and W usually form tubular structures instead of pores [14,49,50].

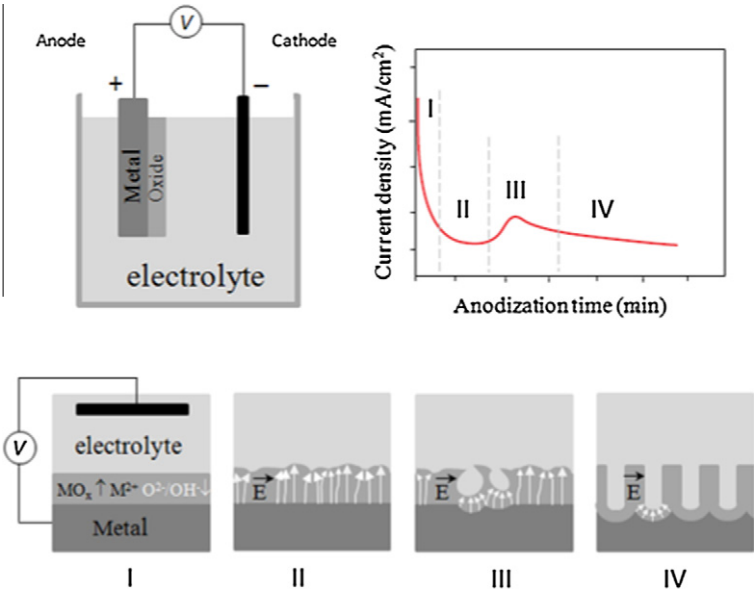

Fig. 3. Schematic diagram of the self ordering process of pore formation by electrochemical anodization including electrochemical cell set-up and typical current density curve of electrochemical anodization. Stages of pore growth: (I) formation of oxide layer; (II) formation of pits by local electric field heterogeneities; (III) initial pore formation; (IV) pore growth under steady-state conditions.

The next section of this review deals with the exploitation of the nanopore formation process in nanostructural engineering. This field is motivated by the desire to generate new and unusual nanopore architectures with advanced properties, paving the way to new applications.

4. Structural engineering of AAO pores

4.1. Controlling lateral pore arrangements and pore shapes by pre-patterning

The self-ordered hexagonal pattern of pore domains prepared by common anodization methods is typically limited to a short-range order spanning only several microns. To fabricate AAO with ordered pore arrangements over macroscale dimensions (mm–cm), and pores with arrangements other than the hexagonal arrangement dictated by the self-ordering process or to introduce different pore geometries including square or triangular ones, several strategies using pre-patterning of the Al surface have been successfully demonstrated. These pre-patterning techniques include: imprinting by a dot-like stamp [33], imprinting by a pyramidal stamp [51], colloid sphere lithography [52], electron-beam lithography [53], focused-ion beam lithography [54], holographic lithography [55], Ar plasma etching [56] and direct writing laser (DWL) lithography [57]. The choice of the technique depends on the scale of the required pore arrangement, the desired pattern and pore size and shape.

Pioneering work in this area comes from the Masuda group who formed an array of shallow depressions on Al substrates by indentation with a Si mold and these depressions served as initiation sites for the hole generation at the initial stage of anodization (Fig. 4a) [34]. By this method, pores with different shapes (square and triangle) were produced according to the fabrication parameters or the arrangement of the initiation sites (Fig. 4a and b). Subsequently, several studies to synthesize AAO with non-hexagonal pore arrangements have been reported. Krishnan and Thompson prepared AAO with a square patterns of nanopores by using mechanical indentation prior to anodization followed by chemical etching [53]. Similar results were demonstrated by Sun et al. (Fig. 4c and e) showing that

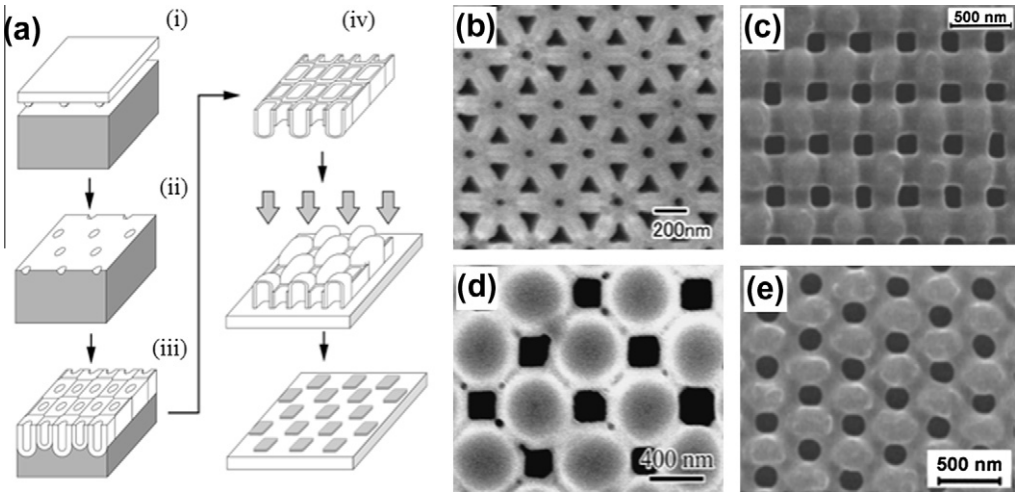

Fig. 4. Schematic of Al pre-patterning and fabrication of AAO with complex pore architectures. (a) (i) texturing of Al by imprinting using Ni mold, (ii) textured Al with ordered array of pits, (iii) anodization of Al, (iv) selective formation of holes through barrier layer; (b) AAO with triangle shape; (c) square shape; (d) checkerboard pattern and (e) rhombus-shape with twofold symmetry. Adapted with permission from Refs. [34,53,55,58,66].

photoresist-grating pattern developed on silica substrate can be used as a mask to deposit an Al film. Consequently, fabrication of AAO with square nanopores can be well controlled and designed over macroscale areas during anodization [55,58].

Further progress in this area has seen the development of a variety of fabrication approaches with exotic patterns and arrangements of AAO structures [52,59,60]. Examples include two-dimensional nanopore arrays [61], alternating regions of Al and AAO arrays [62], patterned lateral pore arrangements [63], microarrays of AAO spots formed by photolithography-based microstructuring [64] and isolated nanopores [65]. AAO with mosaic checkboard patterns was demonstrated by Masuda et al. through imprint-based pre-texturing using a mold with alternating defects in the square lattice of convex structures (Fig. 4d) [66].

4.2. Complex internal pore architectures

AAO membranes with complex internal pore architectures hold considerable prospects for the development of advanced molecular separation and sensing platforms or use as templates for the fabrication of nanostructured nanowires and nanotubes with unique magnetic, electrical and optical properties [67]. Several approaches have been explored to design modulated pore channels and architectures which include multi-step anodization where the type of electrolyte or electrolyte concentration is changed after each step, changing electrolyte temperature during anodization, variation of applied voltage or current during anodization or combining anodization and chemical etching.

It is well established that pore diameters in AAO are dependent on the nature of the electrolyte and the applied voltage used during anodization, so the simplest way to alter internal pore geometries would seem to change these two parameters during the etching. In pioneering work by Li and Papadopoulos, the fabrication of Y-shaped pores (stem 40 nm in diameter and branches 28 nm in diameter) was achieved by voltage reduction by a factor of $1/\sqrt{2}$ during anodization [68]. This work sparked extensive interest in the fabrication of hierarchically Y-branched structures as demonstrated by Meng et al. (Fig. 5) [69]. The multiple branched pore structure was fabricated by a combination of reducing the applied voltage by a factor of $1/\sqrt{n}$ (n = refer number of branch), changing the electrolyte after each anodization step and thinning the barrier layer after each anodization step at the pore bottom by chemical etching. Ho et al. reduced the anodization potential in several steps and applied chemical

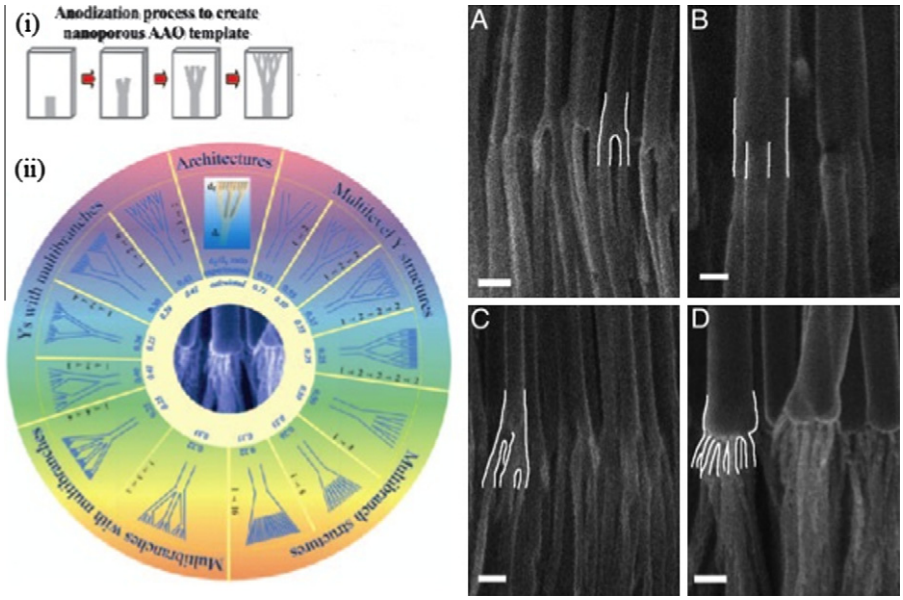

Fig. 5. (Left): (i) Schematic showing the fabrication process, where pores with controlled architectures are developed by consecutive steps of anodization and then used as molds to cast nanotubes and nanowires of complex geometries. (ii) Schematic showing a catalogue of pore architectures categorized in the schematic based on four different hierarchies of branching of stems: multiple generations of Y-branching from one stem, multiple branching from individual stems, combination of Y-branching with each branch undergoing multiple-branching (or reverse), and a combination of multiple branching with each branch developing multiple branches. (Right): Series of SEM images of multiply branched structures of carbon nanotubes (CNT) confirming branched structure of the AAO template. The primary stem branches into 2 (A), 3 (B), 4 (C), and 16 (D) pores, respectively. The junctions are highlighted with white line contours for clarity. Adapted with permission from Ref. [69].

etching after each step to fabricate AAO membranes with 3D multi-tiered branch nanostructures as shown schematically in Fig. 6. Three-tiered branched AAO having an average pore diameter of 285 nm branching into four 125 nm sub-pores in the second tier and four 55 nm sub-pores in the third tier was demonstrated (Fig. 6a–d) [70].

Another example of this concept for fabrication of tree-like nanopores achieved by exponential reduction of anodization potential during oxide growth was reported by Cheng et al. [71]. The synthesis of nonlinear nanopores of AAO membrane on geometrically shaped Al films has been demonstrated by Zakeri et al. [72] who showed that the geometric shape of the Al substrate with two dimensions less than 1 mm strongly affects the fabricated nanopore characteristics such as Y-shaped and dendritic nanopores arrangements. Interestingly, in all reported cases of the hierarchical AAO structures, those were then used as templates to prepare branched carbon nanotubes, nanowires and gold nanotrees [68,69,71–73].

The variation of anodization condition by changing electrolytes allows the fabrication of AAO membranes with periodic diameter-modulation in the pore structures [41]. Gösele et al. cleverly combined the conventional MA and HA process to achieve periodic modulation of pore diameter. The length of each segment was controlled by varying the time of the anodization process (Fig. 7). This approach was extended to form shaped pores with nanofunnel geometry by Krishnan and Thompson [53]. The authors used stepwise anodization processes with two different electrolytes, first with phosphoric acid followed by oxalic acid. Subsequently, an inverted nanofunnel was obtained by switching the electrolytes sequence. More recently, Gösele's group introduced a method called "pulse anodization" where both MA and HA processes were applied in the same electrolyte. The method is based on applying long low current pulses (MA regime) followed by short high current pulses (within the HA regime)

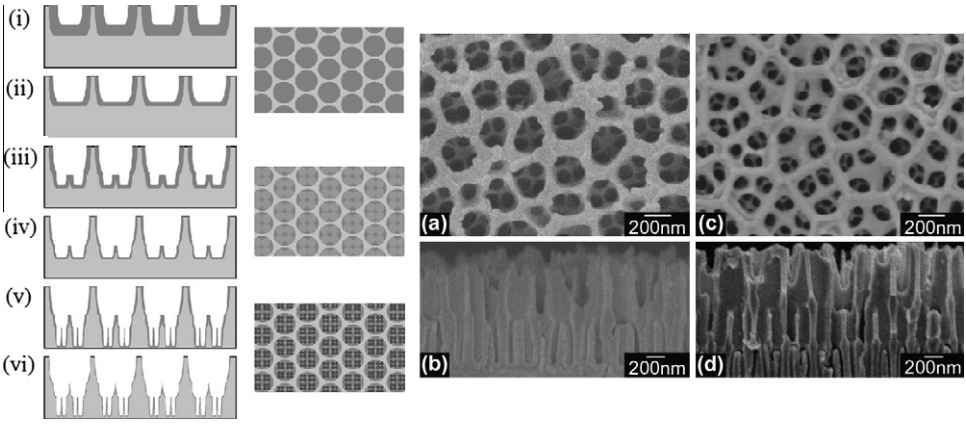

Fig. 6. (Left): Schematic of the sequential fabrication steps of three-tiered branched AAO. (i and ii) First step, first-tier pore anodization and thinning of barrier layer. (iii and iv) Second step, second tier formation at reduced potential followed by thinning of barrier layer. (v and vi) Third step, formation of third-tiered pores at further reduced anodization potential and final pore widening and (middle) corresponding top views of all tiers. (Right): SEM microscopy of the resulting pore structures. (a and b) Top and cross-sectional views of a two-tiered branched AAO prepared by combined anodization in 0.3 M phosphoric acid (130 V) and 0.15 M oxalic acid (80 V) followed by thinning of the barrier layer. (c and d) Top and cross-sectional views of the three-tiered branched AAO prepared by combined anodization in 0.3 M phosphoric acid (130 V), 0.15 M oxalic acid (80 V) and 0.15 M oxalic acid (80 V) followed by thinning of the barrier layer. Adapted with permission from Ref. [70].

(Fig. 8). Although this method demonstrates the ability to create different pore diameters across the AAO structure, it does not allow control over the shape of pore [42,74].

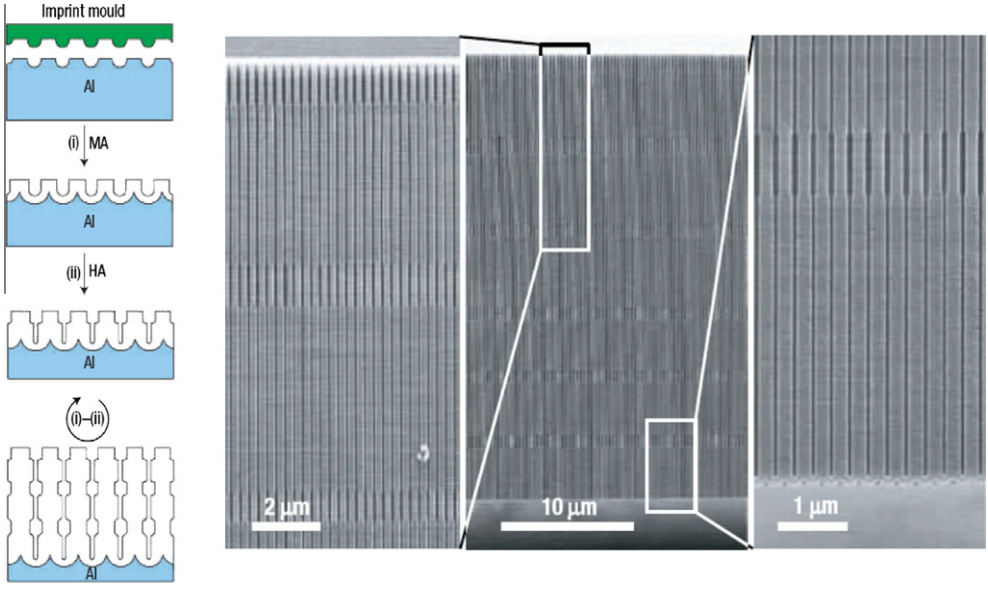

Fig. 7. Long-range ordered AAO membranes with modulated pore diameters. (Left): Scheme for the fabrication of porous alumina with modulated pore diameters by a combination of MA and HA on a pre-patterned aluminium substrate. (Right): SEM micrographs showing the cross-section of the prepared AAO with modulated pore diameters. Magnified cross-section images of the top and bottom parts of the membrane are shown on both sides of the central image. Adapted with permission from Ref. [41].

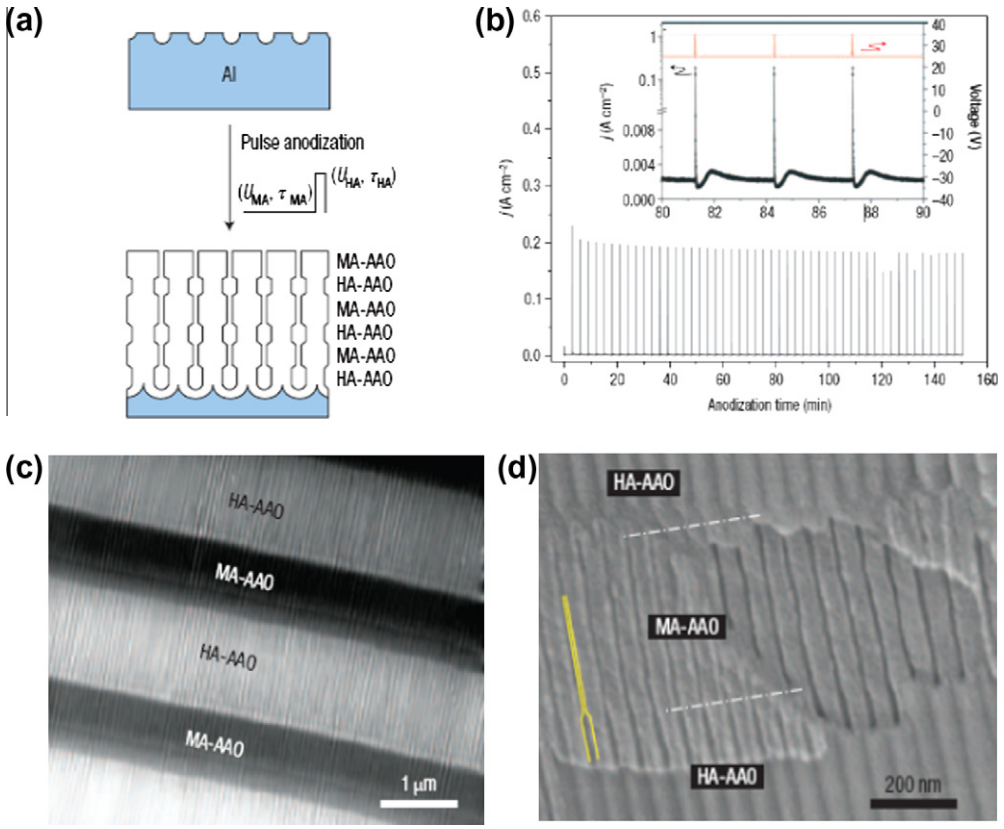

Fig. 8. (a) Scheme for the fabrication of AAO with modulated pore diameters by pulse anodization. (b) A typical current–time (j–t) transient during pulse anodization of aluminium. Pulses consisting of an MA pulse (long) followed by an HA pulse (short) were applied. (c and d) SEM images showing the cross-sectional view of an as-prepared multilayered AAO membrane. Dark and bright image contrast areas correspond to MA- and HA-AAO segments, respectively. Adapted with permission from Ref. [42].

Losic et al. reported a new anodization process, termed cyclic anodization to achieve improved control over internal pore shape. The concept is based on slow and oscillatory changes of anodization conditions ranging from MA to HA regimes (Fig. 9). By changing the period of the current oscillation, control over the geometry of pore structures was achieved and AAO with asymmetrical (ratchet-type) and symmetrical (circular) periodic pore geometries, with different lengths, periodicity and gradients were fabricated [75]. Periodic variations in pore diameter led to photonic crystal behavior in AAO as observed by Biao et al. [76] in optical photographs and transmission spectra (Fig. 10). The color of the sample and the diffraction peak position in the transmission spectra could be controlled easily by using a chemical post-etching step. Similarly, Yamauchi et al. reported on fabricating AAO membranes with conical holes. The conical holes were achieved by repeating and alternating anodization at 40 V and chemical etching with 5% phosphoric acid solution at 30 °C [77]. Losic et al. demonstrated nanosculpturing of AAO membranes with hierarchical pore structures. A typical example is presented in Fig. 11a and b. Three different successive cyclic anodization steps were applied, firstly a cycle with a gradually increasing maximum amplitude, then anodization with a double-profiled cycle and lastly a series of triangular cycles. SEM images of the resulting AAO membrane (ca. 8–10 μm thick) showed hierarchical and multi-modulated pore structures consisting of three stacked porous layers [78]. Chemical etching led to periodically perforated pores (nanopores with nanoholes) as shown in Fig. 11c and d.

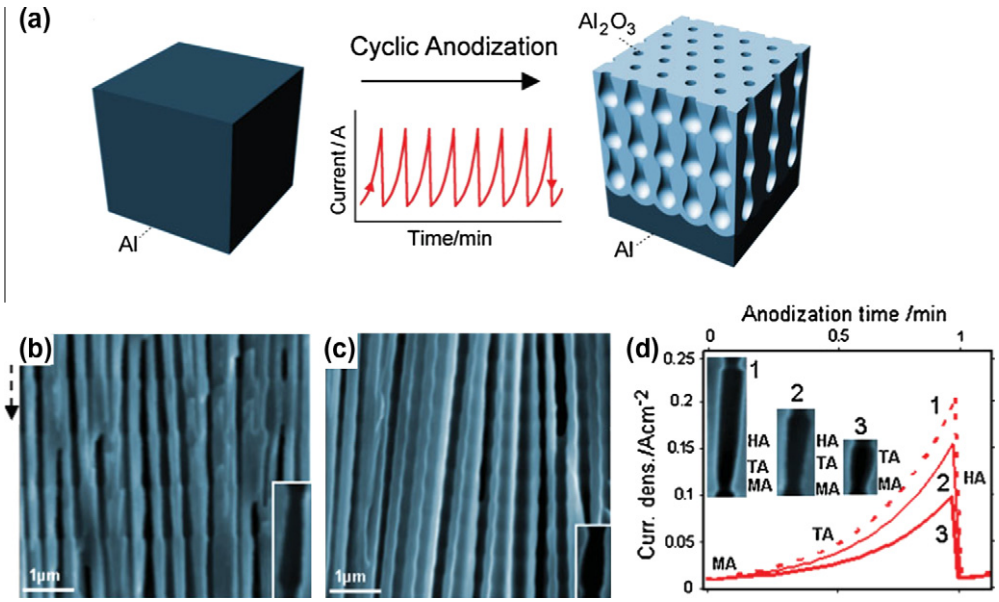

Fig. 9. (a) Scheme of the galvanostatic cyclic anodization approach for structural modulation of AAO with shaped pore geometry. (b) Modulated AAO pores fabricated by asymmetrical current signal (exponential saw-tooth) with two different amplitudes showing pores with asymmetrical and, (c) ratchet-type geometry. (d) Influence of amplitude of current signal on the geometry and the length of modulated segments. Anodization modes (MA, TA, HA) associated with corresponding anodization currents are marked on the pore structures and graphs. Adapted with permission from Ref. [75].

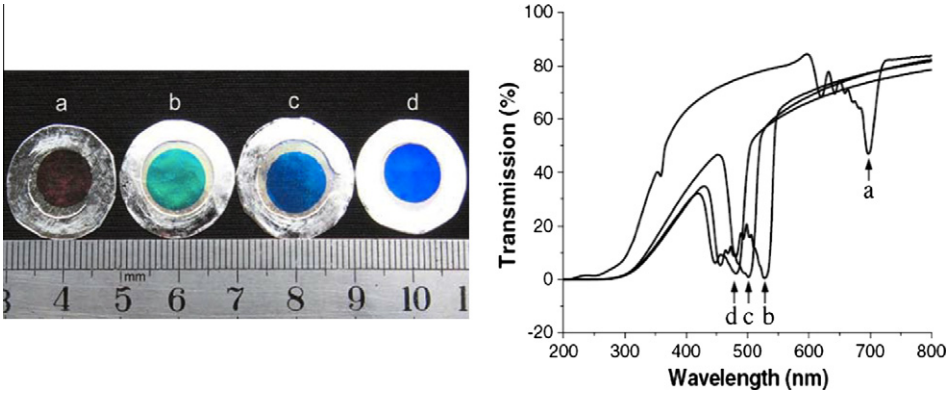

Fig. 10. Optical photograph (left) and corresponding transmission spectra (right) of AAO membranes with modulated structures before chemical etching (a), and after chemical etching for (b) 15, (c) 18 and (d) 20 min. Adapted with permission from Ref. [76].

Biswas et al. [79] investigated the effects of the rapid increase in electrolyte temperature and high voltage up to 160 V, demonstrating rapid etching that led to 3D branched porous AAO membranes. New self-ordered AAO produced at ultra-high anodization voltage (500–600 V) was recently described by Yi et al. The high voltage produced rips and voids between the pores. Subsequent wet chemical etching resulted in AAO with hollow nanostructures (Fig. 12a–g) [80].

In conclusion, AAO nanostructuring is an active research area focused on the development of new fabrication concepts, preparation of more complex pore structures with unique properties suitable for

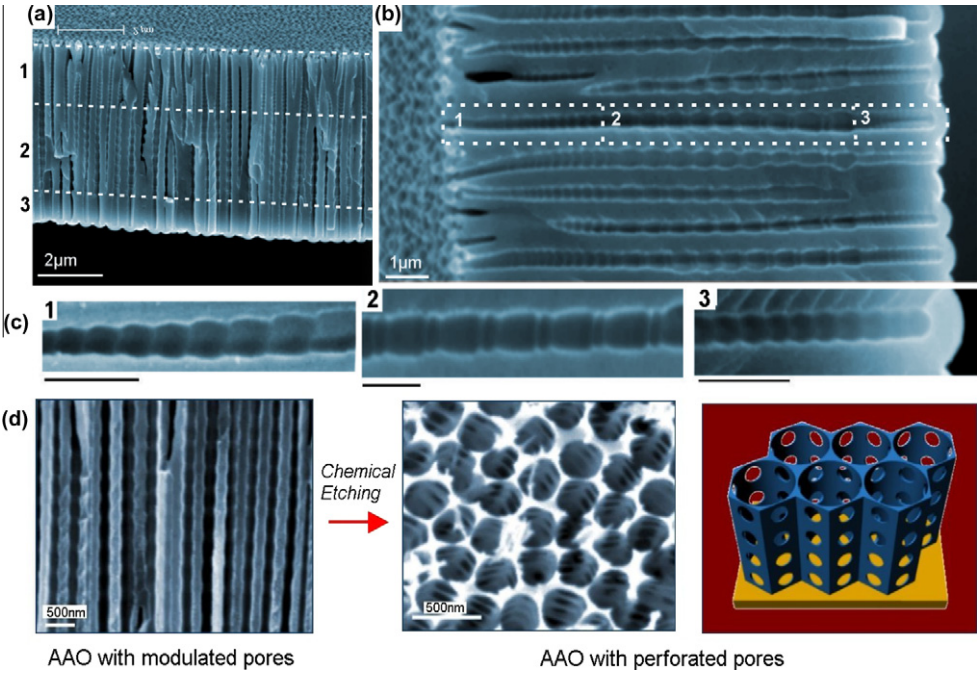

Fig. 11. (Top): (a–c) SEM image of AAO with multilayered pore architectures with different pore shapes and structural modulation fabricated by multiple cyclic anodization in 0.1 M phosphoric acid with three successive galvanostatic anodization steps by three different cyclic signals. (d) AAO with periodically perforated pores (nanopores with nanoholes) by chemical etching. Adapted with permission from Ref. [78].

diverse applications. We can expect more exciting future developments in this field. Template synthesis of metal, carbon, semiconductor and polymer nanowires and nanotubes appears to be the primary motivation for these studies. However, these sophisticated AAO structures should find applications in other areas including molecular separation and in optics, for example as narrow-band filters.

5. Surface modification of nanoporous AAO

In the previous section, we described the recent advances approaches for structural engineering of AAO to generate new properties and applications. In this section, we will show current research on tuning surface properties of AAO using different surface modification strategies. The surface modifications and functionalization of AAO are expected to significantly expand the scope for applications of AAO-based materials. Furthermore, effective combination of structural engineering and surface manipulation will underpin a number of emerging applications.

The AAO surface is insulating and suffers from chemical instability in acidic environment which is a disadvantage for some applications [81,82]. This limitation can be overcome by changing the surface properties and by adding new surface functionalities. The rich content of hydroxyl groups on the AAO surface allow them to be easily modified via modification with organic molecules with the desired functionality. The surface modification techniques that have been explored to improve surface properties and add new functionality to AAO can be divided into two groups: as wet chemical synthesis and gas-phase techniques. The most common approaches for AAO surface modification are summarized in Fig. 13. Wet chemical approaches include self-assembly processes (silanes, organic acids, and layer-by-layer deposition), polymer grafting, sol–gel processing as well as electrochemical and electroless deposition. Subsequent modifications of the thus introduced functionality with biomole-

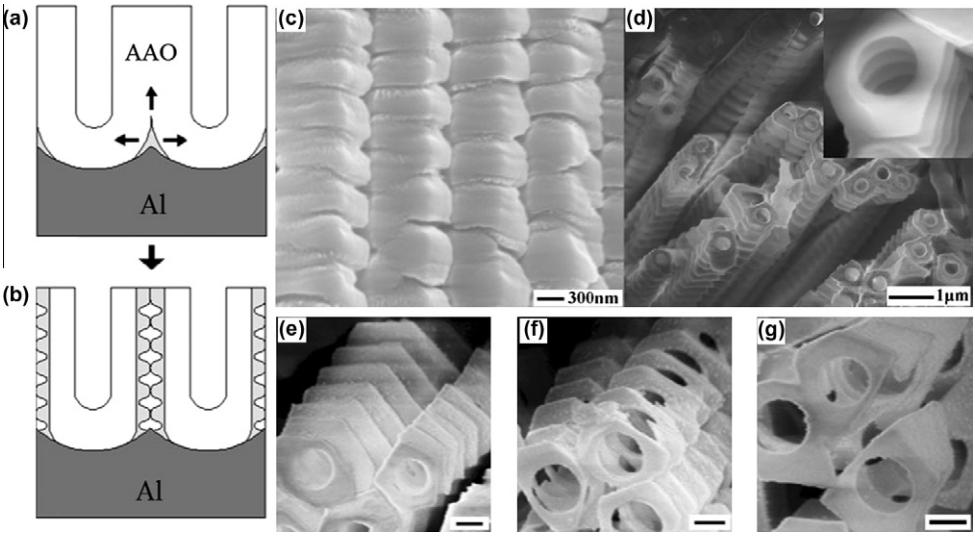

Fig. 12. (a and b) (Left): Schematic diagrams of the fluctuating nanotube growth inside AAO films. (a) Stage of ultra-high Al anodization process showing decomposition of $Al(OH)_3$ from both sides resulting in AAO channels being separated from each other. (b) The following process showing decomposition of hydroxide layer along the side surfaces followed by periodic growth of lateral pores accompanied by current density oscillations and cell separation. (c and d) (Top): SEM images of (c) the cross-sectional section of the AAO film prepared at 600 V and (d) AAO nanostructures fabricated by a subsequent chemical etching (85 min). (e–g) (Bottom): SEM images of AAO hollow nanostructures fabricated by chemical etching processes using different time (e) 90 min, (f) 110 min and (g) 140 min. Scale bars = 200 nm. Adapted with permission from Ref. [80].

cules or nanoparticles can be carried out. Gas-phase surface modification techniques used for surface modifications of AAO include thermal vapor metal deposition, chemical vapor deposition (CVD), plasma processing and polymerization and atomic layer deposition (ALD). Combinations of these two modification technique on AAO have also been described showing ability to tune surface functionalities and properties of AAO for specific applications.

5.1. Wet chemical techniques

5.1.1. Self assembled monolayers

Self-assembled monolayers (SAMs) are organic assemblies formed by spontaneous adsorption, rearrangement and chemical reaction of molecules species from the liquid phase onto solid surfaces [83]. SAMs of the desired functionality are straightforward to prepare on AAO in several ways. The early work focused on SAM with alkanethiols on gold-coated AAO surfaces as envisaged by Martin group [84]. However, the process of gold deposition is tedious and interest on SAM-based modification of AAO has since shifted to the use of organosilanes, which can be applied directly to the native or hydroxylated AAO surface.

5.1.1.1. Organosilane modification of AAO. Chemical modification using silanization is a simple and an effective method to control the wettability and adsorption properties of AAO. Wide varieties of substituted silanes are commercially available and their attachment has a profound effect on the properties of AAO (Table 1). Some of these silane modifiers are widely used as coupling agents or linkers to immobilize other (bio)molecules, polymers, nanoparticles, DNA, cell and suspended lipid bilayers on AAO surfaces. A high density of silane covalently bound on AAO surfaces can be obtained by silanization of hydroxylated AAO membranes (as shown schematically in Fig. 14) [85,86].

The effectiveness of silane modification to change the AAO surface wettability has been demonstrated in several reports. The most popular approach is to functionalize AAO with alkyl- or perflu-

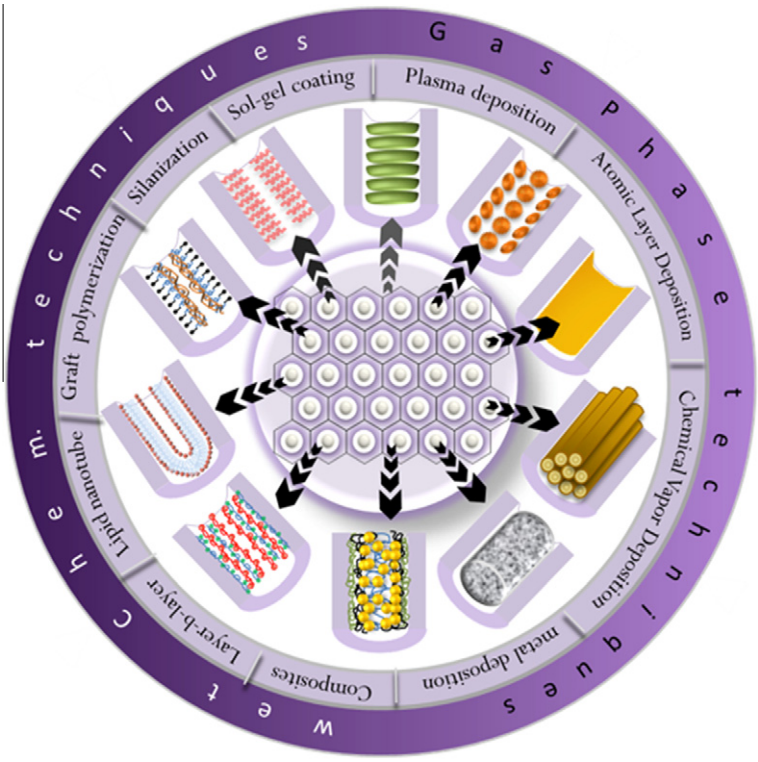

Fig. 13. A wide range of approaches can be used to modify AAO surfaces by wet chemical and gas phase techniques.

oroalkylsilanes [87–89]. The latter change the wettability of the membrane from 20° to 160°. Ku et al. used alkyltrichlorosilanes with tail length from C1–C8 to chemically functionalize the AAO nanopores [90]. They observed that even though AAO immersed in aqueous buffer, the hydrophobic nanopores were filled with air due to the presence of alkyltrichlorosilanes, electrical conduction measured by means of electrical impedance was still observed through a small number of 'hydrophilically defective' pores. In contrast, PEG-silanes have been used to increase the wettability of AAO and to prevent membrane fouling properties in long term use [91], improve biocompatibility of AAO for immunoisolation [92] and also to reduce the effective pore size of the AAO for molecular separations [93].

Post-functionalization of silanized AAO membranes is often carried out to either change the terminal functional group [94,95] or to attach other molecular or nanoscale species including fluorescent dyes, antibodies, peptides, enzymes, DNA, quantum dots, etc. to the reactive functional groups on the membrane surface (e.g. amino, carboxy or aldehyde groups) (Fig. 15) [96–101]. Improved stability of biomolecules immobilized on AAO in comparison to flat surfaces has been reported [102]. Cell adhesive peptide ligands have also been covalently immobilized on 3-aminopropyl dimethylethoxysilane coated AAO membranes to enhance adhesion of osteoblasts (bone forming cells). After silanization. the functionalized AAO membrane was reacted with N-succinimidyl 3-maleimidopropionate followed by arginine–glycine–aspartic acid–cysteine (RGDC) [103]. In another study, different sizes of AAO nanopores were first modified with trichloro(phenyl)silane which then allowed the self-assembly of diphenylalanine (Phe–Phe) dipeptide [104].

Silane-coated surfaces have also been used to suspend lipid bilayers over the pores of AAO membranes functionalized with a grafted polymer layer (vide infra) [105–108]. This was achieved by silanizing AAO with APTES followed by grafting of N-hydroxy-succinimidyl carbonatepolyethylene–glycol (NHS-PEG) and finally vesicle fusion onto the polymer layer. Alternatively, the amine func-

Table 1
Different biosensors based on AAO membranes.

Methods	Biorecognition molecules attached on membrane	Analyte	Refs.
Electrochemical	DNA	Complementary DNA	[298]
Optical	DNA	Complementary DNA	[274,285]
Optical		DNA	[272,285]
Optical		Morin	[281]
Optical	Cytochrome	$NADP^+$	[102]
Electrochemical		Urea	[100,306]
Electrochemical		Ion (Rubby)	[94]
Optical	Streptavidin	Biotin	[99]
Electrochemical	DNA		[96,97]
Electrochemical	DNA		[98]
Optical		Angiotensin I, verapamil	[382]
Electrochemical	IgM	Virus	[213]
Optical	BSA	BSA, Ig	[273,301]
Electrochemical	Anti-HRP	Antibody	[383]
Electrochemical	HRP	Anti-HRP	[383]
Electrochemical	Oligomer	DNA hybridization	[299]
Optical	Dendrimers	DNA hybridization	[276]
Optical	–	DNA pattern	[384]
Optical		Typsinogen and ribonuclease B	[290]
Electrochemical	Cytochrome P450	LDL-Cholesterol	[292]
Electrochemical	Enzyme	Choline	[293]
Electrochemical	Antibody	Virus	[385]
Electrochemical		Amperometric signal	[304]
Electrochemical	Thrombin	Anti Thrombin Ig	[305]
Electrochemical	Glucose oxidase	HRP enzyme	[336]
Electrochemical	Glucose oxidase	Glucose	[245,294]
Electrochemical	Glucose oxidase	Glucose	[386]
Electrochemical	Glucose oxidase	Glucose	[295]
Electrochemical	Yeast	BOD	[387]
Electrochemical	N,N-dimethylformamide, tetrabutylammonium perchlorate divinylbenzene	Glucose	[388]
Electrochemical	Suspended lipid bilayers	Metal ions	[126]

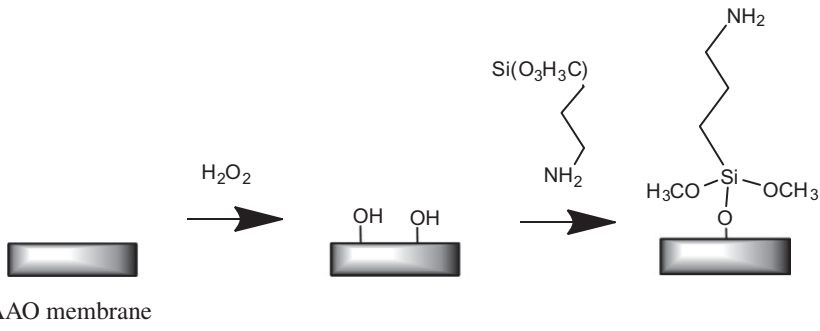

Fig. 14. Common schematic route of silanization used for surface modification on AAO membranes. Adapted with permission from Ref. [85].

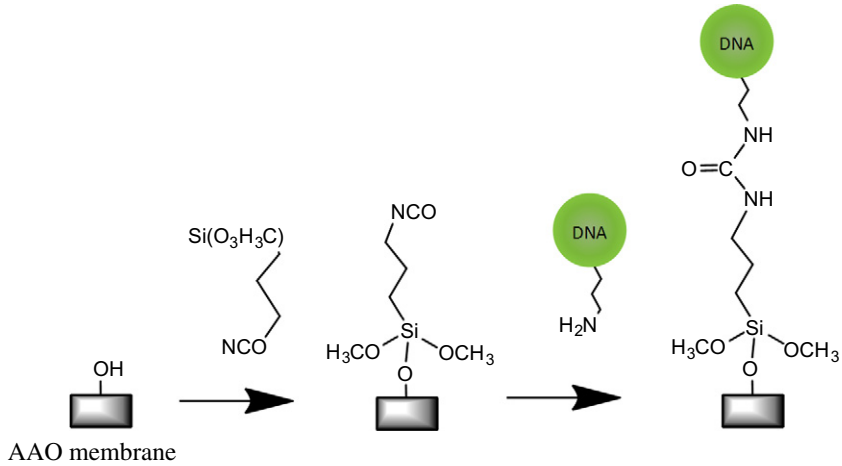

Fig. 15. Silanization of hydroxylated AAO surface with isocyanatopropyl triethoxysilane and subsequent immobilization of amino-terminated DNA.

tion of the APTES-coated surface was reacted with the carboxyl group of 1,2-distearoyl-sn-glycero-3-phosphoethanolamine-N-carboxypolyethylene- glycol 2000 (DSPE-PEG2000COOH) inside AAO pores [107]. It was suggested that PEG chains act as tethering agent and are capable of triggering vesicle fusion as well as help maintain the fluidity of the bilayers [106,107].

Recently, the surface-attached APTES has been used as an initiator for grafting polymer brushes of poly(γ-benzyl-L-glutamate) (PBLG) via surface-initiated polymerization on the AAO membrane surface, generating a membrane with favorable properties for membrane filtration and separation [71]. Li et al. [109] reacted an APTES-functionalized surface with the initiator 2-bromoisobutyryl bromide (BIBB), suitable for grafting of poly(N-isopropylacrylamide (PNIPAM) via atom-transfer radical polymerization (ATRP). The grafting density of PNIPAM on AAO membranes could be controlled by changing the density of the ATRP initiator. Bruening and co-workers demonstrated that the initial step of activating the membrane surface with silane can be excluded by employing a custom-synthesized initiator 11-[(2-bromo-2-methyl)propionyloxy]-undecyltrichlorosilane for grafting poly(2-hydroxyethyl methacrylates (PHEMA) brushes on AAO surfaces [110,111]. Likewise, an APTES-functionalized surface was used to fabricate palladium nanotubes by electroless deposition [112] by sensitizing the membrane with an aqueous solution of $SnCl_2$ and HCl followed by a solution of $PdCl_2$ and HCl. Likewise, Sehayek et al. [113] used an APTES-functionalized AAO membrane as a template to form solid, electrically conductive nanoparticle-decorated nanotubes by passing a citrate-stabilized metal (Au or Ag) nanoparticle solution through the pores of the functionalized AAO membrane. Preparation of bimetallic Au–Pd nanotubes has also been demonstrated using this approach. Accumulation in the wet stage and solidification of nanoparticles upon drying promoted the formation of multiwall metallic nanotubes inside AAO [114]. In a different approach, AAO functionalized with 1H,1H,2H,2H-perfluorodecyltricholorsilane was reported to help minimize the adhesion between the pore wall and polyacrylate nanofibers formed using pressure impregnation and photo-crosslinking inside nanopores [115].

Our group has recently demonstrated multifunctional and multilayered surface modification of AAO nanopores with distinctly different internal and external surface properties [116]. The multilayered surface functionalities was successfully fabricated by combining a series of anodization and silanization cycles with different silanes for instance pentafluorophenyldimethylpropylchlorosilane (PFPTES), APTES and N-triethoxysilylpropyl-(O-polyethyleneoxide)urethane (PEG-silane), achieving a range of functionalities and wettabilities (Fig. 16). This approach also enabled control over the thickness of individual functional layers inside the pore matrix, and to selectively bind gold nanoparticles on amino-functionalized layers. Selective transport experiments with hydrophobic

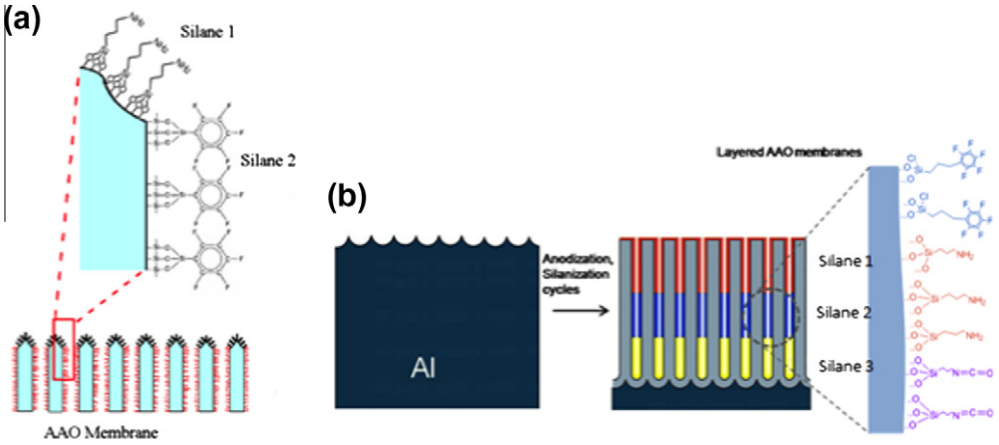

Fig. 16. (a) Schematic of the opening of an AAO membrane with different silane functionality on the very top of the membrane and the inside of the pores. (b) Schematic of anodization and silanization cycles to produce an AAO membrane with multiple silane layers Adapted with permission from Ref. [116].

and hydrophilic molecules on pores with hydrophobic and hydrophilic layer subsequently verified the effectiveness of our modification approach and showed an elegant approach to tune chemical separation properties of AAO membranes [117].

5.1.1.2. Functionalization with organic acids. In addition to organosilanes, the formation of SAMs on metal oxide surface from organic acids has received considerable attention in the past two decades and recently has been applied for modification of AAO. The initial studies by Allara and Nuzzo reported on the adsorption of *n*-alkanoic acids of long carbon chains (16–22 carbons) terminated with a variety of end groups such as methyl, vinyl or propargyl groups [118]. The proposed reaction scheme of *n*-alkanoic on a hydroxylated AAO surface is shown in Fig. 17 [118–120]. Recently, Chang and Suen used two different *n*-alkanoic acids, namely octanoic and octadecanoic acid, to render the AAO membrane hydrophobic. The longer alkyl chain of the latter acid was anticipated to increase hydrophobicity of the surface. Based on bovine serum albumin (BSA) adsorption results, the octadecanoic modified surfaces demonstrated higher protein adsorption (3–19%) as compared to octanoic acid (2–8%) modified surfaces [120]. The same authors extended their work by studying the attachment of three different fluorinated organic acids (trifluoroacetic acid, perfluoropentanoicacid and 2,3,4,5,6-pentafluorobenzoic acid) resulting in hydrophobic AAO membranes. The water contact angle (CA) measurements demonstrated the highest CA of 107° for perfluoropentanoic acid followed by trifluoroacetic and 2,3,4,5,6-pentafluorobenzoic acid with CA of 104° and 98°, respectively. Interestingly, the hydrophobicity of the fluorinated surfaces was significantly lower than that of the octadecanoic acid modified surfaces (CA = 130°) [121]. A variety of fluorinated and non-fluorinated carboxylic acids have been used for surface modification of AAO by Karaman et al. [122]. In contrast to Chang et al. they found

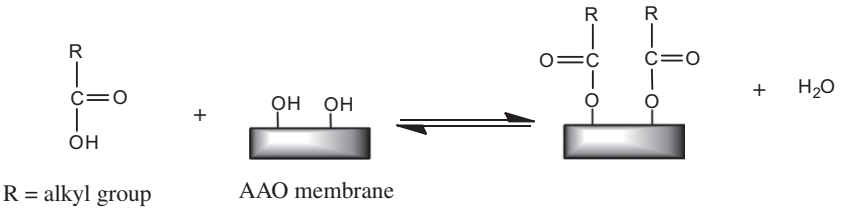

Fig. 17. Reaction scheme of AAO membrane with *n*-alkanoic acid. Adapted with permission from Ref. [120].

that the fluorinated surfaces had a higher CA than the non-fluorinated ones (105° vs. 50–70°). The discrepancy might be due to the shorter short hydrocarbon chains (C3–C4) used in the study by Karaman et al. Other organic molecules such as stearic acid and methyl stearate also chemisorb onto AAO surface [123] with the acid forming a denser monolayer than the ester. Maat et al. showed that it is possible to display alkynes functional groups on the AAO surface using 1,15-hexadecadiyne surfaces and that the alkyne functional group then facilitates the attachment of 11-azidoundecyl lactoside using the Cu(I)-catalyzed alkyne–azide cycloaddition reaction. The lactosylated surfaces showed increased colonization of *Candida albicans* compared to unmodified surfaces [124].

5.1.1.3. Lipid bilayers. Since lipid bilayers are well-established mimics of biological cell membranes, there is great interest in their integration with AAO pore structures in order to assemble artificial bilayer membranes with improved stability over traditional free-standing bilayers (also known as black lipid membranes, BLMs) [125]. Depending on the deposition method, the size of the pores and the surface chemistry, lipid bilayers self-assemble on the top of AAO membranes (forming suspended bilayers) or inside the nanopores (forming conformal bilayers) [126–128].

Steinem et al. prepared suspended lipid bilayers on highly ordered AAO supports and observed long-term stability of this system combined with the ability to monitor ion channel activities [126,129–132]. Their fabrication approach consisted of gold coating an AAO surface followed by formation of a SAM of alkanethiols with a negatively charged head group. Fusion of lipid vesicle featuring positively charged lipid head groups led to a suspended bilayer architecture and prevented vesicle fusion inside the pores as shown in Fig. 18a. The group also prepared so-called nano-BLMs on AAO membranes by "painting" of lipid solution over a gold-alkanethiol modified surface. The resulting lipid bilayer membranes exhibit high membrane resistance up to $1.6 \times 10^8\ \Omega$ suitable for single ion channel measurements (Fig. 18b). In contrast, fusion of lipid vesicles inside AAO nanopores has been achieved using silanes-coated membranes as illustrated in Fig. 19a [106]. Pioneering work by Smirnov and Poluektov led to multilamellar lipid nanotubes (LNTs) by exposure of the AAO to multilamelar vesicles or extruder deposition (Fig. 19b) [127,133]. By the latter technique, the wall thickness of the resultant LNTs can be controlled [134]. The formation of LNT architectures can be confirmed by means of spin-labeling electron paramagnetic resonance (EPR), solid state NMR spectroscopy and fluorescence microscopy using fluorescent lipids [135].

In a different approach, Largueze et al. [107] deposited tethered lipid bilayer membrane inside AAO channels. The lipid bilayer membrane was prepared following the step-by-step techniques inside the

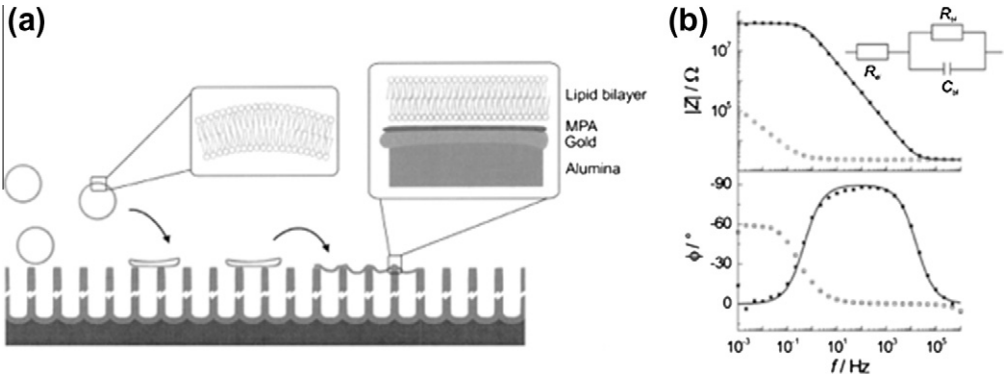

Fig. 18. (a) Schematic presentation of pore suspending bilayers made by fusion of large unilamellar vesicles on 3-mercaptopropionic acid monolayer functionalized Au-coated AAO substrates. (b) Corresponding absolute value of the impedance $|Z|(f)$ and phase shift $\dot{\omega}(f)$ of a functionalized AAO substrate prior to the addition of the vesicle suspension (□) and 30 h after vesicle addition (■). The solid line corresponds to a fit using an equivalent circuit. Electrolyte: 0.1 M NaCl. Adapted with permission from Refs. [126,130].

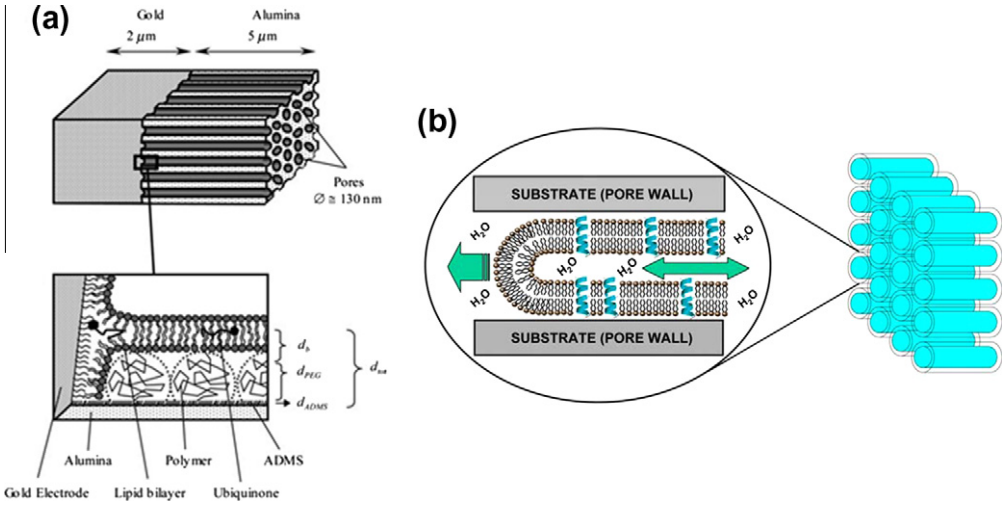

Fig. 19. (a) Top: Structure of the AAO membrane with underlying Au layer as host for self-assembled lipid bilayer. Bottom: Enlarged view of pore bottom showing self-assembled lipid bilayer along the pore wall on polymer-functionalized surfaces [106]. (b) Schematic of single lipid nanotubes (LNTs) propagating inside an AAO pore by capillary action [127].

pores with the last step being PEG-triggered fusion of the surface-attached liposomes. The pore bottom of AAO was first gold-coated and functionalized with an undecanethiol SAM whilst the pore walls were modified by APTES. The system was incubated with liposomes which were then triggered to fuse using PEG. The authors demonstrated the importance to incorporate lipid membrane inside pores to prevent membrane dewetting. These studies showed that by integration of lipid bilayers and nanopore structures it is possible to design sensitive biomimetic nano-channel based sensing devices and use them to study protein membrane interactions.

5.1.1.4. Layer-by-layer deposition. Layer-by-Layer (LbL) deposition is a simple, yet versatile and inexpensive technique, which involves construction of polyelectrolyte multilayers (PEMs) films by alternate dipping of a substrate into polyelectrolyte solutions of alternating charge (Fig. 20a) [154]. The film thickness can be easily controlled at the nanometer scale. The resulting layers can be further functionalized with biomolecules or nanoparticles. The most popular polyelectrolytes used for LbL deposition are polyacrylic acid (PAA), polyallylamine hydrochloride (PAH), polystyrene sulfonate (PSS) and polydiallyldimethylammonium chloride (PDADMAC) [136].

In pioneering work by Balachandra et al., PAA partially complexed with Cu^{2+} ions was first absorbed onto an UV/ozone treated AAO membrane followed by immersion in a solution of PAH. The above procedure was repeated until the desired numbers of bilayers were deposited and conformal and smooth films were formed on the AAO [137]. Most of the studies show AAO pores were not clogged after deposition of five to seven PEM bilayers thus enabling this system to be employed molecular size selective transport [138–141]. The number of PEMs layers combined with different compositions of PEMs (i.e. PSS/PAH, PE-PSS/PAH, $(PSS/PDADMAC)_4PSS$) significantly influenced the flux, transport, rejection rate and selectivity of solutes through these functionalized membranes [138,141,142]. More recently, Ouyang et al. demonstrated the effect of deposition conditions such as pH, electrolyte concentration and the effect of the charge of the outer polyelectrolyte layer on the AAO membrane on molecular separation of cations [142]. PSS/PAH films or composites of PSS/PDADMAC + PSS/PAH showed effective rejection of Mg^{2+} transport from solutions containing NaCl and $MgCl_2$. The selectivity of Mg^{2+} rejection could be enhanced by increasing the charge of the terminated PAH layer by means of increasing ionic strength in the PAH deposition solution.

Dai et al. [143] deposited PEMs of $[PAA/PAH]_3PAH$ followed by immobilization of antibodies on the carboxylic groups of the PAA layers using carbodiimide coupling (Fig. 20b). The resulting coating re-

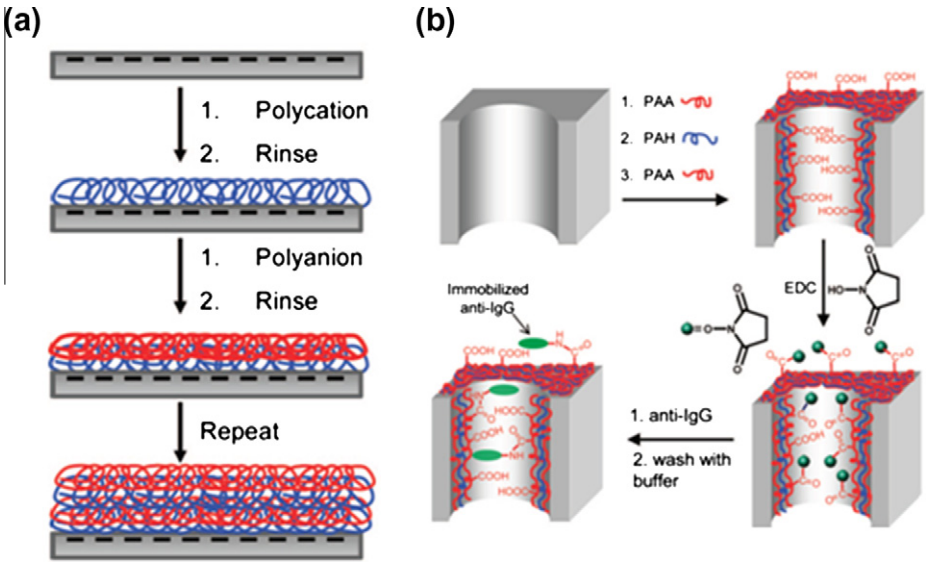

Fig. 20. (a) Schematic of a pore of AAO membrane modified by adsorption of two polyelectrolytes of opposing charge. Adapted with permission from Ref. [154]. (b) Schematic of a pore of AAO membrane modified by adsorption of polyelectrolytes followed by carbodiimide coupling of an antibody. Adapted with permission from Ref. [143].

sisted nonspecific protein adsorption. Charged polyelectrolytes on AAO membranes also allowed the immobilization of citrate-stabilized gold nanoparticles on PEMs under retention of the nanoparticles' catalytic activity as demonstrated by Dotzauer et al. [144].

The interested reader is also referred to a review on the synthesis and properties of LbL films inside AAO pores [145].

5.1.2. Polymer modifications

The covalent attachment of polymer chains inside nanopores is an alternative functionalization approach allowing the fine control of surface chemistry, functionality, density and thickness of the AAO membrane's coating. Polymer layers can be either attached on the top of the pores or inside the pores. Polymer-modified AAO membranes have shown improved binding capacity, selectivity, biocompatibility, stability and lubricant properties in comparison to non-modified AAO membranes. The two most significant approaches for polymer modification of AAO are polymer grafting and plasma polymerization (vide infra). The modification of AAO membranes with polymer brushes by grafting approaches can be achieved via non-covalent and covalent interactions between the polymer chains and the membrane. The arguably simplest method involves physisorption of polymer brushes including poly(2-methoxy-5-(2′-ethyl-hexyloxy)-p-phenylenevinylene (MEHPPV) or poly(2,3,-diphenyl)phenylenevinylene) (DP-PPV) into the pores of AAO membranes as demonstrated by Qi et al. [146]. However, the physisorption of polymer brushes suffers from poor stability. Covalent grafting is generally carried out through either "grafting to" or "grafting from" approaches via atom transfer radical polymerization (ATRP), reversible addition-fragmentation chain transfer polymerization (RAFT) or plasma-induced graft polymerization [147,148]. The resulting polymer brushes contain multiple binding sites that give rise to high binding capacities. Moreover, the polymers can be easily modified with ligands that exhibit specific biological recognition and provide high selectivity. An AAO membrane with PAA brushes was prepared by grafting amino-terminal poly(tert-butyl acrylate (PTBA) to the top layer of an AAO pores modified with carboxylic acid groups, followed by deprotection of the tert-butyl groups [149]. In this case, the pores remained free of polymer.

Sun et al. [110] employed an ATRP approach to modify and control the growth of PHEMA brushes capped with nitrilotriacetate–Cu^{2+} (NTA–Cu^{2+}) complexes that produced membranes with bovine ser-

um albumin (BSA)-binding capacity. Instead of using NTA–Cu^{2+} complexes, the same group extended the work by synthesizing PHEMA–NTA–Ni^{2+} brushes coating inside AAO pores which allow to bind oligohistidine-tagged ubiquitin for protein purification (Fig. 21) [111]. Balacandra and co-workers used the ATRP method to synthesize ultrathin cross-linked poly(ethylene glycol dimethacrylate) (PEGDMA) or linear PHEMA brushes on AAO supports with coating thicknesses of approximately 50 and 20 nm, respectively. Gas permeation studies demonstrated that PEGDMA modified membranes have CO_2/CH_4 selectivity of 20 and O_2/N_2 selectivity of 2, whereas PHEMA modified membranes showed slightly lower selectivity. However, post-modification of the hydroxyl group of PHEMA with pentadecafluorooctanoyl chloride increased the selectivity of CO_2/CH_4 to 8 [150]. The post-modification approach of PHEMA was further extended by the same group by introducing a range of side chains such as octyl, hexadecyl or pentadecafluorooctyl chains rendering the surface hydrophobic and suitable for the separation of volatile organic compounds (VOCs) from water (Fig. 22) [151]. In contrast, Grajales et al. [152] coated AAO surfaces and copolymerized of poly(ethylene glycol methyl ether methacrylate) (PEGMEMA) monomers with different PEG chain lengths thereby avoiding crystallization of PEG side chains and maintaining the amorphous state of the polymer brushes for more than 1 year. The functionalized membrane afforded high permeability of CO_2 and selectivity of CO_2 over H_2. More recently, Lee and Penn [153] have reported a method to derivatize AAO pore walls with epoxide groups and subsequently graft amino-terminated polystyrene chains (PS-NH_2) to these active sites. Other characteristics of polymer brushes grafted on AAO membranes have been reviewed in detail by Bruening et al. [154].

Thermo-responsive polymer brushes of PNIPAM and similar polymers have been intensively explored and received considerable attention in the recent past. The switchable properties such as hydrophilic/hydrophobic switching at the lower critical solution temperature (LCST) make this polymer attractive for a variety of applications [155]. ATRP technology has been used to synthesis PNIPAM grafted on AAO membranes. Li et al. [109] first immobilized APTES on the AAO membrane followed by post-modification with initiator BIBB and subsequently polymerized NIPAM from the surface. The density of PNIPAM could be controlled by adjusting the reaction time of silanes on AAO surfaces whilst

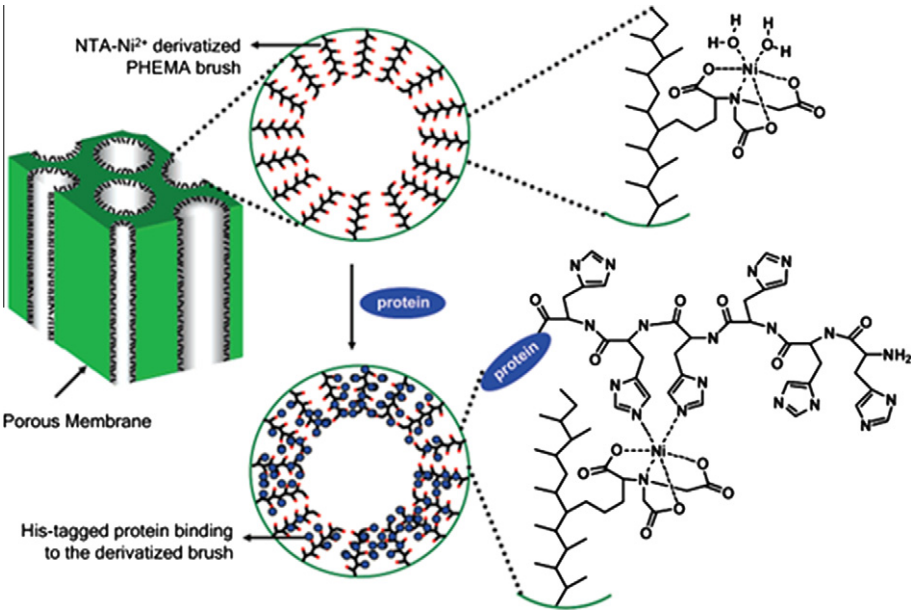

Fig. 21. (a) Schematic diagram showing binding of His-tagged protein to NTA–Ni^{2+}-derivatized PHEMA polymer brushes inside an AAO pore. Adapted with permission from Ref. [111].

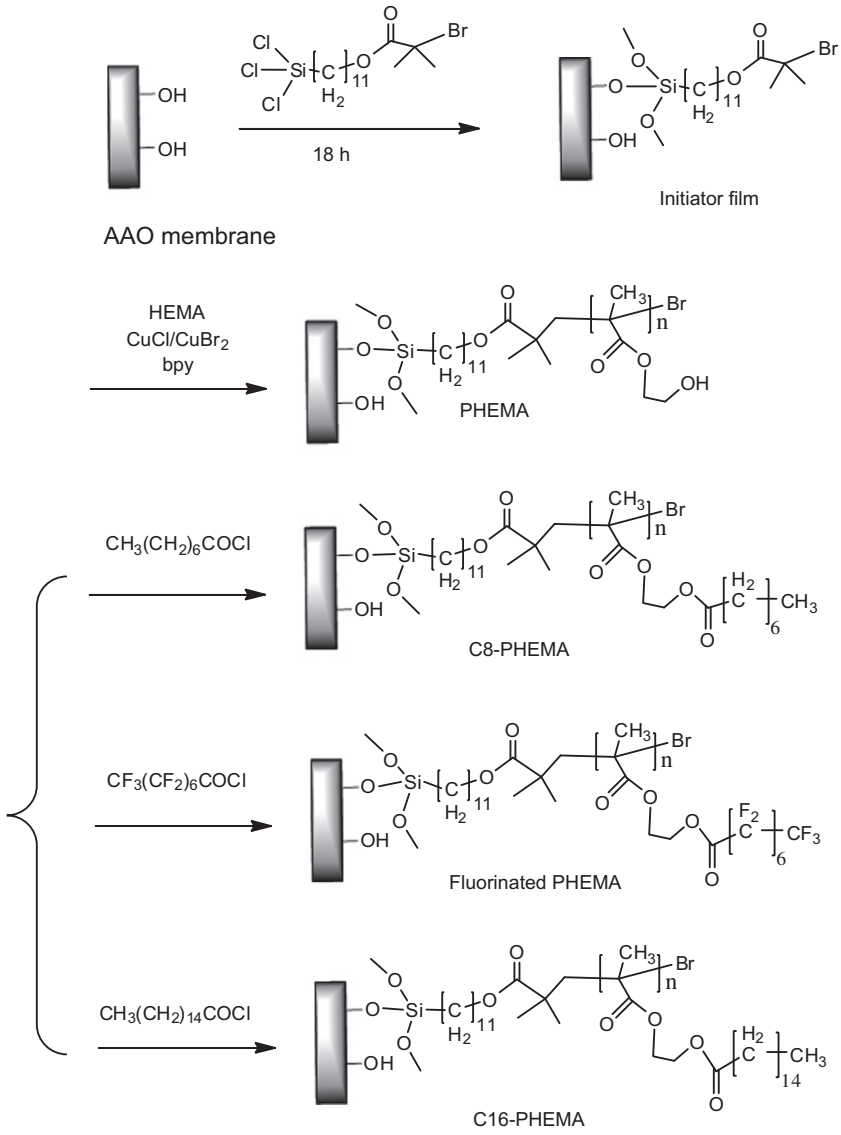

Fig. 22. Scheme showing attachment of a trialkoxy silane initiator to an AAO membrane. ATRP of HEMA from the immobilized initiator, and derivatization of PHEMA with acid chlorides. Adapted with permission from Ref. [151].

the length of grafted PNIPAM was tuned by changing the temperature, time and monomer concentration. Cui et al. used ATRP to synthesize co-polymers of PNIPAM-*co*-*N*,*N*′-methylenebisacrylamide on a BIBB-APTES functionalized AAO membrane [156,157]. Alternatively, Fu et al. [158] used one step approach using an AAO membrane functionalized with the ATRP initiator 1-(trichlorosilyl)-2-[*m*/*p*-(chloromethyl) phenyl]ethane followed by PNIPAM grafting. The length of the polymer controlled the size of the pore opening of the membrane but also the surface roughness and the interfacial energy (Fig. 23). Wang et al. demonstrated the preparation of molecular imprinted polymers (MIPs) using surface-initiated ATRP on an AAO membrane [159].

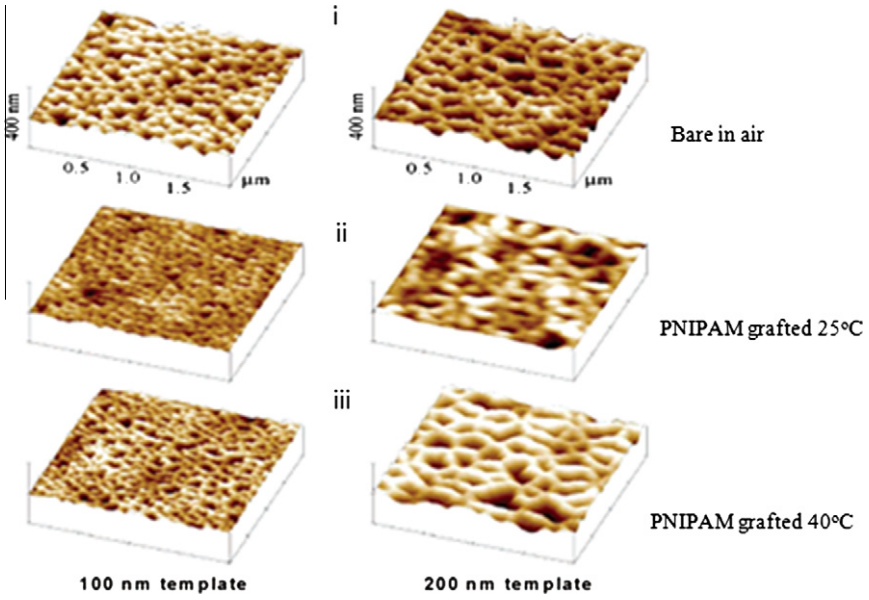

Fig. 23. Topographical AFM images of PNIPAM-grafted AAO: (i) bare AAO membranes (templates) in air; (ii) PNIPAM-grafted membranes in water at 25 °C; (iii) PNIPAM-grafted membranes in water at 40 °C. Adapted with permission from Ref. [158].

The effect of pore geometry on the AAO membrane grafted with poly(methyl methacrylates) (PMMA) by ATRP was demonstrated by Gorman et al. [160]. AAO-grown polymer brushes showed lower molecular weight and broader molecular weight distribution when compared to polymers grown in solution. This shows that confinement effects due to narrow pore size have an effect on the polymer growth kinetics and lead to an increase in polydispersity. Surface grafting of poly(γ-benzyl-L-glutamate) (PBLG) on AAO surfaces was demonstrated by Lau et al. [161]. In their work, APTES-modified AAO was used as surface initiator for polymerization with N-carboxy anhydride of benzyl-L-glutamate monomers to produce high density PBLG. The formation of PBLG inside AAO nanochannels was monitored *in situ* by means of optical waveguide spectroscopy.

Shi et al. fabricated chitosan (CS)-AAO composite membrane with uniform pore size and porosity. The preparation of CS-AAO composite membrane involved activating the hydroxylated AAO membrane with 3-glycidoxypropyltrimethoxysilane (GPTMS) followed by grafting of CS. After exposing composite CS-AAO with $CuSO_4$ solution, the Cu^{2+} capped CS-AAO composite membranes was successfully used as separation and purification of hemoglobin from red cell lysate [162]. In another recent study, thin layer of silica was deposited on the AAO surface to introduce reactive groups for PAA grafting. PAA grafting was achieved by activating the silica-coated AAO with 3-glycidoxypropyl trimethoxysilane resulting in a pH sensitive membrane. The observation of pH sensitive membrane was monitored at a pH between 3 and 5, and at the same time EIS studies showed that the resistance of the membrane increased from $4.3 \times 10^5\ \Omega\,cm^2$ at pH 2 to $1.3 \times 10^6\ \Omega\,cm^2$ at pH 6 [163].

In addition, a number of strategies have been developed for protein immobilization using conducting polymers. For example, Oliveira et al. coated AAO membranes with either polyethyleneimine (PEI) or polyaniline (PANI) and used them as supports for enzymes immobilization. AAO-PEI composite was fabricated following the cross-flow filtration of the polymer solution through the membrane, whereas AAO-PANI was prepared using surface chemical polymerization technique where MnO_2 was used as oxidizing agent for aniline polymerization. After glutaraldehyde activation, horseradish peroxidase and trypsin were immobilized on the composites [164]. Jeon et al. fabricated electrically responsive polymer based on polypyrrole (PPy) doped with dodecylbenzenesulfonate (DBS) anion that was electropolymerized on the upper part of AAO pore structures. Using this approach, the pore size of AAO

could be acutated electrically depending on electrochemical state of PPy/DBS. The actuation processes were confirmed by *in situ* atomic force microscopy and flux measurement [165].

5.1.3. Sol–gel chemistry

The sol–gel assembly process on AAO nanopores involves the hydrolysis of precursor solutions on the AAO substrate by immersion, dipping or spin coating. The solvent is then evaporated and a glassy gel is formed inside the pores [166]. Consequently, the surface is thermally treated in order to remove the remaining solvent from the system. The precursor solution and the surfactant play significant roles in self-assembly process of sol–gel structures forming inside AAO channels [167]. The benefit of surface modification by using the sol–gel technique lies in the ability to (1) synthesize high purity materials at relatively low temperature, (2) prepare homogenous and multi-component structure by mixing precursor solutions and (3) control processing parameters allowing the synthesis of materials with different properties such as structure, thermal stability and surface reactivity (using precursors with additional functional groups) [168,169]. So far, the application of sol–gel techniques on AAO has been dominated by a templating strategy for the preparation of nanocomposite silica [170], carbon [171], metal oxides such as TiO_2 [172], $PbTiO_3$ [173], composite TiO_2–silica [174], $LiCoO_2$ [175], SnO_2 [176], Si [177], NiO [178] and polymer derived SiOC [179] using sol–gel approaches. Tetramethoxysilane (TMOS) and tetraethoxysilane (TEOS) are the most widely used starting materials for silica-based modifications of AAO. In some cases, the AAO template was removed and liberated and free-standing nanotube and nanorod structure were created. In other cases, AAO composites membranes were prepared with reduced pore dimensions and different surface chemistries.

Lee et al. [180] demonstrated preparation of AAO/silica composite membranes using AAO as a template to deposit silica nanotubes by the sol–gel template technique. The prepared silica nanotubes were then reacted with aldehyde terminated silanes. This modification method allowed the conjugation of an antibody that selectively binds to one enantiomer of a therapeutic drug. Recently, Yamaguchi et al. employed a rather simple fabrication procedure of spotting precursor solutions containing cationic cetyltrimethylammonium bromide (CTAB) as structure directing agent and TEOS as the silica source onto the AAO membrane, and obtained aligned and columnar ordered silica nanochannels (Fig. 24) [170]. Platschek et al. [181,182] extended this work by demonstrating systematically adjustable orientation of mesoporous silica structures by combining sol–gel and evaporation-induced self-assembly (EISA). By varying the amount and type of structure directing agent such as CTAB or EO_{20}-$PO_{70}EO_{20}$ (Pluronic 123, P123 or Brij56) and by adding inorganic salts, they investigated the effect of interfacial interactions on the orientation of silica nanochannels confined within AAO membranes. They demonstrated that CTAB promoted the orientation of hexagonally structured mesopores along the AAO channels, whereas non-ionic surfactants such as P123 or Brij56 led to the formation of either circular or columnar orientations. Furthermore, the authors found that the mesophase structure could be tuned by adjusting the moisture content of deposited sample and humidity during drying process. The Steinhart group used the same approach to fabricate silica nanowires containing linear mesocage arrays. In their experiment, a mixture of TEOS, polystyrene-block-poly(ethylene oxide) (PS-*b*-PEO), HCl, ethanol and toluene infiltrated into AAO membrane and EISA then promoted the formation of spherical PS domains in a PEO/TEOS matrix. After gelation for 24 h, the PS-*b*-PEO matrix was removed through calcinations, leaving behind silica nanowires with elongated spherical voids (Fig. 25c) [174].

Wu et al. [183] fabricated silica-P123 composite mesostructures within AAO channels using a sol–gel dip-coating technique. They observed remarkably rigid single and double helical mesoporous silica frameworks formed within the AAO channels which retained their morphologies after removal of the surfactant (Fig. 25a and b). Silica nanorod arrays were fabricated using the same surfactant (P123) but slightly modified sol–gel conditions [184]. An improved and new strategy of synthesizing silica nanotubes with orientation controlled mesopores in AAO membranes was developed by Zhang et al. Rather than using a conventional dipping process, the group slowly added TEOS and a P123 precursor into the channel of AAO one after the other, promoting interfacial growth of silica nanotubes. In addition, they showed that the orientation of the silica nanotubes can be regulated without any modification of the channel surface or applying any external forces as routinely performed in previous studies [185].

Recently, Cazacu et al. [186] produced silica-coated AAO nanochannels using CTAB and TEOS, where the inner silica surface was then functionalized with hydrophobic octadecyltrimethoxysilane

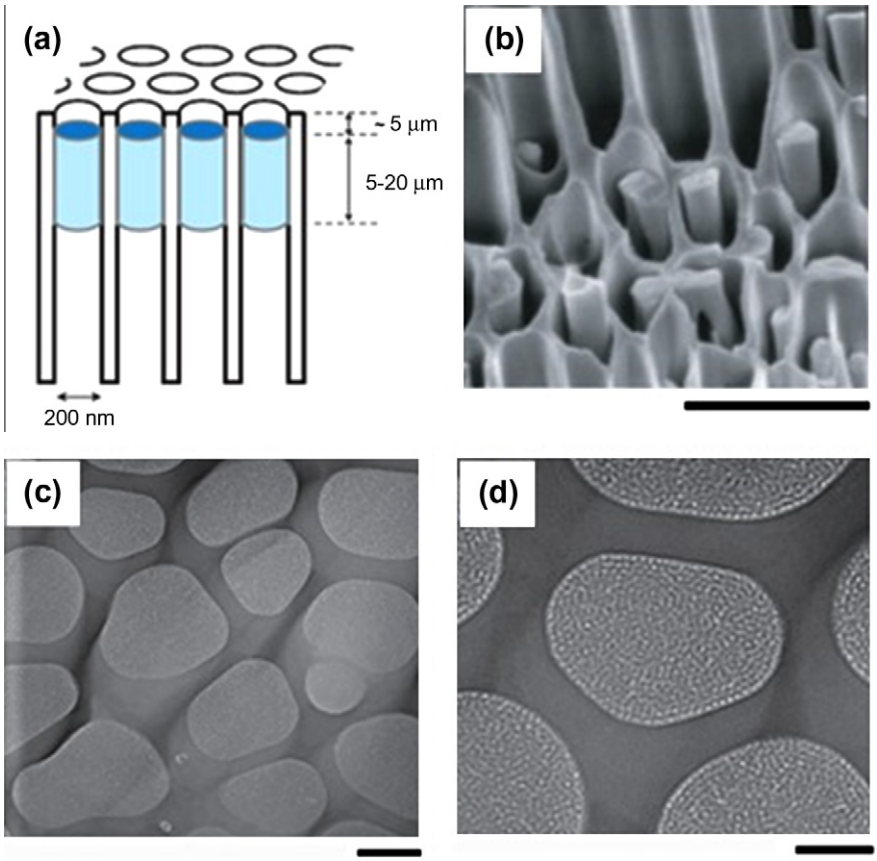

Fig. 24. (a) Schematic illustration of the columnar structures of silica–surfactant nanocomposite formed inside the columnar AAO pores (pores inside pores). (b) Cross-sectional view of the AAO membrane after treatment with cetyltrimethylammonium bromide (CTAB) and TEOS as silica source (scale bar 1 μm). (c) Low magnification TEM images of the AAO membrane with the silica–surfactant nanocomposites inside the columnar AAO pores. (d) High magnification of (c). Scale bars correspond to 100 nm (c) and 50 nm (d). Adapted with permission from Ref. [170].

(ODS). Macrocylic receptors such as hexylureidobenzo-15-crown-5 or hexylureidobenzo-18-crown-6 were then adsorbed on these membranes. The internal structures of the receptor functionalized pores changed in the presence of alkali metal salts and forming stacked macrocyclic ion channel architectures. Likewise, lysine was attached to AAO–silica composites via glutaraldehyde as a cross-linker [187]. Silica nanotubes could also be prepared using less common precursors such as $SiCl_4$ by absorbing these molecules on the hydrated membrane surface followed by a hydrolysis process to form SiO_2 [188].

Relatively little work has been done on non-silica based sol–gel coatings on AAO. Rorvik et al. showed that different concentrations of sol solutions did not have a significant effect on the resulting wall thickness of ferroelectric lead titanate ($PbTiO_3$) nanotube inside AAO membranes [173]. Ordered NiO nanotubes arrays embedded in AAO have been prepared using a nickel–ammonia complex solution as a precursor. The nanotubes were reported to possess polycrystalline structure with diameters of about 200 nm and wall thickness of 60 nm [178]. More recently, high aspect ratio TiO_2 nanotube arrays have been prepared through LbL titania deposition process. In this fashion, AAO was exposed to series of deposition cycles to aqueous protamine and titania precursor-bearing solutions. The ability of protamine to bind to alumina and titania, and to induce the formation of a Ti–O-bearing coating

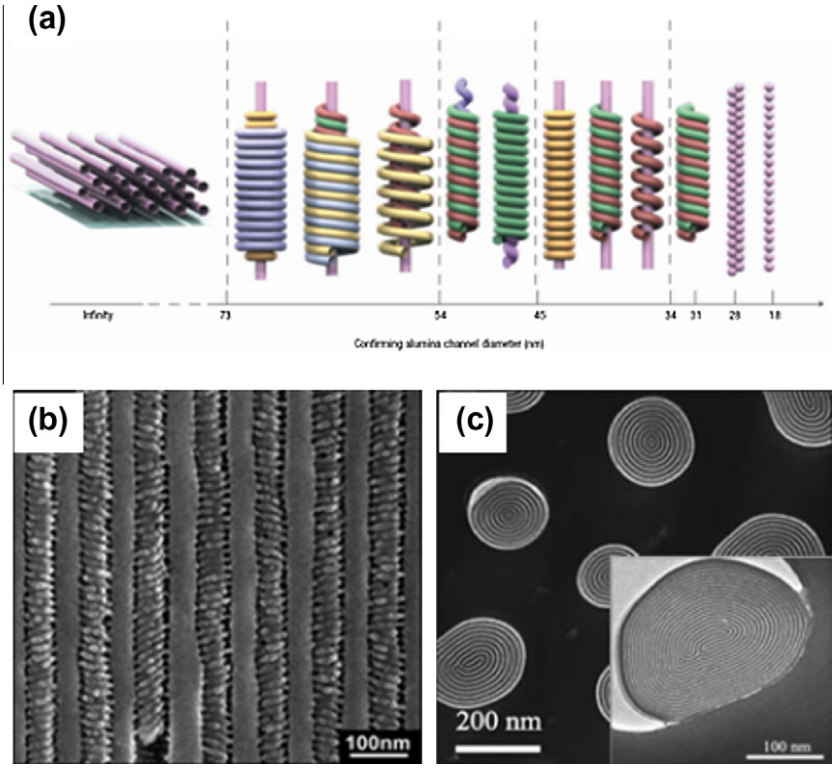

Fig. 25. (a) Summary of the experimentally observed confined evolution of mesostructures within AAO nanochannels of varying diameter. (b) Cross-sectional electron microscope images of the mesostructured silica nanomaterials prepared from the as-made AAO templates with pore diameters of 83 nm. (c) Self-assembly of the ordered silica–surfactant nanocomposites in the channels of the AAO membranes with approximately equal distribution of columnar and circular geometry as well as an AAO pore with a hybrid structure, inset higher magnification. Adapted with permission from Refs. [174,183,185].

upon exposure to the TiBALDH (Ti(IV) bis-ammonium-lactato-dihydroxide) precursor enabled the assembly of a conformal protamine/Ti–O-bearing coating on the nanochannel surfaces within the AAO template. Subsequent protamine pyrolysis produced co-continuous networks of pores and titania nanoparticles which was then used as electrode for dye-synthesized solar cells [189].

Wang et al. recently synthesized mesoporous carbon nanostructures such as carbon fibers with a core–shell structure and carbon ribbons with circular mesopores running parallel to the longitudinal axis of the ribbons within the pores of AAO membranes [171]. In this work, phenol–formaldehyde presol was used as precursor solution combined with varieties of cationic (CTAB) and amphiphilic surfactants such as F127 ($EO_{106}PO_{70}EO_{106}$) and P123. After the sol infiltrated the pores of AAO membrane and changed into a gel during aging process, the membrane was calcined at 600 °C for 3 h to produce carbonized mesoporous walls. Platschek et al. controlled the morphology of the synthesized 1-D mesoporous carbons by tuning the resol-to-surfactant ratio and by employing different types of surfactants. The same group employed titanium tetraisopropoxide (TTIP) as the titania source and P123 as the structure-directing agent to prepare titania nanotubes with mesoporous walls within AAO membranes and used the resulting structures as an electrode in a high rate rechargeable lithium battery [190]. The topic of sol–gel modifications of AAO and template synthesis using AAO template membranes has been extensively covered in a review paper by Bae et al. [191].

5.1.4. Electrochemical deposition of metals

Electrochemical deposition of metals provides a simple, inexpensive and approach for conformal surface modification of AAO. In comparison to chemical vapor deposition (CVD), atomic layer deposition (ALD) and thermal metal deposition, the electrode deposition is low cost and does not require expensive equipment and special conditions (e.g. high vacuum) [192]. The process requires a simple electrochemical cell and potentiostat or power supply which are common instruments available in every chemical lab. In most cases, a thin metal layer (commonly Au) is deposited on one face of the AAO membrane, to serve as working electrode for metal electrodeposition. Most studies employing electrochemical deposition focus on template synthesis of metal nanowires, nanorods, nanotubes and nanoparticles [30,34,84,193–195].

Segmented Ag–Au alloy nanowires prepared inside an AAO membrane via the electrodeposition technique are described by the Gösele group [195]. The Ag component could then be selectively removed using nitric acid. Lee et al. developed an alternating current (AC) technique for dielectrophoretic assembly of gold nanoparticles in AAO membrane [196]. By fabricating sacrificial and shell layers of metal nanowires in the pores of AAO membranes followed by electrodeposition, well-aligned nanochains were prepared after removing the sacrificial layers and subsequent annealing (Fig. 26) [197]. In another study, Lee et al. fabricated hollow multisegmented metallic nanotubes using combined electroless and electrochemical methods. In this work, Sn^{II} was first deposited on AAO pore walls by immersing the AAO membranes in $SnCl_2$ solution. Subsequently, Ag nanoparticles were immobilized on AAO pore walls by spontaneous reduction of Ag^{I} by Sn^{II} via a sensitization–preactivation process. These two steps constituted one single deposition cycle which was repeated several times. Ag nanoparticles immobilized on the surfaces of AAO membranes were isolated from each other without the formation of a continuous conduction path for current transport. Subsequent electrodeposition of Au led to the formation of Au nanotube in AAO channels with a bimetallic stacked

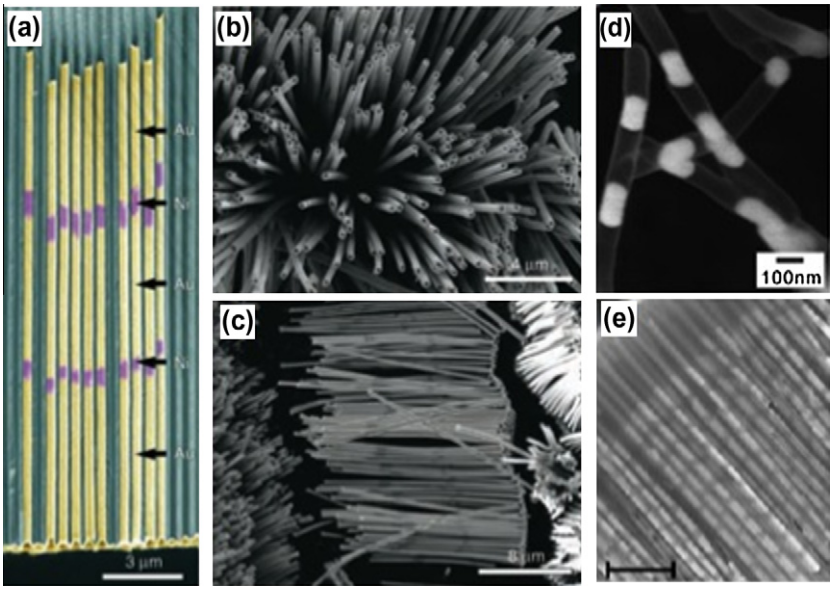

Fig. 26. SEM images of multisegmented metal nanotubes with a stacked configuration of metal inside AAO. (a) Cross-sectional SEM image of Au–Ni–Au–Ni–Au along the nanotube axis. The signals from Au and Ni are shown in yellow and purple, respectively. (b and c) SEM images of multisegmented metal nanotubes after removal of the AAO matrix with NaOH. (c) Clearly shows the stacked configuration of multisegmented metal nanotubes in which the segments with bright and dark image contrasts correspond to Au and Ni, respectively. (d) SEM image of Au nanochains embedded in AAO nanotubes by annealing of the coated nanowires. (e) SEM image of 10 gold segments along separated by Ag gap segments in AAO membrane. Adapted with permission from Refs. [197–199].

configuration [198]. Burdick et al. [199] demonstrated high-throughput fabrication of alternate multisegment deposition of gold with short gaps of Ag. Likewise, Hoang et al. demonstrated growth of multisegmented nanorods comprising Au and sacrificial Ag segments using an electrochemical wet etching approach [200]. Recent advancement in the synthesis of multisegmented nanorods and nanowires consists of metal, semiconductor and conducting polymer prepared by electrochemical deposition have been reviewed by Hurst et al. [192].

The Masuda group recently developed a method to fabricate layered 3D Au nanoparticle arrays inside an AAO matrix for use as a surface-enhanced Raman scattering (SERS) substrate. The electrodeposition of Au nanoparticles inside AAO channel was demonstrated by AC electrolysis of AAO at 25 V in an electrolyte containing chloroauric acid. The number of layers of the Au nanoparticle array was determined by the number of repetitions of this process, and the gap size between Au nanoparticles was determined by the duration of anodization after the electrochemical deposition of Au [201].

5.1.5. Electroless metal deposition

Electroless deposition is a chemical reduction process of metal cations (dissolved in aqueous solution) to an insoluble state [202]. These processes take place simultaneously at the targeted surface without the need for it to be conductive. Metal deposition on the surface is triggered by a catalyst (reducing agent) in solution [203]. Martin et al. first applied this approach to AAO membranes using gold deposition [84]. These gold nanotube/AAO composite membranes were successfully used for molecular separations showing size, charge and chemistry based selectivity [12,204]. By varying the electroless deposition time, hollow tubes can be obtained with short deposition time while solid nanorods can be obtained using longer deposition time [192]. Recently, Cheng et al. used the electroless deposition technique to fabricate SERS-active Au nanoparticles (AuNPs) arrays with tuneable particle gaps on AAO substrates. They reported that pH and the temperature are the main factor controlling the size, shape and aggregation of AuNP, as well as the inter-particle distance [205]. Catalytic and SERS properties of gold nanotubes inside AAO pores were demonstrated as results of clustered gold surface inside nanotubes as a result of gold nucleation process during chemical deposition [206,207].

Wang et al. [112] synthesized a range of metals nanotube arrays in AAO templates including Co, Ni and Cu arrays via electroless deposition on APTES-functionalized AAO membranes. The inner diameter of nanotubes can be tailored by adjusting the deposition times whereas the length of the nanotubes is determined by the thickness of the AAO template (Fig. 27). Other studies conducted by Azizi et al. saw the fabrication of end-closed NiCoFe-B nanotube arrays by immersion of the Pd sensitized AAO membrane into the electrolyte bath containing $NiSO_4{\cdot}6H_2O$, $CoSO_4{\cdot}7H_2O$, $FeSO_4{\cdot}7H_2O$, lactic acid and dimethylamine borane. Zhou et al. found that a high yield of amorphous Ni–W–P nanoparticles with uniform size could be fabricated by electroless deposition inside AAO. The resulting Ni–W–P nanoparticles possessed a low coercivity at room temperature [208]. Zhang et al. synthesized Ag nanotubes with lengths over 10 μm inside AAO membranes [209]. Likewise, Ag nanoparticles with uniform size and smooth surface were deposited inside AAO using this technique [210,211].

5.2. Gas-phase techniques

To improve structural, physical and chemical properties of AAO, gas-phase techniques including thermal vapor deposition, sputtering, pulsed laser deposition, chemical vapor deposition and plasma polymerization are employed to deposit a wide range of materials from metals, metal oxides, complex oxides, ceramics, nitrides to carbon nanotubes [67]. These methods offer many opportunities to improve the properties of AAO for specific applications from tuning the size of pore structures, chemical conversion of alumina and for the replication of pore structures into nanowires and nanotubes.

5.2.1. Metal coating using thermal vapor deposition

Metal modifications of AAO using thermal vapor deposition technique have been explored using metals including gold, silver, platinum, palladium, titanium, nickel, etc. The aim of these modifications was typically to improve conductivity and chemical stability of the AAO material but also to introduce some new properties (catalytic, electrochemical, magnetic, optical and transport) [67]. AAO coated with metal such as Au, Pd, Pt, Ti/TiO_2 has reportedly improved catalytic properties, whereas magnetic

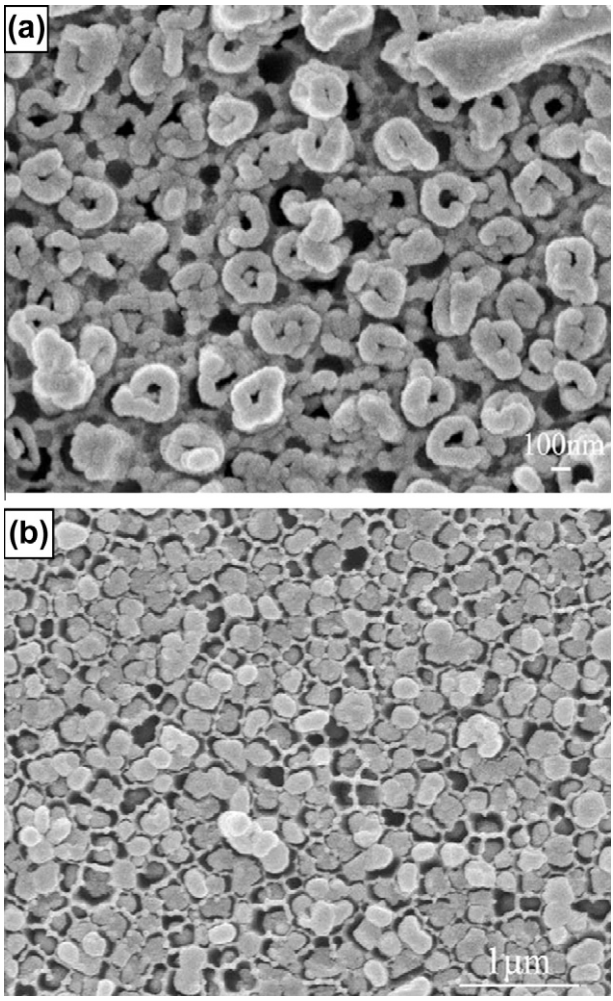

Fig. 27. Top view SEM images of (a) Co nanotube and (b) Co nanowire arrays prepared via electroless deposition with different plating time of (a) 10 min and (b) 30 min. Adapted with permission from Ref. [112].

properties have been introduced by coating with Ni or Co. Metal coating also served as the basis for further chemical modification of AAO to help in binding various chemical and biological species in particular for optical sensing and molecular separation applications. Both thermal and sputtering techniques were used for AAO modifications based on the deposition of thin metal films on the top of AAO surface. The main disadvantage of these techniques is that only the top part of the nanopores can be modified and deposition of internal pore surface is limited.

Gold-coated AAO membranes were also used as a base layer to assemble LbL of α,ω-diorganophosphonate/zirconium (IV). This base layer was critical to achieving a conformal multilayers rather than multilayers suspended over the pores [212]. Platinum-coated AAO membranes were prepared by Toh et al. for selective transport and separations of charged proteins. In this work, both sides of the AAO membranes were sputtered with Pt and electrical potential was applied to create a high electric field during separation experiments of charged proteins. In addition, further size selective separation was achieved by increasing the thickness of sputtered Pt layer [213,214]. Hexagonal arrangements of AAO membranes were exploited by several groups for coating with silver to prepare SERS

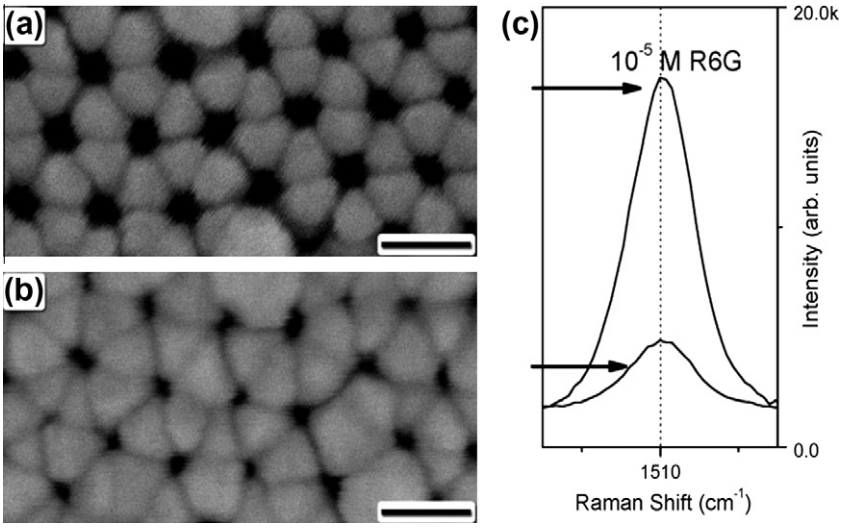

Fig. 28. SEM images obtained from the Ag-coated AAO membranes formed using different Ag sputtering times of (a) 15 and (b) 20 min. The scale bar is 100 nm. (c) SERS spectra of Rhodamine 6G-adsorbed Ag-coated PAA membranes corresponding to those in (a) and (b), demonstrating the intensity variation of the SERS signal at 1510 cm^{-1}. Adapted with permission from Ref. [215].

substrates [215,216]. An Ag layer deposited by using a direct-current magnetron sputtering system was reported to exhibit high Raman signal due to an abundance of silver nanoparticle hot spots (Fig. 28) [215]. The design of a silver nanocap array with uniform and highly reproducible SERS-active properties may open new opportunities for the fabrication of robust, exceptionally sensitive,

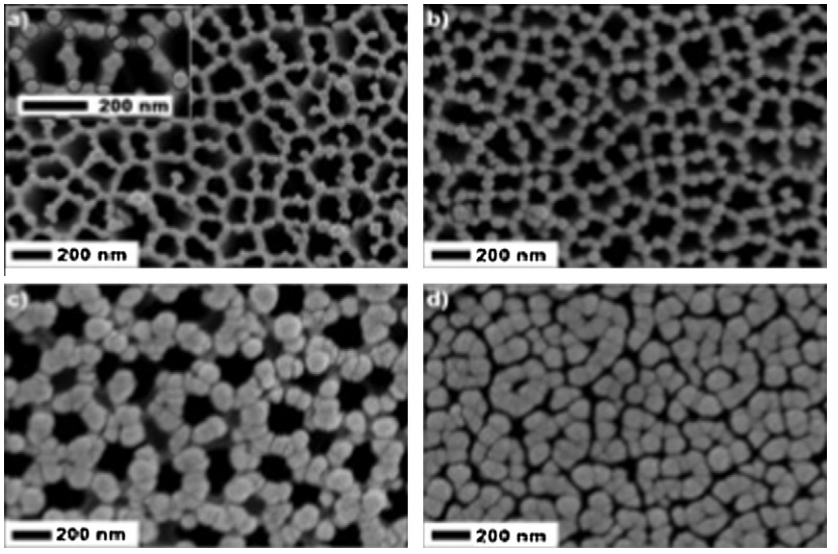

Fig. 29. SEM images of Pt deposited on AAO membranes by pulsed laser deposition. The equivalent thickness, *t*, of the deposit is (a) 40 nm; (b) 68 nm; (c) 160 nm and (d) 320 nm. The Ek of the species impinging on the AAO membrane was kept constant at 4 eV at^{-1}. On the thinnest deposit (a), the inset shows that Pt nanoaggregates are preferentially located at the neck of the pore walls of the AAO membrane. Adapted with permission from Ref. [217].

cost-effective, large-area SERS-based sensors. In an alternative approach, Periera et al. used pulsed laser deposition (PLD) technique to modify AAO channels with a thick film of pure metal i.e. Au, Pt or bimetal of (Pt–Ru) (Fig. 29). This was achieved by optimizing the kinetic energy of the deposited metal in contact with the AAO substrate [217]. Wang et al. combined physical vapor deposition, gating ion milling and thermal annealing techniques for fabrication of metal nanodot arrays on AAO [218].

5.2.2. Plasma polymer deposition

Plasma polymerization is an engineering friendly surface modification technique producing stable and cross-linked films of controlled thickness and with the chemical functionality being determined by the choice of the monomer [219]. This technique is particularly attractive due to the ability to generate reactive and biocompatible polymer surfaces with a range of functional groups including amine, carboxyl, hydroxyl, epoxy and aldehyde groups that can be used for further modification.

The first report of plasma treatment on AAO membranes was by Brevnov et al. [220], who prepared Janus-type membranes with a hydrophilic and hydrophobic side. The hydrophobic side of the membranes with a water contact angle (WCA) of 150° was prepared by deposition of a 120 nm fluorocarbon polymer layer by inductively coupled plasma polymerization of C_4F_8. The plasma polymer film was stable for a month as indicated by a stable WCA. Nevertheless, the pore diameter of these functionalized regions decreased significantly from 160 to 80 nm. The other side of the membrane was left unmodified and showed a WCA of <20°.

In order to improve both structural and surface properties of AAO membranes, Losic et al. successfully implemented surface modification of AAO by plasma polymerization of *n*-heptylamine (Fig. 30) [221]. The diameter of AAO membrane pores could be precisely tuned from 20 nm to <5 nm by adjusting the duration of the plasma treatment (Fig. 30b).

5.2.3. Atomic layer deposition (ALD)

A key feature of the ALD technique pioneered by Suntola and Antson in the 1970s is its ability to prepare highly conformal films on non-line-of-sight surfaces. ALD growth rates of films are typically less than one monolayer per deposition cycle depending on the temperature, substrate and deposition

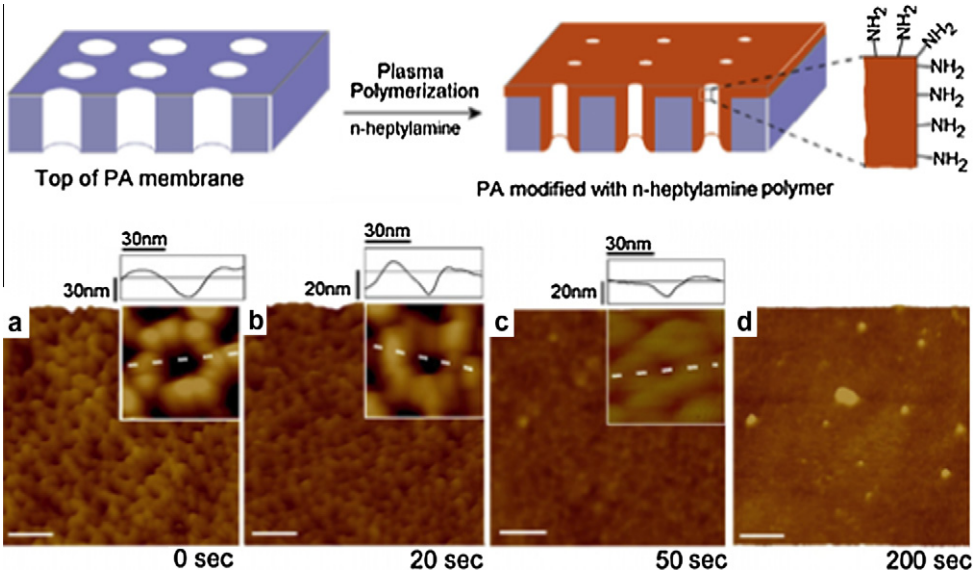

Fig. 30. Top: Schematic diagram of plasma polymerization of *n*-heptylamine on a AAO membrane. Bottom: AFM images (contact mode) of the top surface of bare AAO membranes; (a) and AAO membranes modified with *n*-heptylamine plasma polymer using deposition times of (b) 20 s, (c) 50 s and (d) 200 s. The scale bars are 100 nm. The insets reproduce the structure of single pores. Adapted with permission from Ref. [221].

condition employed. ALD permits the deposition of a broad range of materials including oxides, nitrides, sulfides and metals with coating that shows high mechanical, chemical and thermal stability and attractive optical properties. Therefore it is not surprising that this technique has been exploited for surface modification of AAO [222].

Pioneering work on ALD modification of AAO demonstrated that ALD of silica, titania and alumina can be used to controllably reduce the pore dimensions of AAO, improving its catalytic, optical and transport properties [223–226]. Velleman et al. [87] deposited silica (SiO_2) on AAO by the ALD method to reduce pore diameter followed by surface modification with specific silane chemistry to achieve chemical selectivity in molecular transport. Different ALD strategies have been applied to coat AAO nanopores using single metal oxide (Fe_2O_3, ZnO, TiO), mixtures of metal oxides ($SiO_2/Fe_2O_3/SiO_2$), nitrides (WNx), composite materials ($TiN–Al_2O_3–TiN$) and carbon nanotubes (CNTs) using conventional gase or even liquid phase ALD achieving a range of nanostructured materials with high surface area and properties suitable for photoelectrodes, photonic crystals, photovoltaic devices and nanocapacitors [227–231].

Bachmann et al. [232] have fabricated ordered magnetic Fe_2O_3 nanotube arrays by means of ALD using AAO membranes as templates. More recently, Pitzschel et al. [228] used regulated AAO membrane prepared by a combination of HA and MA anodization techniques for fabrication of layered nanotubes composed of $SiO_2/Fe_2O_3/SiO_2$ using ferrocene and APTES as precursors for ALD. Similarly, Banerjee et al. prepared alternate layers of metal–insulator–metal (MIM) by depositing $TiN–Al_2O_3–TiN$ multilayers inside AAO nanopores yielding nanotubular capacitors with equivalent planar capacitance up to 100 $\mu F\ cm^{-2}$ [227]. In a different strategy, dye-sensitized solar cells (DSSCs) made of ZnO-coated AAO membranes have been prepared by alternate exposure of the membrane to diethyl zinc and water vapor at a temperature of 200 °C, annealing at 400 °C in air for 30 min to increase crystallinity, followed by selective ALD of Al doped ZnO (AZO) on one side of the membrane (Fig. 31) [233]. The Martison group grew indium tin oxide (ITO) inside AAO via ALD to fabricate semiconducting DSSC [234]. The ALD technique also has been applied to produce Ta_2O_5 and TiO_2 thin films on the pore walls of AAO templates [174,230,235].

A comprehensive review on ALD and application of this technique using various metal and metal oxides can be found in Refs. [222,236,237].

5.2.4. Chemical vapor deposition (CVD)

Chemical vapor deposition (CVD) is a chemical process involving the dissociation of gaseous molecules or activation of chemical reactions by heat, light or plasma to form stable and conformal films

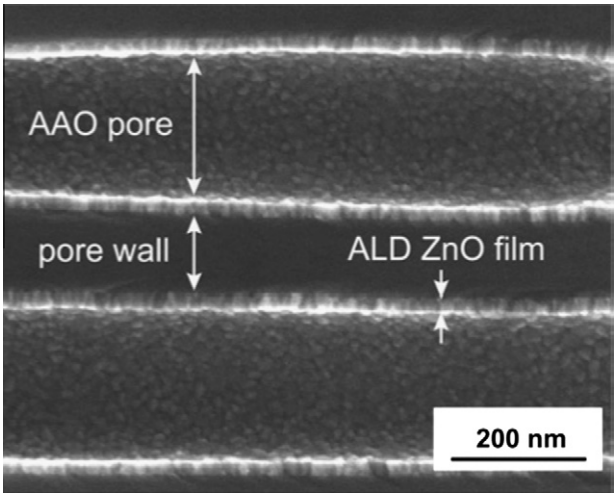

Fig. 31. Cross-sectional SEM image of commercial AAO membrane pores coated with 20 nm of ZnO by ALD. Adapted with permission from Ref. [233].

on a substrate [238]. CVD offers excellent control over coating thickness and coverage, and sustains fast growth rates as compared to other deposition processes. The most popular method for AAO modification is CVD growth of carbon layers and carbon nanotubes (CNTs) inside pores [52,59, 239–241]. Several excellent reviews on CNT preparation via CVD in AAO template are available [60,145,242,243]. Vertically aligned CNT arrays of controllable height were achieved combining CVD, ion milling and chemical etching. In this architecture, carbon layer were grown within the pore using CVD via pyrolysis of acetylene gas at elevated high temperature (600 °C) for 1 h [241]. The CNT arrays were obtained by partially removing the top surface of AAO template by ion milling, followed by chemical etching. Poop et al. used propylene and argon as carrier gas to demonstrate non-catalytic CVD of carbon in an AAO template with the gas flow in the direction of the pore axes [240]. The use of hydrocarbon precursors without of catalyst to fabricate catalyst-free multi-walled CNT inside AAO template also has been demonstrated recently [239,244]. The AAO surface can act as catalyst showing advantages of AAO for catalyst-free synthesis of CNT which are expected to be more biocompatible as the presence of catalyst is usually linked to toxicity of CNTs [244].

Ansari et al. [245] used plasma-enhanced CVD (PECVD) to modify AAO surfaces with metal oxides. In this approach, hydrated $SnCl_4{\cdot}xH_2O$ was used as a precursor and pure oxygen as reactant gas. Since the vapor is carried by plasma, it eliminates the vapor condensation issues on the surface of the substrate. Low temperature deposition process (<400 °C) was possible. Crystallinity of thin films SnO_2 increased with increasing plasma power. A similar approach was used to grow amorphous nanocrystalline silicon films on AAO substrate [246].

6. Emerging applications

The unique properties of AAO membranes such as the highly ordered pore structures, uniform pore size, controllable pore geometry, surface chemistry, and high surface area are main features which made this material an attractive platform for a number of applications. Furthermore, highly ordered pore arrays of AAO have been extensively used as a template in fabrication of various nanostructured materials, providing a more cost-effective alternative to lithographic techniques and eliminating the need for sophisticated, expensive facilities as well as time-consuming processes. A prime example is the fabrication of ordered metal nanowires in AAO templates that can be applied to lithium ion batteries, energy storage, solar cells, recording media, resistors, transistors, switches, molecular junctions and nanoreactors. Other key applications include templated nanostructured conducting polymers and carbon nanotubes with interesting electrical, optical, and photoelectric properties.

A variety of chemo- and biosensors have been developed using AAO as transducers. Another important area is the use of AAO as catalytic membranes. Due to the material's high surface area, a large amount of enzyme or synthetic catalyst can be immobilized within an AAO membrane, affording high reaction rates. Moreover, controlling surface chemistry of AAO membrane allows altering the charge, functionality, permeability, reactivity and selectivity of the material. A range of sophisticated molecular separation tasks have been explored on AAO engineered in terms of surface chemistry and pore size including the separation of enantiomers, multivalent ions, amino acids, proteins and nucleic acids. As another example, suspended lipid bilayers on AAO nanopores and lipid nanotube arrays assembled inside AAO pores provide an ideal model supported membrane for membrane-associated proteins studies. Furthermore, AAO-based materials have been exploited as scaffolds for tissue engineering making use of the controlled cell-material surface interactions. Finally, recent research suggests that the material holds considerable potential as a drug or gene delivery carrier, enabling controlled release of therapeutic molecules.

6.1. Template synthesis

Template synthesis has been shown to be a popular approach for fabricating nanostructured materials. The advantage of this approach is that it does not require sophisticated instrumentation and allows the fabrication of uniform sizes of nanomaterials of broad origin with high yield [191,192,204,247]. The advantages of using AAO as a template are: (1) pore structures with controlled

structural properties (pore diameter, modulated pore structure and lengths) can be easily fabricated, (2) uniformity of pore diameters with high pore density (10^{11} cm^{-2}), (3) cylindrical pore geometry with high aspect ratio and (4) easy dissolution of AAO template with acidic or alkaline solution without affecting the fabricated nanostructures confined inside the nanopores. Alternatively, the nanostructures can remain inside the pores of AAO template and used as a composite material or support for various applications. The high thermal and mechanical stability of AAO membrane allows them to be used as templates in relatively high temperature gas phase synthesis via ALD or CVD.

Since it was first introduced by Martin [84], this method has been employed to prepare variety of one dimensional nanostructured materials made from metals (Ag, Au, Bi, Cu, Co, Fe, In, Ni, Pt, Pd, Pb, Sn, Sb, Zn) [84,248–250], metal oxides ($Co_3O_4Fe_2O_3$, MnO_2, SnO_2, $BaTiO_3$, Bi_2O_3, $PbTiO_3$, SiO_2, SnO_2, V_2O_5, ZrO_2) [251–253], alloys (Co–P, Fe–Pd, Ni–P, Cd–Te–Au, Bi_2Te_3) [254,255], semiconductors (CdSe, GaMnAs, TiO_2, WO_3, ZnO) [193,249,256,257], polymers [(polypyrrole, PANI, polystyrene, poly(sodium 4-styrene sulfonate (PSS), PEI, poly(3-methylthiophene) (P3MT), poly(N-methylpyrrole), polytetrafluoroethylene (PTFE), poly(methyl methacrylates) (PMMA) [258], poly(vinylidene fluoride) (PVDF), divinyltriphenylamine (DVTPA) [256], polyvinyl alcohol (PVA), polyethylene oxide (PEO)], nylon, carbon, composites, silica and biological molecules (protein, DNA). A range of nanostructure have been fabricated including: nanofibers [259], nanowires [260], nanopillars [261–263], nanorods [115], nanotubes [264,265], nanochannels [266], nanocones [77], nanorings, nanobelts and nanodots [251,267,268]. Different approaches have been applied towards the synthesis of those nanostructures including chemical, electroless and electrochemical deposition, sol–gel techniques, solution casting, chemical polymerization, thermal evaporation, chemical vapor deposition and others as discussed in earlier sections (Fig. 32). The templating methods based on AAO substrate have been the subjects of several excellent reviews, which the interested reader is referred to [67,191,192,247,269–271].

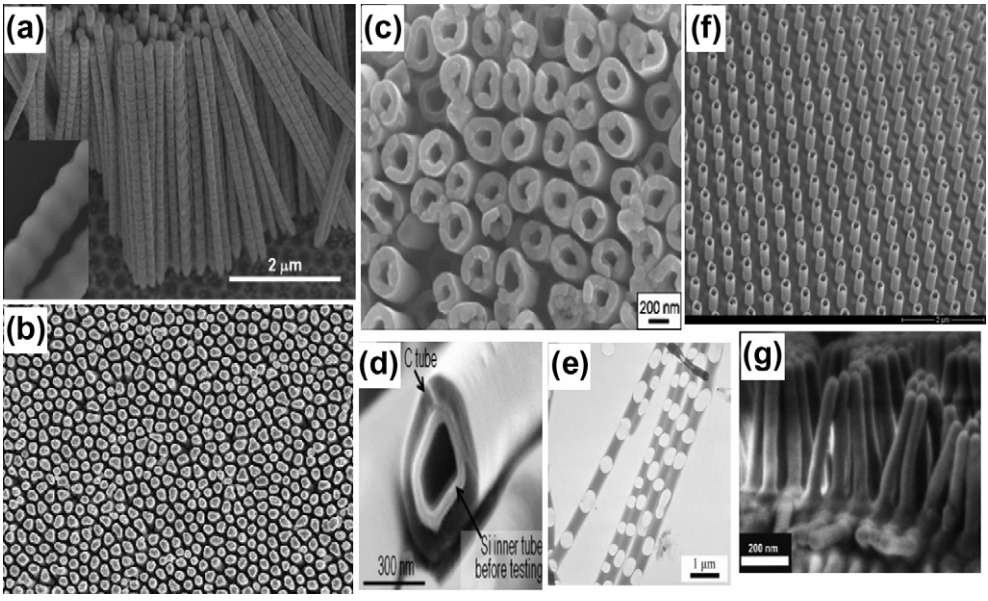

Fig. 32. Template synthesis using AAO membranes. (a) SEM image of corrugated gold nanotubes prepared by electrodeposition of gold on AAO template, inset: larger magnification. Adapted with permission from Ref. [250]. (b) Top-view SEM image of Cu nanotubes after AAO removal. Adapted with permission from Ref. [245]. (c) Top-view of Fe–Pd nanotube array obtained after removing the AAO template. Adapted with permission from Ref. [254]. (d) SEM image of composite Si-in C nanotube after dissolving the AAO template. Adapted with permission from Ref. [353]. (e) TEM image of PMMA nanorods with void spaces after template dissolution. Adapted with permission from Ref. [258]. (f) SEM of ZnO nanotube membrane showing the perfect alignment of the nanotubes. Adapted with permission from Ref. [257]. (g) cross-sectional SEM view of thermally cured divinyltriphenylamine nanorod arrays after removal of the AAO template. Adapted with permission from Ref. [256].

6.2. Sensing applications

6.2.1. Optical chemo- and biosensors

The main advantages of using nanoporous AAO as a platform for biosensors are their chemical inertness and the large surface area [243]. Furthermore, moderate transparency of AAO membranes in the UV and IR regions has allowed direct detection by of absorbances in transmission mode. Absorbance [97], reflection [272–275], fluorescence [99], chemi-luminescence [276], surface plasmon resonance [272] and Raman scattering [277] have been used as transducing mechanisms (Table 1). Various biomolecules including proteins (e.g. hemoglobin, myoglobin, cytochrome), enzymes (e.g. cholesterol oxidase, peroxidase), antibodies, DNA and whole cells have been chosen to develop optical biosensors on nanoporous AAO.

Vlassiouk et al. [97] covalently attached 5′-amino terminated DNA oligonucleotides inside nanopores via glutaraldehyde crosslinking on AAO amino-functional surfaces. Hybridization efficiencies of up to 70% of complementary 21-mer oligonucleotides were determined from UV spectroscopy. Reproducibility studies showed that the sensor platform could be re-used several times and that the complementary DNA could be washed off either by heating or denaturing solutions without affecting the surface-immobilized DNA probes. It is generally acknowledged that the performance of biosensors can be improved by increasing the available surface area of a substrate designed to bind to a biomolecular analyte. For example, Takmakov et al. [99] prepared thin AAO films on flat glass surfaces and bound biotin to the AAO pores via aminosilane-succinimide chemistry. The binding of tagged streptavidin molecules was then monitored using fluorescence microscopy and fluorescence intensity was reported to be as much as seven times increased in comparison to the flat glass surface. The high biotin coverage of up to 2×10^{14} molecules/cm^2 (geometric surface area) was maintained for more than a week in PBS buffer or DI water.

In another important approach, the surface of nanoporous AAO was decorated with FITC-modified polypyrrole for generating a highly sensitive and selective fluorescence ratiometric sensor for 2,3,3′-trichlorobiphenyl (PCBs). This newly developed sensor showed effective sensing to PCBs with a lower detection limit of 1 ppb and highly selectivity demonstrating a new route for developing simple, low cost, reliable and reproducible PCB trace detection [278]. Alternatively, in more simple approach developed by Wang et al., phenyl isothiocyanate was directly immobilized onto AAO membrane achieving a fluorescent membrane for rapid detection of trace PCB with a lower detection limit of 1 μg/L [279].

Oliveira et al. [164] immobilized trypsin or peroxidase under retention of their catalytic activity on PEI or PANI functionalized AAO matrices. They reported that AAO–PEI–trypsin covalently coupled to the surface showed almost three times higher activity as compared to those samples where enzymes were attached by adsorption on a membrane without PEI functionalities. In addition, AAO–PANI–HRP could retain 74% of its initial activity after five batch cycles of substrate turnover.

Photoluminescence (PL) biosensors have also been implemented on AAO substrates. Jia et al. demonstrated that PL intensity of the embedded dye (morin) inside AAO nanopores can be greatly enhanced by the introduction of proteins such as trypsin or human serum albumen [280,281]. Feng et al. [276] introduced graded-band-gap quantum dot modified AAO that could enhance the detection of DNA hybridization. AAO surfaces were first covered with positively charged 3-aminopropyl dimethylethoxysilane followed by assembly of three layers of negatively and positively charged dendrimers via LbL. Afterwards, positively charged dendrimers and negatively charged QDs were alternatingly deposited. Finally, probe DNA was immobilized via carbodiimide chemistry. Changes of PL emission spectra were induced by hybridization of Cy5-labeled complementary 15-mer DNA due to fluorescence resonance energy transfer between the QDs and Cy5.

In another approach, spots of ordered AAO were fabricated via photolithography for DNA-microarray studies. Each spots on the microarray was functionalized with hydrophilic poly-L-lysine (PLL) while the surface covered with photoresist surrounding the AAO spots was hydrophobic. The PLL-coated microarray spots bound high amounts of Cy3 labeled cDNA whilst the surrounding surface did not adsorb the DNA [64]. Tanvir et al. [102] used two different methods to immobilize glucose-6-phosphate dehydrogenase (G6PD) or human cytochrome from liver (CYP2E1) using silane-glutaraldehyde functionalized and sulfhydryl-reactive AAO membranes, respectively, under retention of the

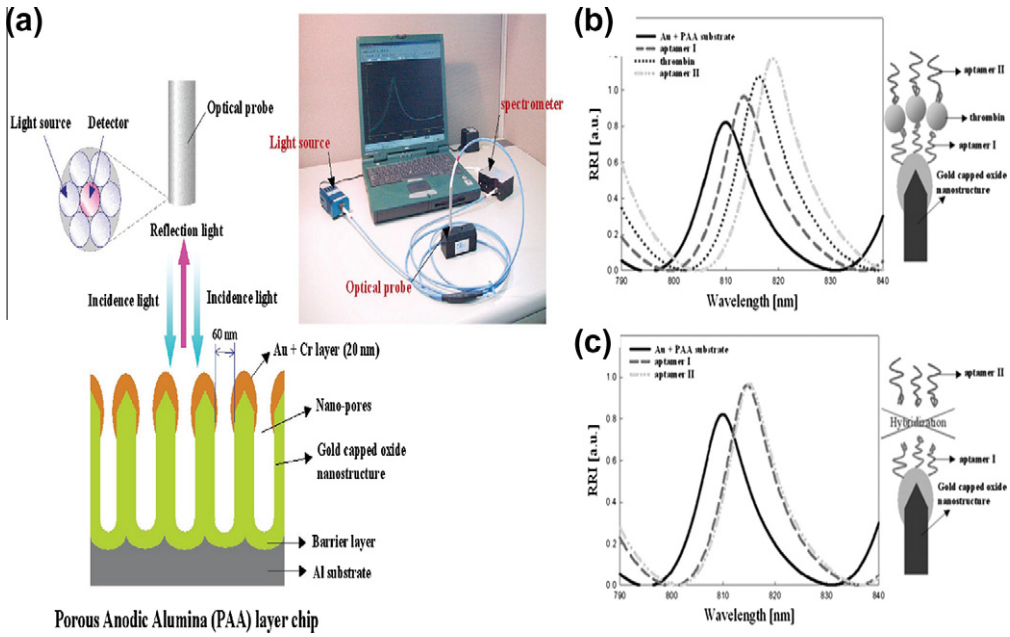

Fig. 33. Sandwich-type binding assay for thrombin using aptamer-functionalized Au-capped AAO pores. (a) Schematic of experimental setup and construction of LSPR and interferometry based label-free optical biosensor with AAO chip. (b) Interferometric and LSPR characteristics of bare AAO layer chip (solid line), 10 μM aptamer I immobilized on Au-capped AAO surface (dashed line), binding reaction between 10 μM aptamer I and 1 μM thrombin on the chip surface (dotted line), and binding reaction between the aptamer I–thrombin complex and aptamer II (dashed double dotted line). (c) Interferometric and LSPR characteristics of bare AAO layer chip (solid line), 10 μM aptamer I immobilized on chip surface (dashed line), and binding reaction between 10 μM aptamer I and 10 μM aptamer II (dashed double dotted line). Adapted with permission from Refs. [272,285].

enzymes' activity. These two individually modified membranes were stacked together in a microfluidic device. The product of substrate transformation by G6PD became the cofactor for CYP2E1 in the CYP2E1-functionalized membrane, activating that enzyme.

Optical interference-based biosensing using nanoporous AAO has been demonstrated by several groups [273–275]. White light reflection from AAO films on Al substrates produces interferences, which are characteristic of the thickness and refractive index of the AAO films. Pan and Rothberg [274] created thin films of AAO membranes with a thickness of approximately 6 μm which were functionalized with biotin and streptavidin. Then, biotin-modified single stranded DNA was applied to the sample and red shifts of reflectance spectra were observed when complementary DNA was hybridized to the surface. Sailor's group [273] described an AAO based interferometric immunosensor that specifically bound immunoglobulin G (IgG) antibodies on protein A adsorbed to the AAO pores. More recently, we improved sensitivity of this type of biosensor by depositing a thin Pt layer on AAO which produced high fidelity interferometric reflectance spectra in both air and water [275]. As for a proof of concept, biosensing of two distinct immunoglobulin antibodies was demonstrated. The influence of pore dimensions on interference properties of AAO was evaluated by Kumeria et al. showing optimal pore diameters and length to achieve highest sensitivity on interference signal [282]. Reflective interferometric gas sensing for detection of hydrogen sulfide was demonstrated using AAO nanopores coated with gold films [283]. In addition to molecular detection, the interference spectroscopy using AAO as platform was further used by Kumeria et al. to develop biosensing microchip for capturing and detecting circulating tumor cells [284].

In another approach, Kim et al. [285] deposited an Au layer on top of AAO nanopores to produce localized surface plasmon resonance (LSPR) effects. Immobilization of thiolated probe DNA and hybridization of complementary target DNA were then detected by means of LSPR and interferometric

measurements. This biosensor afforded detection of hybridization of target DNA and aptamer–protein interactions down to 10 pM and 1 nM, respectively (Fig. 33) [272,285].

In a view of benefits and limitation of porous AAO substrate as biosensor for protein adsorption, Lazzara et al. studied the adsorption–desorption kinetics of proteins in porous AAO in comparison to flat surface. By means of time-resolved optical waveguide spectroscopy, they concluded that the adsorption of protein is mainly governed by the rate of protein entrance into the pores whilst the desorption from the pores strongly depends on the rate constant of adsorption (k_{ad}) since the resident time of the proteins is governed by the rebinding probability [286].

AAO-based chemosensors respond to the presence of a specific analyte in a variety of ways. For example, Ko et al. used SERS of AAO membranes decorated with Au nanoparticles as a tool for label-free detection of explosives [287]. In their work, the surface of AAO membranes was modified with polyethlenimine (PEI) to prevent pore blocking and attachment of Au nanoparticles on the outer surface of the membranes. The array of nanoparticle-decorated pores showed about five orders greater enhancement of molecule detection than a conventional planar nanoparticle array. Detection of 2,4-dinitrotoluene was reported down to 0.1–0.05 ppt and total amount of the detected material on the substrate was 5–10 zg [287]. The concept had been further extended to decorate AAO with mixed nanoclusters composed of Au nanorods and other nanoparticles (Fig. 34). Using this approach, peroxide-based liquid explosives such as hexamethylene triperoxide diamine (HMTD) were detected below 2 pg, which is about three orders of magnitude lower than the current detection limit [288]. Instead of Au nanoparticles, Ji et al. employed Ag nanoparticle as SERS-active material to fabricate 3D ordered Ag nanostructures on the inner walls of the pores in AAO using 4-mercaptopyridine as probe molecule. The fabricated substrate showed excellent SERS enhancement which was attributed to the optical waveguide effect of vertical alumina-pore arrays [289].

Wada et al. used surface-assisted laser desorption/ionization (SALDI) to detect biomolecules on AAO surfaces [290]. Since surface electroconductivity is one of the requirements for this technique, the AAO surfaces were coated with Au or Pt while the underlying AAO surfaces functioned as a thermal insulator. This approach allowed ionization of small proteins such as trypsinogen at low femtomoles concentrations.

6.2.2. Electrochemical biosensors

Biomolecules such as enzymes can be covalently or non-convalently immobilized onto electrode surfaces including metal-coated AAO membranes to build electrochemical biosensors. Glucose oxidase

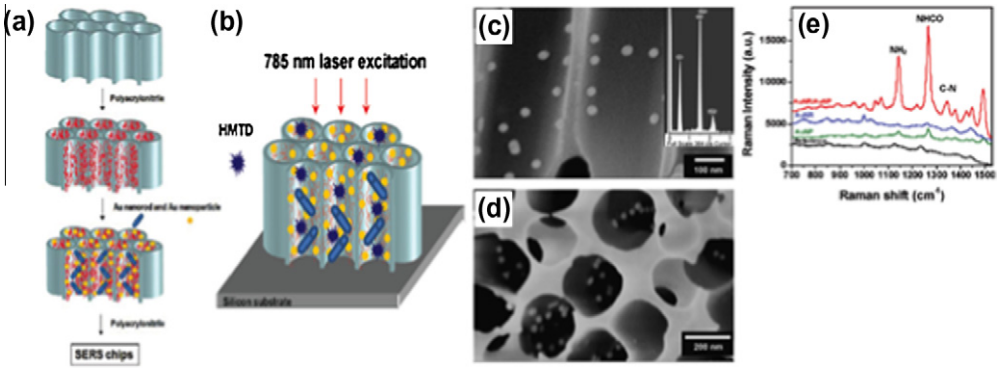

Fig. 34. (a) Schematic diagram showing fabrication of AAO substrate with gold nanoparticles and nanorods. (b) Schematic representative of Raman spectroscopy measurement of hexamethylene triperoxide (HMTD) on AAO substrate with mixed gold nanorods and gold nanoparticles. Adapted with permission from reference [289]. (c) Cross-sectional and (d) angle-view SEM images of AAO membranes decorated with Au nanoparticles. The inset in (c) shows the energy-dispersive X-ray spectrum, which indicates the presence of Au inside the pore walls. (e) Comparison of Raman spectra (SERS) of HMTD measured on AAO substrates with mixed gold nanorods and gold nanoparticles, gold nanorods, gold nanoparticles, and AAO without HMTD. (Black line corresponds to reference spectrum.) Substrates for different concentrations and characteristic signature peaks are labeled in different colors. Adapted with permission from Ref. [287,288].

(GOx) and horseradish peroxidise (HRP) enzymes are the predominant model systems selected to convert a redox reaction into an electrical signal using an electrode transducer [245,291]. This is due to specific binding and catalytic activities of both enzymes. Additionally, enzymes such as urease [100], cholesterol oxidase [292] and choline oxidase (ChOx) [293] have been used in AAO based biosensors. Other biorecognition elements such as antibodies [257], nucleic acids [87,258], cells and micro-organisms [259] have also been successfully immobilized on metal-coated AAO membranes to monitor binding events in bioelectrochemical reactions.

To improve the analytical performance of glucose biosensors by electrocatalytic reduction of enzymatically liberated H_2O_2, Xian et al. [294] fabricated nanoelectrode arrays of Prussian Blue (PB) via electrochemical deposition inside AAO pores. Prior to PB deposition, a thin layer of Au was deposited by vacuum evaporation onto one side of the AAO membrane. GOx was then successfully crosslinked on PB arrays. The PB acted as a mediator and the resulting nanoelectrode arrays showed linear current vs. concentration curves over three orders of magnitude of glucose concentrations with a lower detection limit of 1.0 μM. A common problem of enzyme biosensors is loss of enzyme activity due to the leaching of adsorbed enzyme. To overcome this problem, coating layers have been used as stabilizing agents. For example, Drader et al. [295] improved sensitivity and enzymatic stability of an AAO-based GOx biosensor using a protective chitosan layer. The biosensor showed linear response over a wide concentration range up to 20 mM of glucose. Increasing pore diameter from 30 to 200 nm and reducing thickness from 150 μm to 60 μm improved the response time.

In turn, Ansari et al. [245] focused on the detection of glucose using nanostructured SnO_2 films on AAO surfaces. A thin layer film of SnO_2 on AAO surfaces was deposited via PECVD. GOx was immobilized on the SnO_2 modified surface via physisorption and glucose detection was achieved from 10 to 360 mg/dL. Shimomura et al. [293] developed an amperometric biosensor for the detection of H_2O_2, which is the co-product of choline oxidation. In this work, hybrid silica nanochannels confined inside AAO channels were prepared by sol–gel chemistry. ChOx was conjugated to the silica-coated AAO nanopores for 48 h at 4 °C. This sensor had a detection range of 5.0–800 μM with a response time of 2 min. It maintained 85% of the initial response for up to 80 d of storage. González et al. [296] covalently immobilized anti-HRP on AAO surfaces via carbodiimide chemistry which had been previously modified by APTES and reacted with succinic anhydride. The label-free biosensor was able to detect HRP at concentrations down to 10 nM. Immobilization of cytochrome P450 side chain cleavage (P450scc) enzymes for detection of LDL-cholesterol on AAO membrane by CV was demonstrated by Stura et al. with a sensitivity of 1.1 mg/mL [292]. The sensor could be used for up to 30 d at 4 °C. Maghsoodi et al. [297] fabricated an amperometric glucose biosensor based on an enzyme electrode on CNT grown inside AAO membrane using catalytic CVD of methane using Fe/MgO as catalyst. GOx immobilized on the CNT layer showed a linear amperometric response to glucose concentration without a mediator with a detection limit and sensitivity of 0.1 μM and 635 $\mu A\ mM^{-1}\ cm^{-2}$, respectively.

Electrochemical impedance spectroscopy (EIS) is an ultrasensitive technique to monitor changes in electrical properties occurring from biorecognition events at the surface of modified electrodes. AAO-bilayer membrane biosensors have been prepared by Steinem et al. for EIS of ion channel activity. Their approach is based on distinct surface chemistries on the top and bottom parts of the membrane, preventing the fusion of unilamellar vesicles within the pores and facilitating fusion on the top surface of the AAO to form pore-suspended bilayers. A significant increase in resistance up to $R_m = 8 \times 10^7\ \Omega$ was observed, indicating insulating bilayer formation. This value was sufficient to monitor ion channel activity of membrane protein F (OmpF) from *Escherichia coli* [126].

Takmakov et al. [298] immobilized single-stranded DNA recognition elements on APTES-glutaraldehyde functionalized AAO surfaces. Immobilization of DNA inside AAO pores led to a significant decrease in resistance measured by EIS as compared to unmodified surfaces Wang et al. [299] detected DNA hybridization using a dynamic polymerase-extending (PE) method by means of combined CV and EIS on AAO membranes (Fig. 35). The sensitivity of this technique was reported to be 0.5 nM for detecting complementary target DNA.

In the tethered lipid membrane based biosensor developed by Largueze et al. [107] the deposited gold layer on the bottom part of an AAO membrane served as electrode layer. Ubiquinone, a redox lipophilic mediator embedded within the acyl chains of the lipid bilayer membrane, was used to

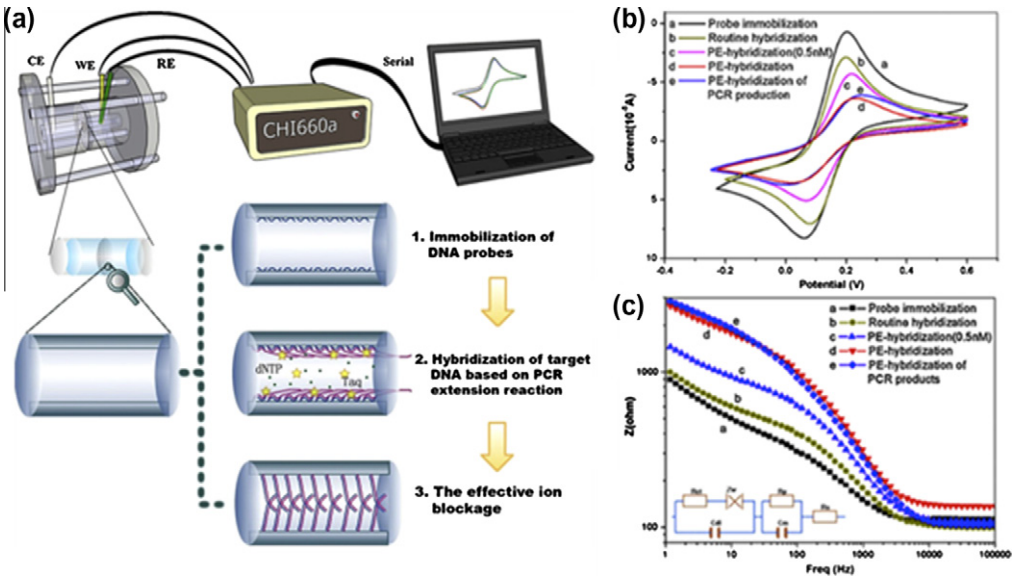

Fig. 35. (a) Schematic of an electrochemical DNA biosensor system and the mechanism of the dynamic polymerase-extending hybridization method (WE: working electrode; RE: reference electrode; CE: counter electrode). (b) CV in the region for $[Fe(CN)_6]^{3-/4-}$oxidation/reduction for the target DNA hybridization with different methods. (c) Impedance Bode plots after different reactions steps. Adapted with permission from Ref. [299].

determine diffusion coefficient, changes and stability of the bilayer membrane using cyclic voltammetry (CV) experiments.

The specificity and sensitivity of antigen recognition by antibodies has also been harnessed for electrochemical biosensors. For example, Yu et al. [300] fabricated a microchip using patterned AAO membrane for *E. coli* detection. The chip featured PEG microwell arrays prepared by a photolithography approach and featuring hydrophobic and hydrophilic regions. Anti-*E. coli* antibody was added and attached following the pattern of hydrophobic regions in the microwells and the target bacteria were selectively captured inside the wells. Binding events were monitored via EIS where low resistance was observed when AAO nanopores were covered by the bound bacteria. The sensitivity of this microchip was reported to be 10^2 CFU/mL as compared to conventional microelectrode arrays featuring detection limits of between 10^4 and 10^7 CFU/mL. Toh et al. developed an AAO-based electrochemical immunosensor where immunoglobulin G (IgG) was first immobilized on a AAO membrane via physisorption followed by blocking of free surface sites with BSA. A layer of Al (~400 nm) was sputtered onto a Pt wire electrode tip and anodized to alumina using a pipette anodization method. The biosensor operated via monitoring the electrode's Faradaic current response toward ferrocenemethanol, which is extremely sensitive to the formation of immunocomplexes within the pores of AAO membrane and was implemented for detection of a range of antigens [163,301,302].

An alternative to the enzyme-based biosensor are gold nanotube array in AAO membranes which show enzyme-free operation [303,304]. Zhou et al. synthesized such nanotube arrays inside an AAO membrane via electroless deposition which significantly enhanced the membrane's surface roughness. The resulting nanoscale roughness increased the catalytic activity towards the electro-oxidation of glucose and showed linear relationship to glucose concentration with detection limit of 10 μM [303]. In a recent example, a rapid nanochannel/gold nanoparticle based sandwich-immunoassay capable of filtering and subsequent detection of immunoglobulin in whole blood was reported [305]. In this work, dual electrostatics/steric blockage in the pores due to specific binding of thrombin and further signal amplification using a redox indicator ($[Fe(CN)_6]^{4-/3-}$) was tuned by primary and secondary immunoreactions with proteins labeled with gold nanoparticles. Nanopore blockage by

gold nanoparticles was enhanced by silver deposition further decreasing the diffusion of the signalling indicator through the nanochannel. Using this approach, detection of thrombin down to the picomolar level was achieved [305].

Yang et al. [100] reported a novel ebiosensor for urea based on a piezoelectric transducer. Urease was immobilized within AAO nanopores via physisorption, cross-linking with glutaraldehyde or cross-linking followed by chitosan coating. The sensor detected urea with high selectivity, wider linear range (0.5 μM to 3 mM), shorter response time (30 s), lower detection limit (0.2 μM) than those previously reported. The authors also reported that enzyme immobilized onto large pore diameters resulted in higher activity but poorer stability compared to smaller pore diameter [306].

6.3. AAO membranes for molecular separation

Molecular transport mediated by pore structures within the range of 1–100 nm diameter can be exploited for membrane-based molecular separation [307]. There are numerous ways in which nanoscale features can interact differentially with molecules on the basis of their size, shape, and charge. Nanoporous membranes are therefore promising platforms for fast and efficient separation. The key criteria for selective molecular transport are controllable pore diameters, narrow pore distribution, high porosity and controllable surface chemistry, all of which are fulfilled in AAO membranes. Indeed, AAO membranes have been applied for numerous applications including molecular separation, transport and catalysis. Separation tasks including separation of multivalent ions, proteins and DNA (including the combination with DNA amplification and sequencing) will be discussed below.

6.3.1. Molecular and ion separation

Many techniques have been devised to control the pore size and surface charge of AAO membranes in an effort to manipulate transport properties and selectivity based on the size, charge and hydrophobicity of molecules [308]. As we described in Section 4, numerous wet chemical synthesis and gas-phase techniques have been applied to controllably reduce the size of AAO pores. Au-plating introduced by the Martin group has been particularly well explored to precisely tune the pore diameter down to several nm [84,204,309,310]. In addition, SAMs of alkanethiols have been formed on the Au-plated surface to introduce chemical selectivity.

In the past years, an understanding of ion transport through AAO membranes and the dependence on parameters such as pore diameter, surface chemistry, solution pH, ionic strength and concentration has been developed [95,137,140,142,311–316]. For example, the Jarvinen group showed that increasing the pH from 5 to 8 could reduce the membrane surface charge of unmodified AAO membranes thus improved the selectivity of divalent and trivalent cation transport.

By increasing the pore diameter from 20 to 100 nm, the diffusion coefficients for divalent cations increased threefold [311]. Further work focused on the development of selective gate membranes with narrow pore openings down to 7 nm by depositing an Au layer on AAO surfaces [312]. The Au-coated layer was further functionalized with alkanethiols to afford a hydrophobic surface for trialkyl phosphine oxide-based metal ion carriers. When uranyl nitrate and lithium nitrate were used as feed solution and sodium acetate as receiving solution, 100% of the metal ion was transported across the membrane by facilitated transport via the phosphate or phosphine oxide carrier. High selectivity of uranium over europium ions was achieved when both metals were present in the feed solution, since the former ion selectively bound to the phosphine oxide carrier. At the same time, the membrane blocked transport of other ions such as H^+, Ca^{2+}, NO_3^- and CH_3COO^- [312]. The same group studied the effect of an alkanethiol-functionalized Au-coated membrane on other compounds such as trichlorophenol (TCP) giving five times faster flux than the unmodified membrane. The long chain of alkanethiol provided a hydrophobic barrier, sealing the pores towards transport of ions in the absence of a carrier [313].

Similarly, Smuleac et al. successfully captured Hg^{2+} ions with high binding capacity using polythiol-functionalized AAO membrane with 200 nm pore diameter. The functionalized AAO surface was prepared by silanization of the membrane with 3-glycidoxypropyl trimethoxysilane. Subsequent attachment of poly-L-glutamic acid (PLGA) and reacting the carboxylic acid groups with the amino group of cystine, cysteine or polycysteine afforded the polythiol-functionalized surface [95].

Steinle et al. [94] functionalized the inner surface of AAO membrane with ODS to render it hydrophobic. As a consequence, the amount of ions transport through the membrane dramatically decreased. Interestingly, the pore of this membrane could be re-opened again towards ion transport by adding a surfactant molecule. This 'on/off' design mimicked the function of an ion channel membrane. Similar on/off characteristics were obtained as a function of pH using carboxy-functional silanes. Odom et al. used a homologous series of molecules (phenol, *p*-cresol, 2,4-dimethylphenol and 2,4,6-trimethylphenol) and observed that the transport rate across the ODS-modified membrane correlated with the hydrophobicity of the permeant molecule [89]. Ku et al. investigated the fundamental characteristics of electrical conductivity across the C18-modified membranes [90]. Although the membrane was rendered hydrophobic and excluded water from the nanopores, electrical currents through the membrane could still be detected through "hydrophilically defective" pores, as determined by means of EIS and ^{29}Si NMR. Velleman et al. used ALD to precisely control the pore opening of silica-coated AAO membrane, which was then functionalized with hydrophobic perfluorodecyldimethylchlorosilane (PFDS) to render the surface hydrophobic. Separation studies with two selected molecular dyes showed that the PFDS-functionalized AAO membrane showed high selectivity and sensitivity towards hydrophobic dyes over hydrophilic dyes [87].

In supported liquid membranes (SLMs) based on AAO membrane, the outer surface of AAO is rendered hydrophobic to improve selectivity and flux rates for effective molecular separation [313,317]. For instance, a thiol modified Au-coated AAO membrane sealed with dodecane was employed. The flux rate of TCP through these membranes was five times faster than control experiments through unmodified membranes and showed excellent selectivity [313]. The influence of interfacial properties of the top pore surface on molecular transport through nanopores is also highlighted in recent work by Velleman et al. [207].

In comparison to the Au-coated surface, Yang et al. developed SLM based on a perfluoroalkanoic acid modified AAO membrane. The fabricated SLM showed excellent selectivity and high flux (10^{-7} - $cm^2\ s^{-1}$) for transporting organic compounds with a fluorine tag. Interestingly, the permeability of solutes decreased by increasing the pore diameter from 20 to 100 nm, a trend that is in contrast to most transport studies where molecular transport scales with pore diameter [317]. Silica-surfactant nanochannels inside AAO nanopores have been used by several groups for separation and catalytic studies [170]. For example, Yamaguchi et al. showed excellent extraction capability towards charged organic molecules, which could be controlled by varying the hydrophobicity of the surfactant tail [30,43,44,169,170,180,186,318–324]. The nature of the extraction mechanism depended on the charge of the solute (Fig. 36) [318]. Shi et al. found that lysine attachment to glutaraldehyde-activated AAO-silica composite membranes gave an increase in the adsorption capacity (from 1.22 mg/g to 17.57 mg/g) of bilirubin from a bilirubin–albumin solution when the temperature was raised from 25 °C to 37 °C [187]. In contrast, decreasing adsorption of bilirubin was observed with increasing ionic strength and increasing albumin concentration. Yamaguchi et al. [315] reported diffusion of metal complexes ($Fe(CN)_6^{3-}$, $Ru(NH_3)_6^{3-}$, ferrocenecarboxylic acid (Fc–COO^-), (ferrocenylmethyl)-trimethylammonium (Fc–NMe^{3+}), *N*,*N*-(dimethylamminomethyl)-ferrocene ($FcNMe_2$), ferrocenemethanol (Fc-OH) inside silica-surfactant nanochannels with diameter of 3.4 nm formed inside AAO nanopores. The diffusion coefficients of $Fe(CN)_6^{3-}$ and $Ru(NH_3)_6^{3-}$ through this nanopore were on the order of 10^{-11} $cm^2\ s^{-1}$, five orders magnitude smaller than those in a bulk aqueous solution. Charged ferrocene (Fc–COO^-, Fc–NMe^{3+}) derivatives showed smaller diffusion coefficients compared to their neutral counterparts ($FcNMe_2$), presumably due to the influence of charge-charge interactions with the pore wall.

In another channel-forming approach, the non-covalent attachment of macrocyclic receptors (hexylureidobenzo-15-crown-5 or hexylureidobenzo-18-crown-6) in AAO membranes produced structures resembling ion channels that facilitate transport of Na^+ or K^+ ions under potential gradient (Fig. 37) [186]. The silica coating can also significantly increase the magnitude of the zeta potential of the AAO surfaces and improve the electroosmotic effect. Saumitra et al. used silica-coated AAO membranes with smaller pore size range from 30 to 100 nm to study electroosmotic flow rate at a low applied voltage of 3 V using 2.5 mM buffer [188].

LbL deposition of PEMs on AAO membrane is another approach to prepare ion-selective membranes [47,140–142,144,322]. Pioneering work by Bruening and co-workers used Cu^{2+}-complexed PAA to control the charge density within PAA/PAH films to enhance anion selectivity. Alternating

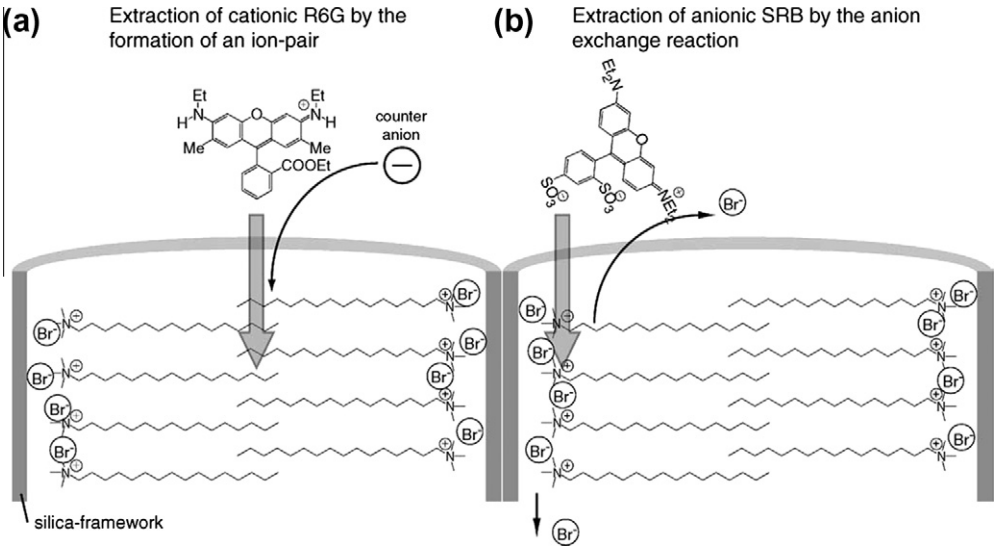

Fig. 36. Schematic illustration of an silica–surfactant–AAO nanochannel and the extraction mechanisms for (a) cationic rhodamine 6G (R6G) and (b) sulforhodamine B (SRB). Adapted with permission from Ref. [318].

deposition of PAA partially complexed with Cu^{2+} and PAH followed by removal of Cu^{2+} and deprotonation resulted in fixed $-COO^-$ sites on the film. Those membranes showed a fourfold increase in selectivity for Cl^- over SO_4^{2-} as compared to membranes with PAA/PAH coating without copper. In addition, changing the outer membrane coating from negatively charged PAA to positively charged PAH decreased the selectivity of the membrane towards Cl^- over SO_4^{2-} tenfold [137]. Hong et al. [141] compared the performance of PSS/PDADMACandPSS/PAH films on AAO membranes in the separation of monovalent anions. They reported that the $(PSS/PDADMAC)_4$ PSS membrane exhibited a much higher selectivity of Cl^- or Br^- over F^- ions compared to the PSS/PAH coating.

Furthermore, the flux through $(PSS/PDADMAC)_4$PSS films was threefold higher than the typical flux in commercial nanofiltration membranes which exhibit minimal selectivity. Ouyang et al. successfully used PEMs consisting of PSS/PAH or hybrid composite of PSS/PDADMAC-PSS/PAH to remove Mg^{2+} from solutions of NaCl and $MgCl_2$, achieving 95% rejection of $MgCl_2$. They also showed that pH, ionic strength and charge of the PEMs significantly influenced monovalent/divalent cation selectivity [142]. In contrast, the selectivity of PSS/PDADMAC membranes towards phosphate ions varied with the number of deposited layers. For example, when the number of PSS/PDADMAC bilayers was increased from 4.5 to 5.5, phosphate rejection decreased from 86% to 75% and chloride/phosphate selectivity dropped to 4.1 [141].

Vapor polymer deposition method was used to convert an inert AAO membrane to polyrhodamine-modified AAO membranes for removal of heavy metal ions from aqueous solution. After impregnating the AAO membrane with ferric chloride as an oxidant, rhodanine monomer was introduced during the vapor deposition polymerization method. The AAO-polyrhodanine membrane showed a removal capacity for Hg (II) of up to 4.2 mmol/g polymer [325].

6.3.2. Separation of amino acids and proteins

The application of AAO membranes for the separation of amino acids and proteins is described in several reports [93,110,111,139,143,162,187,213,214,326,327]. Bruening et al. demonstrated the separation of a mixture of glycine, L-alanine, L-serine, L-glutamine and L-lysine in a $(PSS/PAH)_7$PEM-modified alumina membrane [139]. For protein separation, this group employed a different concept based on the grafting of PHEMA polymer brushes from AAO membranes using ATRP [110,111]. This process yielded a remarkable binding capacity of 0.9 mg of BSA/cm^2 of external membrane surface (150 mg/cm^3 of membrane). AAO membranes modified with polymer brushes such as PHEMA have also been

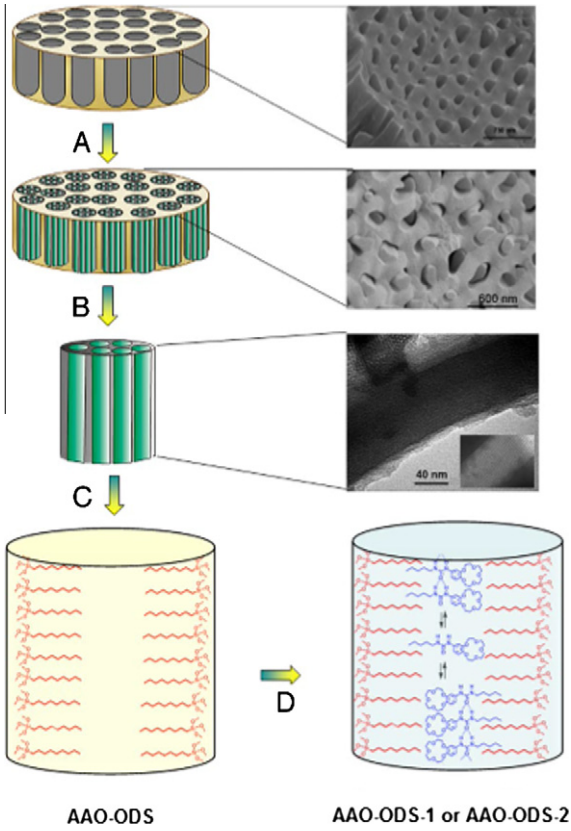

Fig. 37. Schematic representation of the synthetic route to obtain functionalized silica mesoporous AAO filled with mesostructured silica (arrow A), then calcinated (arrow B), reacted with ODS (arrow C), and finally filled with the hydrophobic carriers 1 or 2 (arrow D). Adapted with permission from Ref. [186].

used for protein purification. Polymer brushes derivatized with nitrilotriacetate–Ni^{2+} complexes allowed the purification of polyhistidine-tagged ubiquitin (HisU) in less than 30 min with a binding capacity of 120 mg of HisU/cm^3. Adsorption isotherms showed that saturation of the brushes occured at a HisU concentration as low as 0.04 mg/mL and that these brushes could bind up to 23 monolayers of HisU [111].

AAO nanopores on a silicon substrate have been used for the separation of BSA and bovine hemoglobin (BHb), exploiting the electrostatic sieving effect with high throughput (>10^{-8} M cm^{-2} s^{-1}) and high selectivity (>42) [327]. Recently, Sun et al. employed ATRP to grow PAA polymer brushes in AAO membrane for the high-capacity affinity-based separation of proteins [110]. In a simpler approach, Chang et al. investigated adsorption and desorption of BSA on octanoic and octadecanoic acid functionalized AAO membranes in batch and flow processes by means of liquid chromatography [120]. BSA adsorption capacities of octanoic and octadecanoic acid-modified membrane were 0.003 and 0.004 μmol/cm^2, respectively. Interestingly, the adsorption performance was retained over three cycles of adsorption–desorption.

Shi et al. [162] used chitosan-functionalized AAO membranes in the presence of a chelating agent (Cu^{2+}) to increase membrane active sites. This metal-chelated affinity membrane was used to separate hemoglobin (Hb) from hemoglobin phosphate and hemolysate. The adsorption and affinity capacity of membrane produced by this approach towards Hb was 17.5 mg/g and 91.2%, respectively. In contrast, silica nanocomposites formed inside AAO nanopore with a pore diameter of 3.4 nm showed good size

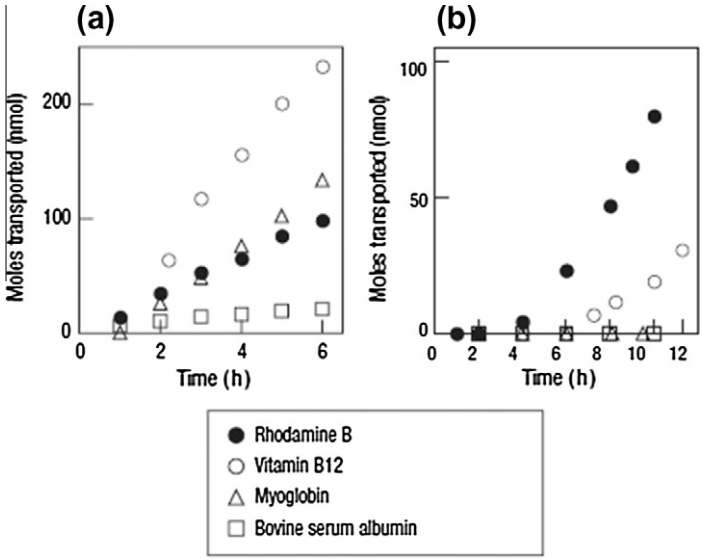

Fig. 38. Time-dependent transport of molecules through the AAO membrane. The amount of moles of four different molecules transported through the AAO membrane without (a) and with (b) the silica–surfactant nanocomposite. Adapted with permission from Ref. [170].

exclusion properties and facilitated the transport of rhodamine B (1.0 nm) and vitamin B12 (2.4 nm) while preventing the transport of larger molecules such as myoglobin (4.0 nm) and BSA (7.0 nm) (Fig. 38) [170]. Likewise, separation of enantiomers of peptide drugs through antibody-functionalized silica nanochannels inside an AAO membrane was achieved [180]. An AAO membrane modified with PEO has been generated that excludes antibodies but permits access of insulin and glucose and therefore potentially enable encapsulation of pancreatic islet cells for treatment of type I diabetes [328].

Applying an external voltage to the functionalized AAO membrane constitutes an alternative method to improve selectivity of AAO membranes for protein separations. Cheow et al. [213,214] investigated the effect of varying electrical potential on Pt-coated AAO membranes for separation of BSA, lysozyme (Lys) and myoglobin (Mb). By varying applied potentials across the membrane, Lys was transported 10–16 times faster than BSA and Mb was transported 4–5 times faster than BSA.

Recently, the electrostatic sieving effect of a thin AAO membrane on protein separation (BSA and BHb) has been investigated. High throughput ($>10^{-8}$ M cm^{-2} s^{-1}) and high selectivity (>42) of both proteins has been achieved [327]. In another approach, a protein trapping device was developed based on an AAO hybrid structure of nanochannels and ion channels. The presence of ion channels in the barrier layer of AAO bottom was confirmed by electrokinetic experiments. By applying a transmembrane potential, electrophoresis of negatively charged protein was induced to the nanochannels and the protein was unable migrate across the barrier layer due to size exclusion effect. The concept was extended by incorporating the AAO hybrid structure into a microfluidic system. As a result, a rapid and efficient trapping of protein at a high concentration factor (10^4–10^5) in AAO nanochannels was realized within 30 s [329]. These two examples revealed the suitability of AAO membranes for size-based sorting.

6.3.3. DNA separation

Separation of DNA has numerous applications in biotechnology and medicine. For example, the ability to separate and quantify DNA lengths and its types is vital to the early detection of diseases. However, the separation of DNA is a difficult analytical task, which requires sophisticated, expensive and robust devices [330]. An important issue is the clogging of separation devices with DNA molecules, limiting the device performance [331]. Therefore, low cost and mechanically robust nanopore-based transporters with well-defined surface-charge properties offer significant opportunities in this field. Sano et al. developed a size exclusion separation method that used AAO membranes in

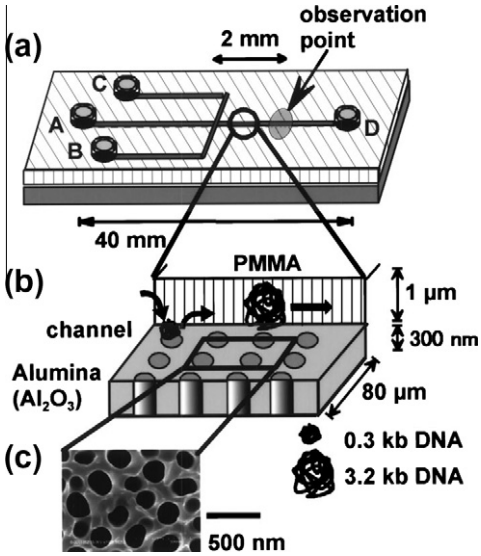

Fig. 39. (a) Schematic illustration of an AAO based microfluidic channel (chip). The chip has four reservoirs: A, B, C, and D. (b) Magnified view of the separation channel. The radius of each pore was controlled to allow smaller molecules to enter the pores while stopping larger molecules from entering. (c) SEM micrograph of the nanopores. Adapted with permission from Ref. [332].

a microfluidic channel as size separation platform for DNA. In this approach, DNA biomolecules with smaller size were frequently trapped in the pores and hence eluted more slowly than the larger biomolecules passing through the channel (Fig. 39) [332]. Vlassiouk et al. [97] reported efficient detection and affinity separation of single stranded DNA using AAO membranes with covalently immobilized DNA. After the binding and separation phase, the target DNA was eluted by inducing de-hybridization at elevated temperature. Higher separation efficiencies of up to 85% were obtained for mixtures of complementary and non-complementary single stranded DNA. CV and EIS results showed that hybridization efficiency of DNA was drastically reduced on filters with larger pore diameter (i.e. 200 nm) as compared to 20 nm due to the increased size mismatch between the pore diameter and the DNA length [96]. Chang et al. developed anion exchange membranes comprising of AAO coated with tertiary and quaternary ammonium group [333]. Two different strategies (batch adsorption and chromatography) were chosen to partially separate plasmid DNA, RNA and a mixture of DNA and RNA. The separation efficiency of plasmid DNA for these membranes was recorded as 53% and 65% for batch and chromatography processes, respectively. The rather poor separation performance could be attributed to the large pore size (200 nm) used in the study.

The ALD approach was employed to fabricate sub-40 nm pore AAO membranes to separate DNA from bacteriophage (phi29) virus in a mixture. When a mixture of empty capsids and DNA containing virus was centrifuged at 3000 rpm, the empty capsids deformed and passed through 40 nm diameter pores and retained on the bottom surface of the AAO membrane whereas the particles packaged with DNA were mainly retained at the top surface of the AAO membrane [334].

6.4. Catalysis

AAO membranes with their high surface area per unit volume and chemical inertness are ideal platforms for catalytic applications. Many industrial catalytic processes involve the combination of high temperature and chemically harsh environments [335]. Using AAO, catalysis can also be combined with molecular separation. Several studies have focussed on the placement of various catalytic active components including metal, metal oxide nanoparticles, organic catalysts or enzymes inside of AAO nanopores [105,144,322]. Bruening et al. [144] prepared catalytic membranes using LbL of PAA/PAH layer in which gold nanoparticles were sandwiched (Fig. 40). This membrane catalyzed the reduction

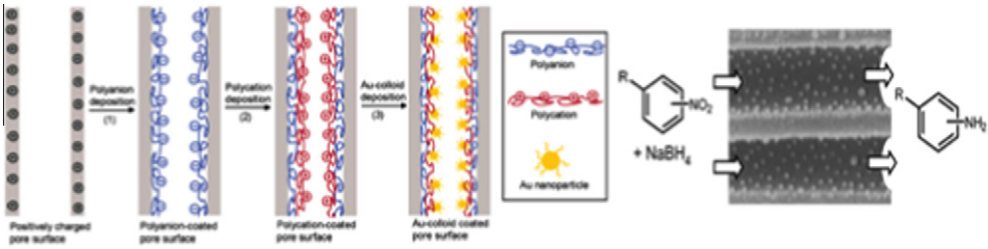

Fig. 40. Schematic diagram of AAO membrane used as a catalytic membrane. Adapted with permission from Ref. [144].

of 4-nitrophenol (4-NP) to 4-aminophenol (4-AP). Subsequently, the group fabricated membranes that selectively catalyzed the reduction of nitro groups in the presence of other reducible compounds i.e. cyano, chloro and styrenyl moieties [322].

Stair et al. [335] used ALD to precisely control the deposition of V_2O_5 and diameters of the AAO scaffold pores. The catalytic membrane was prepared by depositing 10 nm of alumina by ALD into an AAO with 40 nm pores. Subsequently, a single vanadia monolayer was deposited by wet impregnation using ammonium metavanadate. Oxidative dehydrogenation of cyclohexane and benzene through a V_2O_5 coated AAO membrane showed high catalytic activity and selectivity.

Recently, Wang et al. [336] explored an asymmetric reaction where an enzyme and its substrate were fed to an AAO membrane from opposite sides. Asymmetric biochemical reactions were demonstrated using the HRP enzyme as a model catalyst. The AAO membrane on 60 μm thickness with a nominal pore size of 200 nm was integrated into polymeric microfluidic layers to generate microreactor. The reaction rate of the enzyme with its substrate was detected colorimetrically and was controlled by the diffusion of the substrate through the membrane.

Oliveira et al. prepared two different AAO membranes coated with PEI-trypsin and PANI-peroxidase to study their catalytic activities in batch and flow-through mode. The hydrolysis rate of N-α-benzoyl-DL-arginine-p-nitroanilide to p-nitroaniline was 2.95 and 3.8 nmol release per minute under batch and flow-through system, respectively. At the same time, in the oxidation of o-phenylenediamine (OPD) to 2,3-diaminophenazine (DAP) by PANI-peroxidase coated AAO, the enzyme maintained its initial activity up to 98% and 74% in continuous and batch mode, respectively [164].

6.5. Biomedical applications

6.5.1. Biocompatibility, cell growth and tissue engineering

High biocompatibility is a prerequisite for new biomaterials and it is defined as the ability of a material to perform with an appropriate host response in a specific situation [337]. The main biocompatibility studies that have been performed on nanoporous AAO relate to *in vitro* cell culture studies and applications as orthopedic implants [92,103,338–345].

The use of nanostructured biomaterials in bone engineering is biologically inspired because bone is a naturally occurring porous ceramic material composed of nanosize organic and mineral phases that forms a highly hierarchical macrostructure. Earlier studies using oxide ceramics showed that a porous surface with pore diameter of ~100 μm is optimal for bone in-growth to maintain blood supply to connective tissue, but recent studies using nanoporous AAO have revealed that much smaller pores of AAO allow bone in-growth [92,338,339]. Study of osteoblast response on nanoporous AAO membranes with pore diameters of 30 to 80 nm confirmed the growth of extensions of osteoblasts into the nanopores which produced an active matrix in the form of a fibrous scaffold that contain calcium and phosphorus, the typical elements of the bone matrix [339]. A similar conclusion was reached by Popat et al. who reported that AAO membranes showed significantly improved osteoblast adhesion and proliferation in comparison with amorphous alumina, Al metal and glass [338]. These studies show the potential of AAO to be used as a biocompatible platform for bone growth and orthopedic implant applications.

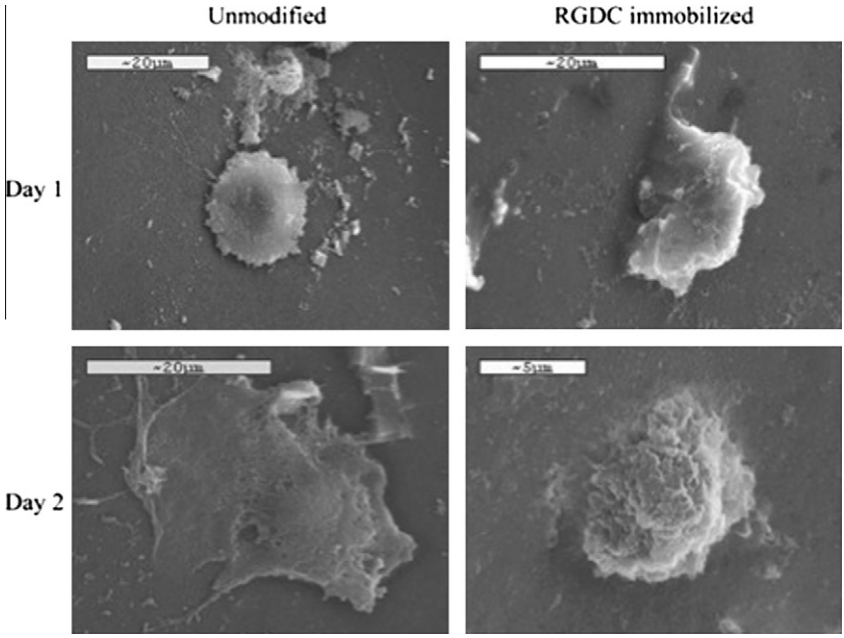

Fig. 41. SEM images showing osteoblast morphology after 1 and 2 days in culture on unmodified and arginine–glycine–aspartic acid–cysteine (RGDC)-immobilized AAO membranes. Adapted with permission from Ref. [103].

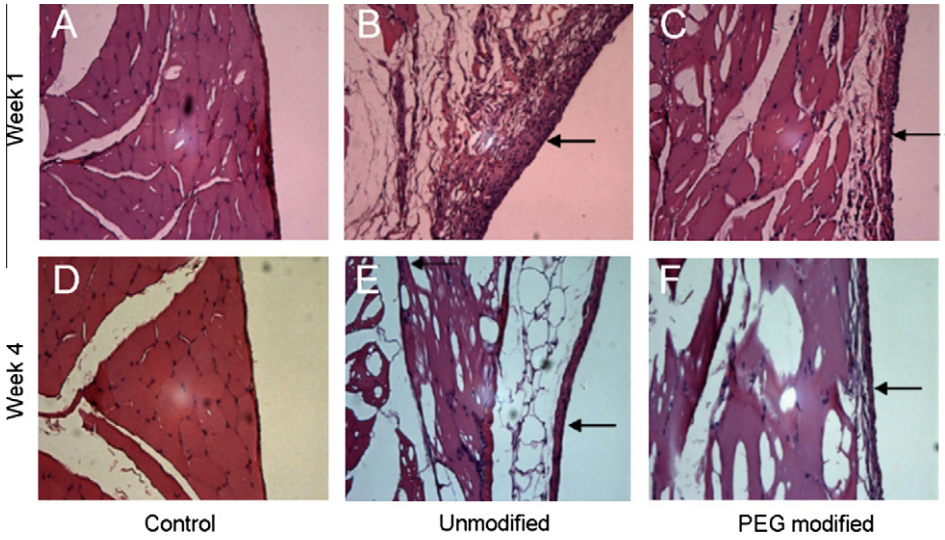

Fig. 42. Histological examination of tissue exposed to no material (A) and (D), unmodified AAO capsules (B) and (E), and PEG-modified AAO capsules (C) and (F) after 1 and 4 weeks. Arrows indicate the portion of the tissue that was exposed to the capsule. Adapted with permission from Ref. [92].

Improved osteoblast adhesion and growth on AAO with the same pore diameters (30–80 nm) was reported by physisorbing vitronectin or covalently immobilizing a cell adhesion mediating peptide

(RGDC) via amino-silane-maleimide grafting chemistry (Fig. 41) [103]. RGDC-modified AAO showed favorable osteoblast adhesion after 1 d in culture and cell matrix production was visible after 2 d. In an *in vitro* biocompatibility study by Flamme et al. toxic effects of AAO on β-cells were absent, whilst the viability of cells was reduced by 94% when cell were treated with latex particles [92]. On the other hand, *in vivo* implantation of PEG-coated AAO capsules into the intra-peritoneal cavity of rats showed moderate inflammation after 1 week, indicated by the presence of macrophages and lymphocytes in the granulation layer. However, the inflammation response decreased after 4 weeks (Fig. 42).

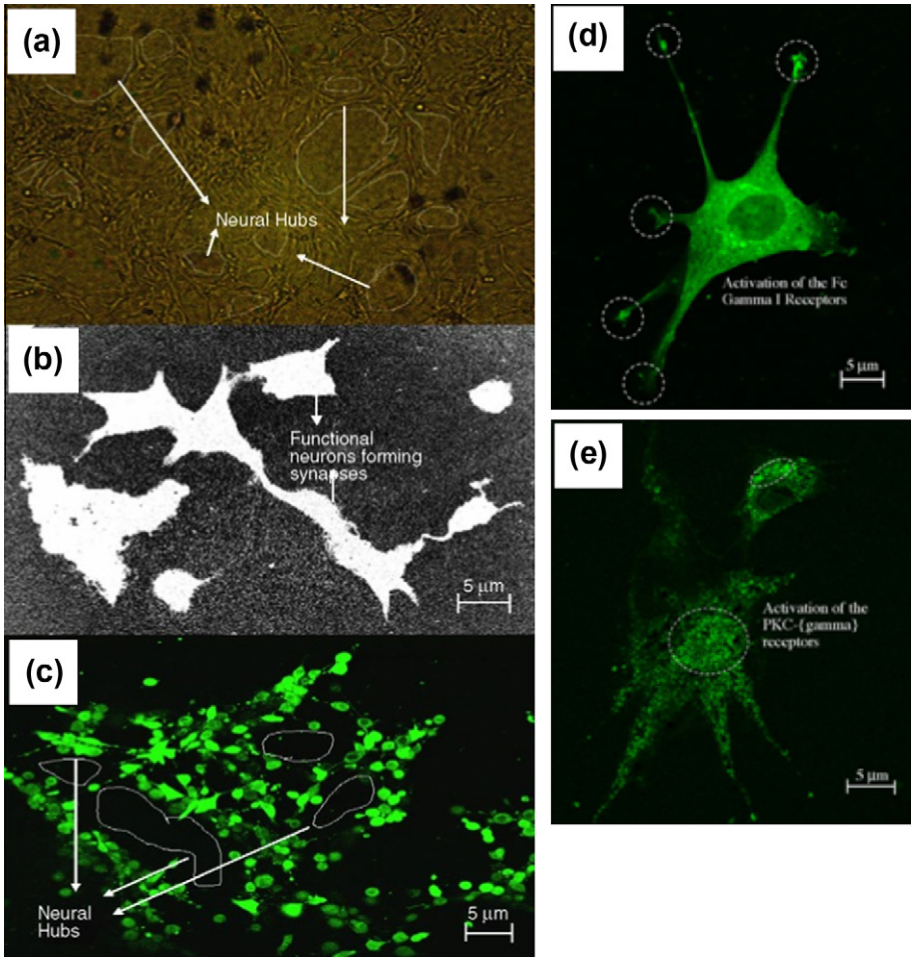

Fig. 43. (a) Optical micrograph representing the development of neural hubs on AAO membrane after 24 h seeding and incubation on the AAO substrate. (b) SEM image of synaptic neurons establishing communication hubs on the AAO membrane. (c) Fluorescent optical micrograph of differentiating neurons on AAO substrate. The neurons were preloaded with fluo-3 calcium stains to establish their viability. (d) Fluorescence confocal micrograph demonstrating the activation of the specific groups of ion channels glucose–insulin (PKC-γ) receptors at the neurite terminals (circled area), resulting in potassium ion transients due to the effect of glucose on the neuronal cell membrane. (e) Fluorescence confocal micrograph demonstrating the activation of the Fc-γ I receptors on the neuron cell membrane at the soma (circled area), causing in potassium ion transients due to the effect of IgG on the neuronal cell membrane. The cells were pre-loaded with green fluorescent protein (GFP) and the fluorescent transients were visualized during the interaction of the glucose molecules with the cell membrane. Adapted with permission from Ref. [347].

Karlsson and Tang [343] prepared a series of AAO membranes coated with serum, collagen I, fibrinogen, IgG and albumin to study *in vitro* viability of osteoblastic cells (MG63). A clear effect of pore size on cell viability was also observed on protein-coated AAO membranes. Incubation of cell with collagen-coated membrane gave highest cell numbers on both 20 and 200 nm pore sizes. Cells cultured on fibrinogen-coated membrane seemed to be more viable on 20 nm pore size as compared to 200 nm pores size. This could be related to the size and shape of fibrinogen. Fibrinogen is less likely to penetrate the smaller 20 nm pores due to steric reasons thus, leading to accumulation of fibrinogen on the surface.

Rat-derived neuronal cells were also used to characterize adhesion and biocompatibility on modified AAO membranes. Wolfrum et al. [346] employed three different coatings on AAO membrane: PLL, extracellular matrix (ECM) gel and concavalin A (ConA) to promote cell adhesion on AAO membranes. It was observed that rat neurons showed good adhesion and cell neurite formation on surfaces coated with ECM gel. Prasad et al. used PLL-coated AAO membranes as a platform to record *in situ* cellular electrical activities in response to therapeutic drugs (glucose and IgG) [347]. Micron-sized gold pads were patterned on PLL-coated AAO membrane and extra cellular signal were recorded when neurons forming functional synapses responded to specific drug molecules via a variation in the voltage signal (Fig. 43). The presence of glucose and IgG caused current signals of 160 pA to 5 nA, respectively.

Biofouling of AAO membranes was studied by Popat et al. who showed that biofouling could be eliminated by surface modification with PEG-silane [345].

Several studies also investigated the biocompatibility of uncoated AAO membranes [341,348–350]. For example, Karlsson et al. used primary human osteoblast-like cells to investigate cellular

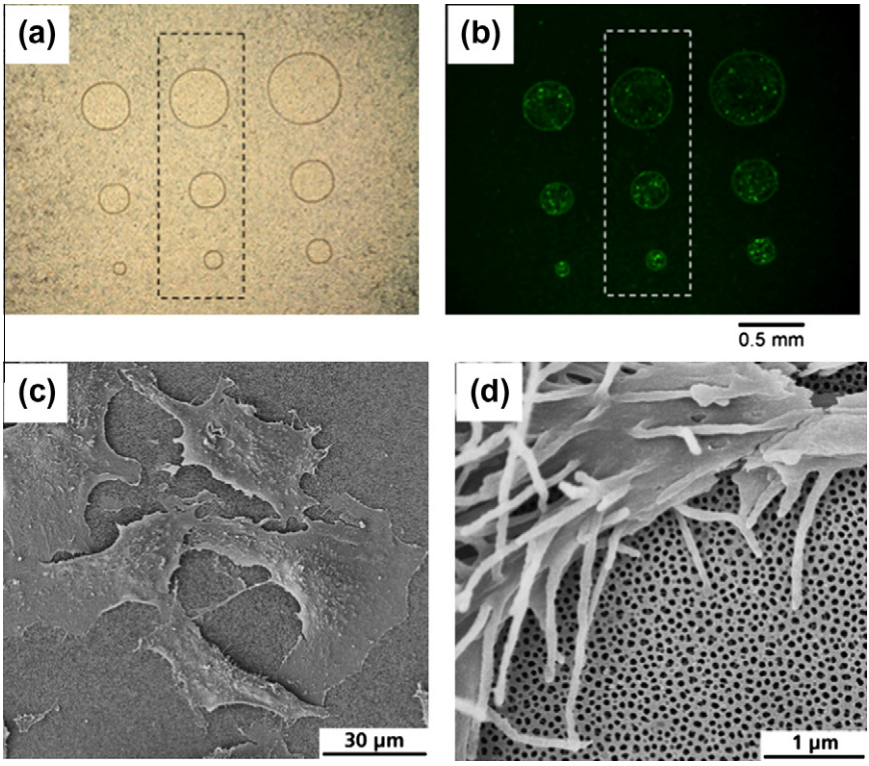

Fig. 44. (a) Brightfield and (b) fluorescence micrographs of HeLa cells on a AAO culture substrate with a 3 × 3 array of holes with diameters of 0.1–0.6 mm beneath. Adapted with permission from Ref. [347]. (c) SEM image of HepG2 cells on self-supporting AAO membrane (pore diameter 76 ± 10 nm) and (d) magnification of a cell border of (c). Adapted with permission from Ref. [341,343,348,349].

interactions on unmodified AAO membranes (Fig. 44). Their results showed normal osteoblastic cell growth during 2 weeks in culture. This was followed by an increase of alkaline phosphate (ALP) production which indicates the osteoblastic phenotype was retained on the AAO membrane [341]. Another study by Hoess et al. used two different pore sizes (70 and 260 nm) of the unmodified AAO membrane and a hepatoma cell line (HepG2). They observed the cells easily adhered on the membrane surface with 260 nm pore size making membrane protrusions (filopodia) able to penetrate into the pores of the underlying AAO which is not observed on AAO with smaller pores [343]. Kant et al. investigated the influence of the various AAO pore structures on the growth of human neuroblastoma with SK-N-SH cells as the neuronal model cell. This study demonstrated that pore organization could have a direct influence on the orientation and phenotype of neuronal cells, opening up bio-engineering possibilities. The most extensive cell response was found on surfaces with mixed pore and brush structures (Fig. 45a–c). This surface gave the highest cells attachment and frequent neuron-like phenotype with cytoplasmic processes and extensive cell–cell interactions [351].

The use of AAO as a biomaterial has been explored in several domains including: the development of therapeutic devices for bone and dental tissue engineering and coronary stent implants [46,352]. A major challenge in orthopedic research is to design surfaces that will promote osteogenesis *in vitro* and *in vivo*. A few studies have demonstrated that AAO scaffolds could be used to establish an effective means for alloplastic substitution of teeth. Effective biological sealing could be achieved through a screw and blade-vent implants. The later implant technique showed a partial interposition of

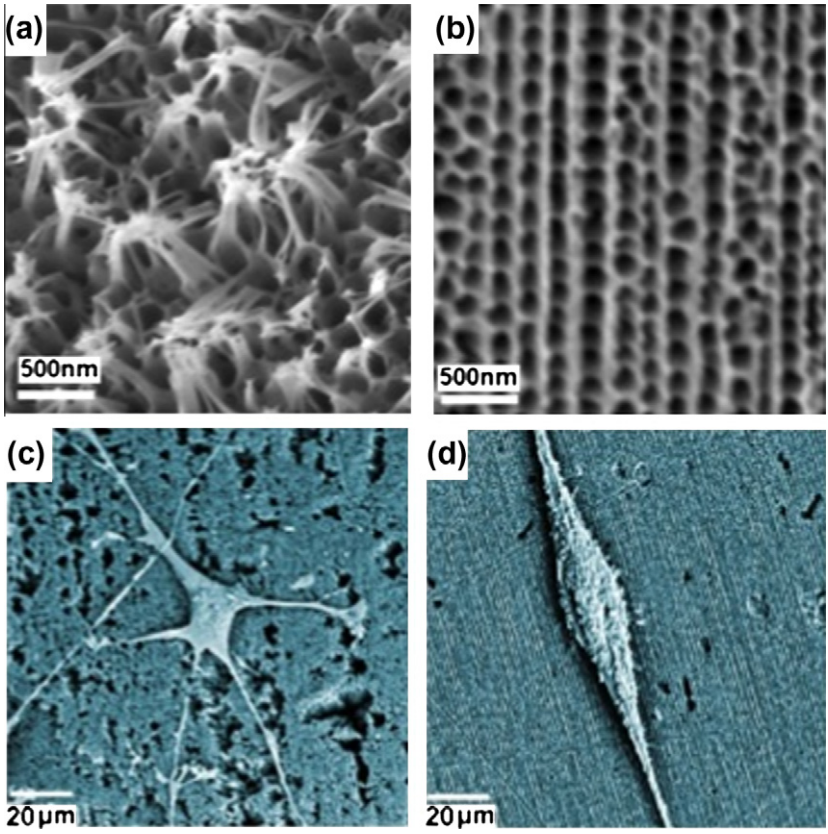

Fig. 45. SEM images of single neuroblastoma cells grown on different types of AAO showing influence of pore structures on cell morhology. (a and b) AAO with nanobrushes show an extensive branching and interconnection of cells. (c and d) Aligned pores show a linear morphology of neuroblastoma cell directed by aligned pore structures. Adapted with permission from Ref. [351].

connective tissue whilst the screw implant exemplified a tight attachment of bone over the whole implant surface. One of the major problems for the dental application is to fabricate ceramic implants with complex shapes while maintaining accurate dimensional control of features from the macro- to the microscale along with good material properties. For example, clinical failures of AAO-based dental implants in animals have been observed. This study suggests that the residual of unwanted surface microporosity adjacent to the gingival cuff results in an inflammatory reaction that prevents the establishment of an effective biological seal between the oral cavity and the alveolus [353].

Bone regeneration in a scaffold *in vivo* involves formation, penetration and migration of osteoblast and mesenchymal cells from the surrounding bone tissue, as well as vascularization. Suitable implant porosity and pore size are expected to enhance osteogenesis and numerous studies have verified this hypothesis [354,355]. In addition, the surface microtopography can also significantly affect tissue neoformation. For example, *in vivo* implantation of PEG-coated AAO capsules into the intra-peritoneal cavity of rats showed moderate inflammation [92]. Bose et al. showed that coating of AAO scaffolds with hydroxyapatite (HAp) helped improve the biological response of the scaffolds *in vitro* using rat pituitary tumor cells [356]. Furthermore, highly adherent layers of AAO on the surface of titanium alloys show improved proliferative activity in comparison with surfaces without AAO [357].

6.6. Drug delivery

A range of nanoscale materials has been explored in recent years for drug delivery applications to address the problems associated with conventional drug therapies such as limited drug solubility, poor biodistribution, lack of selectivity and unfavorable pharmacokinetics [358]. Among them are nanoporous and nanotube carriers due to their unique features, such as low fabrication cost, controllable pore/nanotube structure, tailored surface chemistry and high surface area [359,360]. Implantable systems for local delivery of therapeutics based on porous platforms fabricated by electrochemical process including pSi, AAO and TNT have been widely explored [16]. Good mechanical stability, chemical inertness, biocompatibility, controllable pore size and pore volumes, along with tunable surface chemistry have made AAO to be an excellent platform for loading large amount of drugs and facilitating their controlled release.

To address the problem of sustained release of poorly soluble drugs from implants, Simovic et al. demonstrated extended drug release based on applying a thin plasma polymer film on the top of AAO membrane after drug loading (Fig. 46a) [361]. A plasma polymer layer with different thickness deposited on AAO allowed the control over pore diameter and hence the rate of drug releases (Fig. 46b–f). It was possible to achieve favorable zero order release kinetics from AAO implants by controlling deposition of a plasma polymer layer. More recently, this group explored AAO as therapeutic implants for elution of drug nanocarriers using several polymer micelles as model nanocarriers [362]. The release kinetics of drug-loaded polymeric micelles from AAO was two-phased with a burst release of 31–55% in the first 6–8 h, followed by a slow release phase over ~8–22 d. This release pattern is especially useful in bone implant therapies that require a large initial dose followed by a prolonged dose over a few weeks. Additionally, by applying plasma polymer film on the top of AAO, the release could be extended considerably, the burst release almost suppressed and zero order drug release kinetics over a period of more than 4 weeks achieved. Peng-Fei et al. demonstrated the effect of temperature on the permeation of vitamin B12 through PNIPAM-grafted AAO membranes [109,158]. Above the LCST, permeation of vitamin B12 was more pronounced than below due to the collapsed polymer state, increasing the effective pore diameter. The length of PNIPAM chains had a more dramatic effect on the switchability than the density of the grafted polymer [109].

The concept of switchable drug release from AAO has been recently demonstrated by Jeon et al., designing an electrically responsive AAO membrane based on an electropolymerized PPy/DBS coating on the outer part of the AAO membrane. The pore size of the PPy/DBS AAO membrane could be reversibly actuated by the electrochemical state and pulsatile release of the model protein drug (FITC-BSA) demonstrated (Fig. 47). The stimulus could be applied on-demand and the response time was short (less than a few seconds). A high flux of drugs could be obtained in the open state as a result of high pore density ($16.1–6.4 \times 10^9/cm^2$) and the short constricting channel (~1.5 μm) length. Considering these results, drug release of accurate drug dosage control depending on a patient state would be

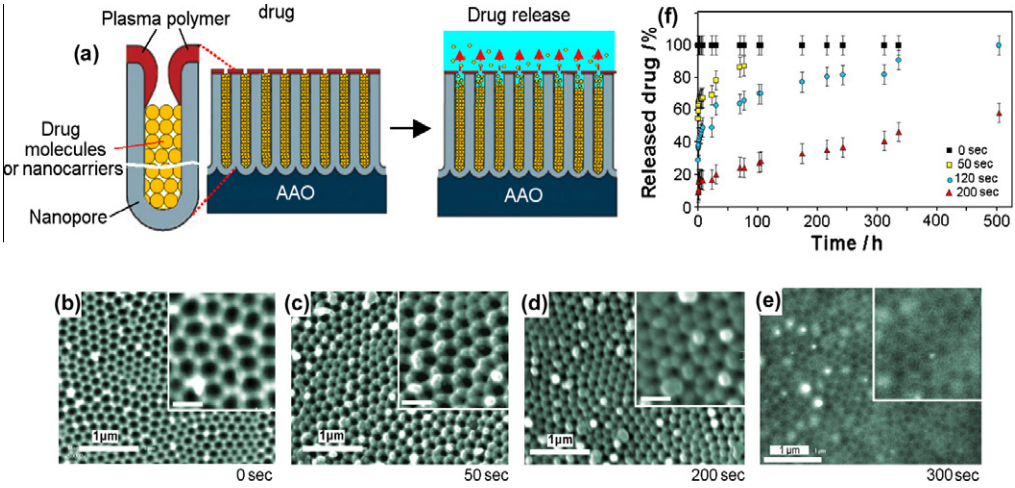

Fig. 46. (a) Scheme of plasma polymer modification of AAO platform loaded with drug or drug nanocarriers (polymer micelles) to achieve controlled and extended drug release. (b) SEM images of the top surface of AAO porous layer modified with allylamine plasma polymer using deposition times of (b) 0 s; (c) 50 s; (d) 200 s and (d) 300 s. Scale bars in insets are 200 nm. (f) Controlled release of model drug vancomycin from plasma modified AAO during 500 h or drug release. Adapted with permission from Ref. [361].

possible which is relevant to emergency therapy of acute angina pectoris and migraine, hormone-related diseases, and metabolic syndromes [165].

For details on drug delivery systems based on nanoporous membranes, readers are referred to a recent review [363].

6.6.1. Drug eluting stents

Coronary stent implantation is a successful procedure for the treatment of coronary artery disease. However, restenosis still remains one of the biggest challenges in interventional cardiology. To overcome this, the concept of drug-eluting stents with drugs being trapped in polymer films coated onto the stents had been recently introduced [364]. Although the clinical use of polymer stents has been approved, their inflammatory reaction is still a serious limitation. An alternative approach is the design of stents with an AAO layer filled with anti-inflammatory and cytostatic drugs [364,365]. A

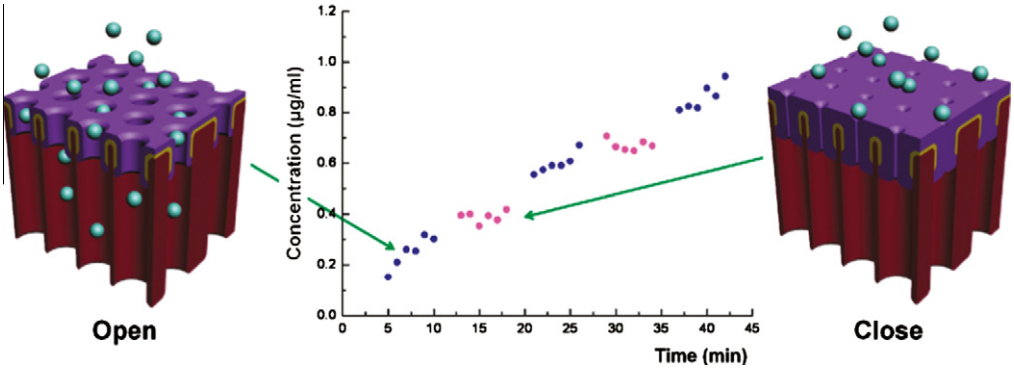

Fig. 47. Schematic of electrically-responsive electropolymer-coated AAO membrane showing reversible change of pore size (and the drug release rate) between oxidation and reduction states. Adapted with permission from Ref. [165].

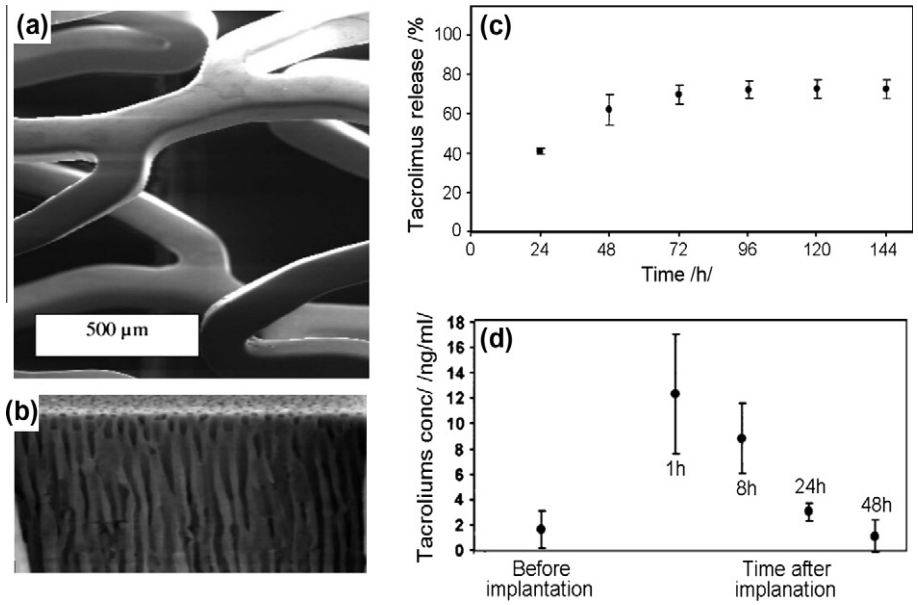

Fig. 48. (a and b) SEM image of stents coated with AAO (cross-section of AAO layer on the top) with pore size between 5 and 15 nm and pore density 10^{12} cm^{-2} allowing drug loading with tacrolimus. (c) *In vitro* drug release, cumulative tacrolimus release within the first 144 h; after 72 h, about 75% of the loaded 60 μg tacrolimus has been eluted and about 25% is still trapped in the AAO coating. (d) *In vivo* drug release. Time course of tacrolimus concentration in whole blood after stent implantation in the carotid arteries of rabbits. Adapted with permission from Ref. [364].

SEM image of a stainless-steel stent with an AAO layer prepared by electrochemical anodization of an Al film deposited on a stainless-steel stent is shown in Fig. 48 [364]. Wieneke et al. performed *in vitro* and *in vivo* drug release studies of these stents using AAO with different pore diameters loaded with tacrolimus (an immunosuppressive drug) [364,366]. The impact of AAO pore diameters (5–20 nm) and depth of the porous layers (1–4 μm) on the drug release behavior was investigated. Animal experiments in rabbits showed that the AAO layer on coronary stents alone as well as in combination with tacrolimus led to a reduced infiltration of lymphocytes and macrophages in response to stent implantation, thus suggesting this new approach has the potential to overcome existing problems of inflammatory response and to translate into clinical application. However, further improvement of biocompatibility and controlled release capability is required.

6.6.2. Biocapsules for immunoisolation

The concept of encapsulation of therapeutic cells using microfabricated capsules with semi-permeable barriers in order to shield cells from the immune system has been pursued as a potential treatment for a number of diseases such as diabetes mellitus, Parkinson's and Alzheimer's [367]. Typical immunoisolation devices consist of polymeric membranes, but there are several issues associated with the use of these membranes, including poor chemical resistance, inadequate mechanical strength and broad pore size distributions [368]. In comparison to polymer membranes, AAO membranes offer many advantages in designing implantable biocapsules including mechanical strength, chemical resistance, adjustable pore size and surface chemistry, and easy incorporation into microfabricated devices.

The use of therapeutic AAO biocapsules with controlled drug release for immunoisolation was firstly demonstrated by Gong et al. [369]. Fig. 49a shows a capsule consisting of a uniformly porous layer with pore diameters of 25–55 nm, which was fabricated by electrochemical anodization. To prove the controlled release capacity of these capsules, the release of model drug molecules such as fluorescein (400 Da), and conjugates of FITC and dextran of varying molecular weight (4, 20, 70, and 150 kDa) was explored. The study demonstrated that nutrients and small molecular weight proteins

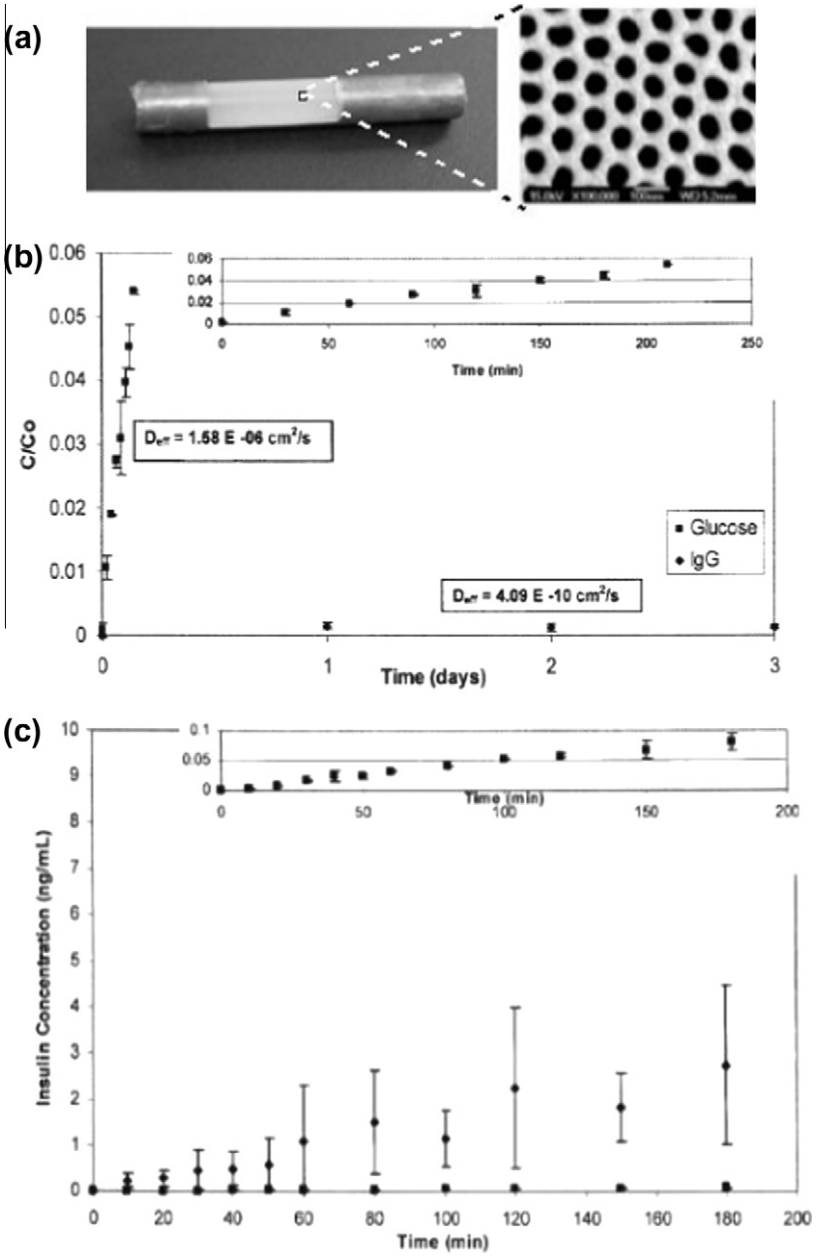

Fig. 49. (a) Photos of completed AAO capsule. (b) Normalized release of glucose (squares, D_{eff} 1.58E−06 cm^2/s) and IgG (diamonds, D_{eff} 4.09E−10 cm^2/s) through a AAO membrane with a nominal pore size of 75 nm. *C* is the concentration at time *t*, *Co* is the loading concentration. Inset: Glucose release on a 210-min time scale. (c) Insulin release from encapsulated (experimental, squares) and unencapsulated (control, diamonds) MIN6 cells following a step increase in glucose. The nominal pore size used for the encapsulated cells was 75 nm. Inset: Enlarged graph of experimental data. Adapted with permission from Ref. [369].

(∼3.5 nm diameter) would be able to diffuse through the membrane, whilst preventing transport of larger molecules (>30 nm diameter), such as antibodies. They also demonstrated the feasibility of

using nanoporous AAO capsules for the encapsulation of cells. AAO capsules (pore diameter 46–75 nm) incorporated with insulin-secreting MIN6 cells could act as effective semipermeable devices allowing transport of glucose and insulin whilst impeding the transport of larger proteins such as immunoglobulin [369–371]. Fig. 49b shows fast release of glucose and the prevention of IgG release over 4 d. The release profile of insulin produced by MIN6 cells through AAO in response to an increase in glucose level is shown in Fig. 49c. The cells also retained their viability in close proximity to the AAO membrane showing future perspectives of this approach for clinical immunoisolation.

6.7. Other applications and aspects

In recent years, emerging applications such as fuel cells, solar cells, molecular junctions and photonic crystals using AAO substrates have received increasing attention. For instance, AAO-based metal–insulator–metal (MIM) nanocapacitors for energy storage have been fabricated by Banerjee et al. [227] who deposited the sequence of TiN–Al_2O_3–TiN multilayer structures on AAO by ALD (Fig. 50). Self-alignment of each individual layer facilitated the formation of a highly controlled nanocapacitor inside AAO nanopores with an overall thickness of 25 nm. In this work, the authors reported equivalent planar capacitance (EPC) density up to 100 $\mu F\,cm^{-2}$ surpassing previously reported values of nanostructured electronic capacitors. In another example, Liu et al. synthesized RuO_2/poly(3,4-ethylenedioxythiophene) (PEDOT) composite nanotubes grown in an AAO substrate by step-wise electrochemical deposition method. The high surface area of the nanotubular structures led to high specific capacitance values and fast charging/discharging capability [372]. Another type of application was investigated by Liu et al. who fabricated ZnO nanowires and intramolecular

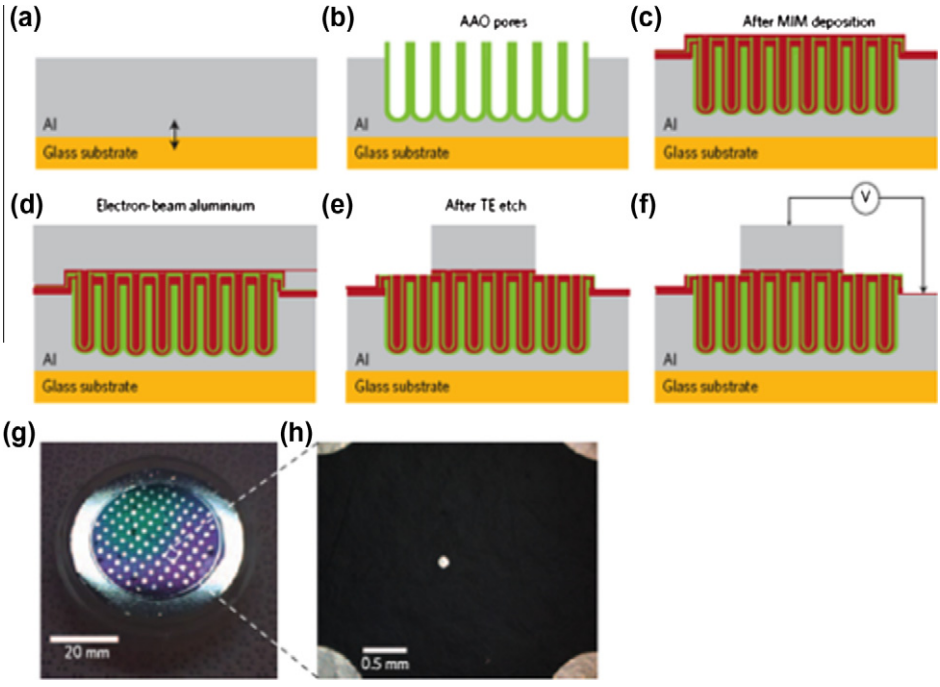

Fig. 50. Process sequence to prepare MIM (metal–insulator–metal) capacitors. (a) Al foil is anodically bonded to a glass substrate. (b) AAO formation. (c) MIM deposition via ALD processes. (d) Electron beam deposition of Al. (e) Photolithography, masking and etching of the Al electrode, then the top electrode (TE) TiN, to define the capacitor area. (f) Electrical testing using the Al foil (which is in contact with the bottom electrode TiN) as a back contact and electron-beam Al as the top contact. (g) Two-inch wafer with capacitors of different areas defined on the surface. (h) A zoom-in image of an actual 'dot' capacitor tested. Each such dot capacitor is 125 μm wide and contains $\sim 1 \times 10^6$ nanocapacitors. Adapted with permission from Ref. [227].

p–*n* junctions embedded in an AAO substrate and studied their electrical properties. *I*–*V* measurements of ZnO nanowires in AAO substrate confirmed that the wires' average resistivity was about one order of magnitude higher than that of non-templated ZnO nanowires [229].

Dye-sensitized solar cells (DSSCs) that display excellent photovoltage and light-harvesting efficiency have received considerable attention recently. For example, Hupp et al. fabricated high surface area photoelectrodes by depositing ZnO inside AAO. A continuous and conformal polycrystalline film of AZO was produced by ALD spanning the length of the pore channels. The power conversion efficiency of this DSSC was reported to be ~1.6% [233]. The same group developed new photoelectrode composites of TiO_2 coated ITO grown inside AAO to produce a transmissive and conductive high-area electrode (Fig. 51). Photovoltaic performance of this photoelectrode exhibited higher current density than control devices (lacking a current collector) with conversion efficiency of 1.1% [234]. These two strategies exploit the high aspect ratio, inertness, robust and translucency of AAO, which makes it a particularly suitable candidate for solar cell electrodes. Recently, Nakayama et al. [373] used a different configuration of solar cells where optically thin GaAs photovoltaic layers decorated with Ag nanoparticles were deposited on AAO. The authors observed that the surface plasmonic resonances and scattering of Ag nanoparticles could be tuned by shape and density of the nanoparticles to optimize the absorption of incident light.

Magnetic nanotube assemblies inside AAO have been pursued by Soroka and co-workers assembling multilayer nanotubes made of TiO_2/iron oxides with well-defined interfaces made by ALD. These structures showed weak ferromagnetic behavior [230]. Bachmann et al. showed the effect of confinement and anisotropy of iron oxide deposited inside AAO (Fig. 52) [374]. By adjusting the size, geometry and thickness of deposited iron oxide by ALD, the magnetization of these nanotubes was manipulated either in vortex or transverse mode. Another notable work is the discovery of nanowires grown inside AAO for electron field emission (EFE) application [375]. Vertically aligned nickel nanowires were grown inside AAO using electrochemical deposition with the AAO substrate acting as insulating spacer. Nanowires grown in 100 nm pore size AAO exhibited higher EFE as compared to 200 nm pore size. The length and diameter of the nanowires also influenced EFE performance.

Optical properties of nanoscopic metal or metal oxide grown in AAO pores have become a hot topic in the last decade. For instance, ZnO deposited in AAO substrates showed higher intensity PL as compared to ZnO deposited on flat Al substrate [376]. Zong et al. investigated the optical properties of transparent copper nanorod and nanowire arrays embedded in AAO. The existence of transverse and longitudinal resonance peaks of surface plasmon resonance were believed to be affected by the diameter of the nanorods and the polarization direction, respectively [377]. In addition, optical properties of SiC nanowire arrays synthesized using ordered AAO was investigated by Li et al. (Fig. 53). These arrays displayed unique Raman spectra where the TO (Γ) phonon line was not only much stronger than the LO (Γ) phonon line, but both lines also shifted. The difference was caused by size confinement effects and stacking faults of oriented nanowires [378].

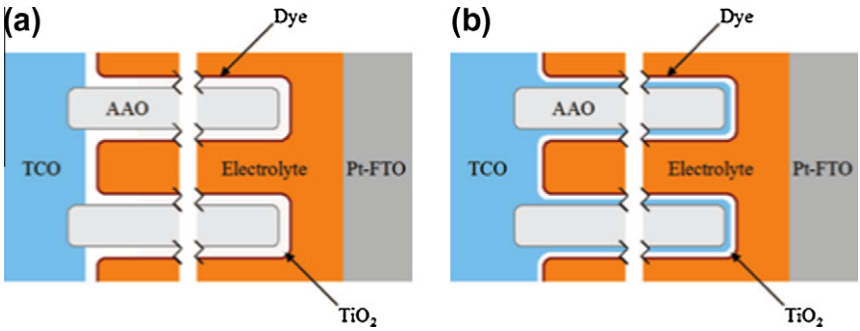

Fig. 51. Idealized two-dimensional cross-section of (a) a nanotube DSSC photoanode and (b) a concentric nanotube DSSC photoanode with ITO lining the pores. Adapted with permission from Ref. [234].

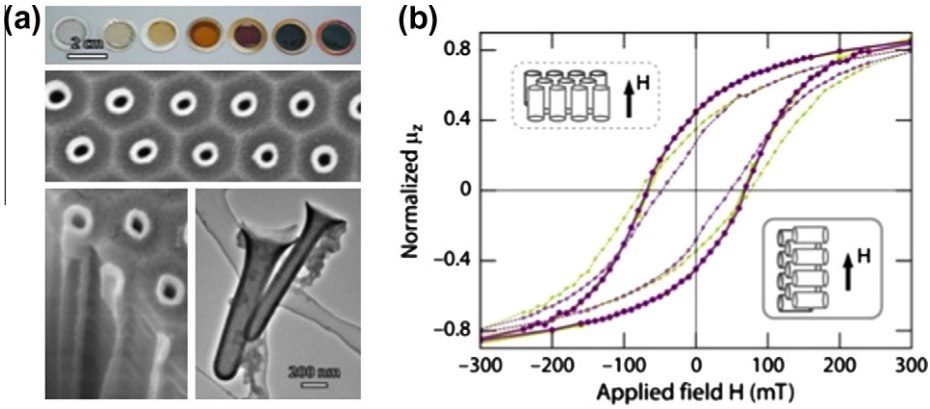

Fig. 52. (a) Structure of iron oxide nanotubes. From top to bottom and left to right: photograph of a series of samples of Fe_2O_3 tubes in the AAO membranes with 50 nm outer diameter and increasing wall thicknesses (0, 1, 2, 4, 8, 12, and 16 nm, respectively); SEM image of $ZrO_2/Fe_2O_3/ZrO_2$ tubes of 180 nm outer diameter embedded in the matrix, observed in cross-section, and at a break of the sample; TEM image of short Fe_3O_4 tubes of 180 nm diameter. (b) Comparison between the magnetic hysteresis of Fe_3O_4 nanotube arrays in a magnetic field applied perpendicular (solid thick curves) and parallel (thin dashed curves) to the z axis of the tubes. The light green curves correspond to tubes prepared with 500 ALD cycles and the dark purple ones with 700 cycles. Adapted with permission from Ref. [374].

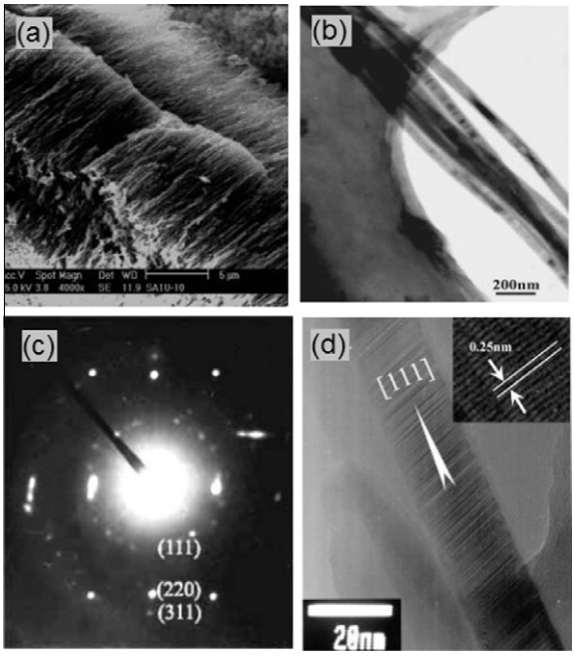

Fig. 53. (a) FE-SEM image of oriented SiC nanowire arrays grown with the assistance of an AAO template. (b) TEM image of several parallel SiC nanowires. (c) The corresponding SAED pattern taken from several SiC nanowires shows three discrete polycrystalline diffraction rings, which correspond to the (111), (220), and (311) crystallographic planes of cubic b-SiC. (d). HRTEM image of an oriented SiC nanowire. Adapted with permission from Ref. [378].

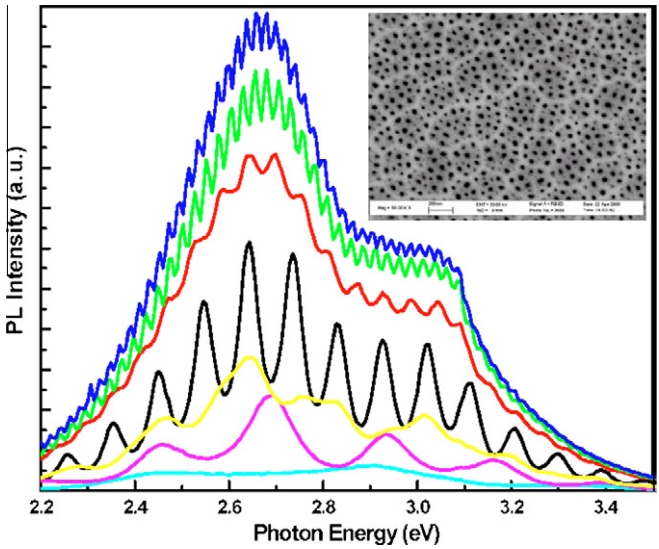

Fig. 54. PL spectra of the AAO films with the same pore diameter but different thicknesses (differentiated by line color from turquoise (lower) to blue (upper)) correspond to 10, 20, 30, 60, 120, 300 and 480 min of anodization time, respectively. The colors were attributed to the interference within a Fabry–Pérot optical cavity which are sensitive to film thickness and refractive indexs. All samples were anodized from polished Al foils. The inserted SEM image of AAO film indicates a porosity of 8%. The scale bar is 200 nm. Adapted with permission from Ref. [380].

Further recent work investigated the behavior of gold nanorod arrays coupled with a semicontinuous nanoparticle film developed using AAO substrates as template. Nonlinear enhancement effects occurred upon plasmonic coupling and interference between a percolating Au nanoparticle film and a free standing Au nanorod array [379]. Others have focused on the optical behavior of naked AAO membranes. Analysis of the laser-induced PL fringes on AAO membranes was exploited to measure thickness and refractive index of the membranes. The PL fringes were attributed to the interference within a Fabry–Pérot optical cavity. The separation between two neighboring PL peaks was highly sensitive to film thickness and refractive index (Fig. 54) [380]. Chen et al. showed that the intensity of PL spectra of AAO membrane increased linearly with membrane thickness. They also suggested that the two sub-peaks observed in the PL emission could be attributed to two luminescence centers in the membrane caused by oxygen defects and oxalic acid impurities [381].

7. Summary and concluding remarks

Over the past several years, significant progress has been made with regards to structural engineering and surface modification of nanoporous AAO material. Much of this progress has been application-driven. In this review, we have drawn together innovative approaches on controlling and designing structural growth of AAO with different sizes, arrangements, structures, geometries and pores architectures. Access to these structures is achieved by changing anodization conditions such as current, voltage and type of electrolytes during electrochemically self-ordering of AAO. Better control of pore arrangement accompanied by nanoimprinting techniques has given rise to high resolution and efficiency for nanofabrication of AAO. Important areas such as template synthesis and molecular separations benefit from these developments. With regards to template synthesis, the dimensions of desirable inverse nanostructures such as diameter, length and degree of orientation can be manipulated by controlling the shape of the AAO template. For example, AAO membrane with periodic pore architecture have been used to fabricate high quality photonic crystals. Furthermore, the current

state-of-art template synthesis employing AAO templates allows fabrication of bamboo-like conducting carbon nanotubes decorated with Au nanoparticles.

Researchers are also pushing the boundaries of molecular separations using AAO with pores of controlled shape and size, internal surface modification and explore the effect of external parameters, such as pH, flux, concentration gradient and ionic strength.

The recent progress on surface modification and functionalization of AAO membranes based on wet chemical synthesis and gas-phase techniques has also been reviewed in detail. Examples of innovative surface modification approaches and their impact on properties of the resulting materials as well as applications enabled by these surface modifications have been highlighted. Fabrication of complex AAO nanostructures combined with even greater control over surface functionality is expected to lead to unique nanostructures and nanodevices with unprecedented functional properties for the next generation devices including the exploration of their application with a focus on the different research area ranging from medicine to material science and electronics. As such, there is no doubt that AAO membranes will play an important role in a plethora of emerging nanodevices.

Acknowledgement

The authors kindly acknowledge support from the Australian Research Council. AMMJ thanks the Malaysian government and Universiti Teknologi MARA, Malaysia for a postgraduate scholarship.

References

[1] Davis ME. Ordered porous materials for emerging applications. Nature 2002;417(6891):813–21.
[2] Liu K, Yao X, Jiang L. Recent developments in bio-inspired special wettability. Chem Soc Rev 2010;39(8):3240–55.
[3] Xia F, Jiang L. Bio-inspired, smart, multiscale interfacial materials. Adv Mater 2008;20(15):2842–58.
[4] Colombo P. In praise of pores. Science 2008;322(5900):381–3.
[5] Adiga SP et al. Nanoporous membranes for medical and biological applications. Wiley Interdiscipl Rev: Nanomed Nanobiotechnol 2009;1(5):568–81.
[6] Majd S et al. Applications of biological pores in nanomedicine, sensing, and nanoelectronics. Current Opin Biotechnol 2010;21(4):439–76.
[7] Stroeve P, Ileri N. Biotechnical and other applications of nanoporous membranes. Trends Biotechnol 2011;29(6):259–66.
[8] Whitesides G, Mathias J, Seto C. Molecular self-assembly and nanochemistry: a chemical strategy for the synthesis of nanostructures. Science 1991;254(5036):1312–9.
[9] Cölfen H, Mann S. Higher-order organization by mesoscale self-assembly and transformation of hybrid nanostructures. Angew Chem Int Ed 2003;42(21):2350–65.
[10] Gomar-Nadal E, Puigmarti-Luis J, Amabilino DB. Assembly of functional molecular nanostructures on surfaces. Chem Soc Rev 2008;37(3):490–504.
[11] Gooding JJ et al. Self-assembled monolayers into the 21st century: recent advances and applications. Electroanalysis 2003;15(2):81–96.
[12] Martin CR, Kohli P. The emerging field of nanotube biotechnology. Nat Rev Drug Discov 2003;2(1):29–37.
[13] Schmid G. Materials in nanoporous alumina. J Mater Chem 2002;12(5):1231–8.
[14] Ghicov A, Schmuki P. Self-ordering electrochemistry: a review on growth and functionality of TiO_2 nanotubes and other self-aligned MO structures. Chem Commun 2009(20):2791–808.
[15] Grimes CA. Synthesis and application of highly ordered arrays of TiO_2 nanotubes. J Mater Chem 2007;17(15):1451–7.
[16] Anglin EJ et al. Porous silicon in drug delivery devices and materials. Adv Drug Deliv Rev 2008;60(11):1266–77.
[17] Stupp SI, Braun PV. Molecular manipulation of microstructures: biomaterials, ceramics, and semiconductors. Science 1997;277(5330):1242–8.
[18] Wehrspohn RB. Ordered porous nanostructures and applications. In: Lockwood DJ, editor. Nanostructure science and technology, vol. 1. 2005, Springer.
[19] Ren Y, Ma Z, Bruce PG. Ordered mesoporous metal oxides: synthesis and applications. Chem Soc Rev 2012;41(14):4909–27.
[20] Li AP et al. Hexagonal pore arrays with a 50–420 nm interpore distance formed by self-organization in anodic alumina. J Appl Phys 1998;84(11):6023–6.
[21] Nielsch K et al. Self-ordering regimes of porous alumina: the 10 porosity rule. Nano Lett 2002;2(7):677–80.
[22] Furneaux RC, Rigby WR, Davidson AP. The formation of controlled-porosity membranes from anodically oxidized aluminium. Nature 1989;337(6203):147–9.
[23] Woo L, Jae-Cheon K. Highly ordered porous alumina with tailor-made pore structures fabricated by pulse anodization. Nanotechnology 2010;21(48):485304.
[24] Yi L, et al. Novel AAO films and hollow nanostructures fabricated by ultra-high voltage hard anodization. Chem Commun 2009;46(2):309–11.
[25] Fan Z et al. Nano-porous anodic aluminium oxide membranes with 6–19 nm pore diameters formed by a low-potential anodizing process. Nanotechnology 2007;18(34):345302.
[26] Lee K, Tang Y, Ouyang M. Self-ordered, controlled structure nanoporous membranes using constant current anodization. Nano Lett 2008;8(12):4624–9.

[27] Lee W, Kim J-C, Gösele U. spontaneous current oscillations during hard anodization of aluminum under potentiostatic conditions. Adv Funct Mater 2010;20(1):21–7.
[28] Friedman AL, Brittain D, Menon L. Roles of pH and acid type in the anodic growth of porous alumina. J Chem Phys 2007;127(15):154717 [7].
[29] Chu SZ et al. Large-scale fabrication of ordered nanoporous alumina films with arbitrary pore intervals by critical-potential anodization. J Electrochem Soc 2006;153(9):B384–91.
[30] Ono S, Saito M, Asoh H. Self-ordering of anodic porous alumina formed in organic acid electrolytes. Electrochim Acta 2005;51(5):827–33.
[31] Sulka GD, Stepniowski WJ. Structural features of self-organized nanopore arrays formed by anodization of aluminum in oxalic acid at relatively high temperatures. Electrochim Acta 2009;54(14):3683–91.
[32] Li AP, Muller F, Gosele U. Polycrystalline and monocrystalline pore arrays with large interpore distance in anodic alumina. Electrochem Solid-State Lett 2000;3(3):131–4.
[33] Masuda H, Fukuda K. Ordered metal nanohole arrays made by a two-step replication of honeycomb structures of anodic alumina. Science 1995;268(5216):1466–8.
[34] Masuda H et al. Square and triangular nanohole array architectures in anodic alumina. Adv Mater 2001;13(3):189–92.
[35] Choi J, Wehrspohn RB, Gösele U. Mechanism of guided self-organization producing quasi-monodomain porous alumina. Electrochim Acta 2005;50(13):2591–5.
[36] Masuda H, Hasegwa F, Ono S. Self-ordering of cell arrangement of anodic porous alumina formed in sulfuric acid solution. J Electrochem Soc 1997;144(5):L127–30.
[37] Vrublevsky I, Parkoun V, Schreckenbach J. Analysis of porous oxide film growth on aluminum in phosphoric acid using re-anodizing technique. Appl Surf Sci 2005;242(3–4):333–8.
[38] Schneider JJ et al. Freestanding, highly flexible, large area, nanoporous alumina membranes with complete through-hole pore morphology. Eur J Inorg Chem 2005;2005(12):2352–9.
[39] Thompson GE, Wood GC. Porous anodic film formation on aluminium. Nature 1981;290(5803):230–2.
[40] Diggle JW, Downie TC, Goulding CW. Anodic oxide films on aluminum. Chem Rev 2002;69(3):365–405.
[41] Lee W et al. Fast fabrication of long-range ordered porous alumina membranes by hard anodization. Nat Mater 2006;5(9):741–7.
[42] Lee W et al. Structural engineering of nanoporous anodic aluminium oxide by pulse anodization of aluminium. Nat Nano 2008;3(4):234–9.
[43] Ono S et al. Controlling factor of self-ordering of anodic porous alumina. J Electrochem Soc 2004;151(8):B473–8.
[44] Singh GK, Golovin AA, Aranson IS. Formation of self-organized nanoscale porous structures in anodic aluminum oxide. Phys Rev B 2006;73(20):205422.
[45] Jessensky O, Muller F, Gosele U. Self-organized formation of hexagonal pore structures in anodic alumina. J Electrochem Soc 1998;145(11):3735–40.
[46] Losic D, Simovic S. Self-ordered nanopore and nanotube platforms for drug delivery applications. Expert Opin Drug Deliv 2009;6(12):1363–81.
[47] Parkhutik VP, Shershulsky VI. Theoretical modelling of porous oxide growth on aluminium. J Phys D: Appl Phys 1992;25(8):1258.
[48] Houser JE, Hebert KR. The role of viscous flow of oxide in the growth of self-ordered porous anodic alumina films. Nat Mater 2009;8(5):415–20.
[49] Macak JM et al. Smooth anodic TiO_2 nanotubes. Angew Chem Int Ed 2005;44(45):7463–5.
[50] Hahn R, Macak JM, Schmuki P. Rapid anodic growth of TiO_2 and WO_3 nanotubes in fluoride free electrolytes. Electrochem Commun 2007;9(5):947–52.
[51] Lee W et al. Wafer-scale Ni imprint stamps for porous alumina membranes based on interference lithography. Small 2006;2(8–9):978–82.
[52] Lu MH, Zhang Y. Microbead patterning on porous films with ordered arrays of pores. Adv Mater 2006;18(23):3094–8.
[53] Krishnan R, Thompson CV. Monodomain high-aspect-ratio 2D and 3D ordered porous alumina structures with independently controlled pore spacing and diameter. Adv Mater 2007;19(7):988–92.
[54] Chen B, Lu K, Tian Z. Novel patterns by focused ion beam guided anodization. Langmuir 2010;27(2):800–8.
[55] Sun Z, Kim HK. Growth of ordered, single-domain, alumina nanopore arrays with holographically patterned aluminum films. Appl Phys Lett 2002;81(18):3458–60.
[56] Maria-Chong AS et al. Soft imprinting: creating highly ordered porous anodic alumina templates on substrates for nanofabrication. Adv Funct Mater 2007;17(10):1629–35.
[57] Stasi V et al. Aluminium pre-patterning for highly ordered nanoporous anodized alumina. Photon Nanostruct – Fund Appl 2007;5(2–3):136–9.
[58] Kustandi TS et al. Wafer-scale near-perfect ordered porous alumina on substrates by step and flash imprint lithography. ACS Nano 2010;4(5):2561–8.
[59] Jee SE et al. Fabrication of microstructures by wet etching of anodic aluminum oxide substrates. Chem Mater 2005;17(16):4049–52.
[60] Pereira A et al. Laser-fabricated porous alumina membranes for the preparation of metal nanodot arrays. Small 2008;4(5):572–6.
[61] Li A-P et al. Fabrication and microstructuring of hexagonally ordered two-dimensional nanopore arrays in anodic alumina. Adv Mater 1999;11(6):483–7.
[62] Barela MJ et al. Fabrication of patterned arrays with alternating regions of aluminum and porous aluminum oxide. Electrochem Solid-State Lett 2005;8(1):C4–5.
[63] Gowtham M et al. Controlled fabrication of patterned lateral porous alumina membranes. Nanotechnology 2008;19(3):035303.
[64] Grasso V et al. Nanostructuring of a porous alumina matrix for a biomolecular microarray. Nanotechnology 2006;17(3):795.

[65] Huang Q, Lye W-K, Reed ML. Observation of isolated nanopores formed by patterned anodic oxidation of aluminum thin films. Appl Phys Lett 2006;88(23):233112–3.
[66] Harada M et al. Anodic porous alumina masks with checkerboard pattern. Appl Phys Exp 2010;3(1):015001.
[67] Lei Y, Cai W, Wilde G. Highly ordered nanostructures with tunable size, shape and properties: a new way to surface nano-patterning using ultra-thin alumina masks. Prog Mater Sci 2007;52(4):465–539.
[68] Li J, Papadopoulos C, Xu J. Nanoelectronics: growing y-junction carbon nanotubes. Nature 1999;402(6759):253–4.
[69] Meng G et al. Controlled fabrication of hierarchically branched nanopores, nanotubes, and nanowires. Proc Natl Acad Sci USA 2005;102(20):7074–8.
[70] Audrey Yoke Yee H et al. Controlled fabrication of multitiered three-dimensional nanostructures in porous alumina. Adv Funct Mater 2008;18(14):2057–63.
[71] Cheng W et al. Tree-like alumina nanopores generated in a non-steady-state anodization. J Mater Chem 2007;17(33):3493–5.
[72] Zakeri R et al. Synthesis and characterization of nonlinear nanopores in alumina films. Chem Mater 2007;19(8):1954–63.
[73] Papadopoulos C et al. Electronic transport in y-junction carbon nanotubes. Phys Rev Lett 2000;85(16):3476.
[74] Lee W, Scholz R, Gösele U. A continuous process for structurally well-defined Al_2O_3 nanotubes based on pulse anodization of aluminum. Nano Lett 2008;8(8):2155–60.
[75] Losic D, Lillo M, Losic Jr D. Porous alumina with shaped pore geometries and complex pore architectures fabricated by cyclic anodization. Small 2009;5(12):1392–7.
[76] Biao W et al. Preparation of photonic crystals made of air pores in anodic alumina. Nanotechnology 2007;18(36):365601.
[77] Yamauchi Y et al. Evolution of standing mesochannels on porous anodic alumina substrates with designed conical holes. J Am Chem Soc 2008;130(31):10165–70.
[78] Losic D, Losic Jr D. Preparation of porous anodic alumina with periodically perforated pores. Langmuir 2009;25(10):5426–31.
[79] Biswas KG et al. Self-supporting nanowire arrays templated in sacrificial branched porous anodic alumina for thermoelectric devices. Appl Phys Lett 2009;95(7):073103–8.
[80] Yi L et al. Novel AAO films and hollow nanostructures fabricated by ultra-high voltage hard anodization. Chem Commun 2009:309–11.
[81] Routkevitch D et al. Electrochemical fabrication of CdS nanowire arrays in porous anodic aluminum oxide templates. J Phys Chem 1996;100(33):14037–47.
[82] Lin YS. Microporous and dense inorganic membranes: current status and prospective. Separat Purif Technol 2001;25(1–3):39–55.
[83] Ulman A. Formation and structure of self-assembled monolayers. Chem Rev 1996;96(4):1533–54.
[84] Martin CR. Nanomaterials: a membrane-based synthetic approach. Science 1994;266(5193):1961–6.
[85] Szczepanski V, Vlassiouk I, Smirnov S. Stability of silane modifiers on alumina nanoporous membranes. J Membr Sci 2006;281(1–2):587–91.
[86] Schift H et al. Controlled co-evaporation of silanes for nanoimprint stamps. Nanotechnology 2005;16(5):S171–5.
[87] Velleman L et al. Structural and chemical modification of porous alumina membranes. Micropor Mesopor Mater 2009;126(1–2):87–94.
[88] Hendren ZD, Brant J, Wiesner MR. Surface modification of nanostructured ceramic membranes for direct contact membrane distillation. J Membr Sci 2009;331(1–2):1–10.
[89] Odom DJ, Baker LA, Martin CR. Solvent-extraction and langmuir-adsorption-based transport in chemically functionalized nanopore membranes. J Phys Chem B 2005;109(44):20887–94.
[90] Ku AY et al. Evidence of ion transport through surface conduction in alkylsilane-functionalized nanoporous ceramic membranes. Langmuir 2006;22(20):8277–80.
[91] Popat KC et al. Surface modification of nanoporous alumina surfaces with poly(ethylene glycol). Langmuir 2004;20(19):8035–41.
[92] La Flamme KE et al. Biocompatibility of nanoporous alumina membranes for immunoisolation. Biomaterials 2007;28(16):2638–45.
[93] Lee SW et al. Transport and functional behaviour of poly(ethylene glycol)-modified nanoporous alumina membranes. Nanotechnology 2005;16(8):1335–40.
[94] Steinle ED et al. Ion channel mimetic micropore and nanotube membrane sensors. Anal Chem 2002;74(10):2416–22.
[95] Smuleac V et al. Polythiol-functionalized alumina membranes for mercury capture. J Membr Sci 2005;251(1–2):169–78.
[96] Vlassiouk I, Takmakov P, Smirnov S. Sensing DNA hybridization via ionic conductance through a nanoporous electrode. Langmuir 2005;21(11):4776–8.
[97] Vlassiouk I et al. "Direct" detection and separation of DNA using nanoporous alumina filters. Langmuir 2004;20(23):9913–5.
[98] Wang X, Smirnov S. Label-free DNA sensor based on surface charge modulated ionic conductance. ACS Nano 2009;3(4):1004–10.
[99] Takmakov P, Vlassiouk I, Smirnov S. Application of anodized aluminum in fluorescence detection of biological species. Anal Bioanal Chem 2006;385(5):954–8.
[100] Yang Z et al. Piezoelectric urea biosensor based on immobilization of urease onto nanoporous alumina membranes. Biosens Bioelectron 2007;22(12):3283–7.
[101] Hobler C, Bakowsky U, Keusgen M. A functional immobilization of semiconductor nanoparticles (quantum dots) on nanoporous aluminium oxide. Phys Status Solidi (a) 2010;207(4):872–7.
[102] Tanvir S et al. Covalent immobilization of recombinant human cytochrome CYP2E1 and glucose-6-phosphate dehydrogenase in alumina membrane for drug screening applications. J Membr Sci 2009;329(1–2):85–90.
[103] Leary Swan EE, Popat KC, Desai TA. Peptide-immobilized nanoporous alumina membranes for enhanced osteoblast adhesion. Biomaterials 2005;26(14):1969–76.
[104] Demirel G, Buyukserin F. Surface-induced self-assembly of dipeptides onto nanotextured surfaces. Langmuir 2011;27(20):12533–8.

[105] Abdul MMJ, et al. Pore spanning lipid bilayers on silanised nanoporous alumina membranes. SPIE, 2008.
[106] Demé B, Marchal D. Polymer-cushioned lipid bilayers in porous alumina. Eur Biophys J 2005;34(2):170–9.
[107] Largueze JB, El Kirat K, Morandat S. Preparation of an electrochemical biosensor based on lipid membranes in nanoporous alumina. Colloids Surf B – Biointerfaces 2010;79(1):33–40.
[108] Lazzara TD et al. Phospholipids as an alternative to direct covalent coupling: surface functionalization of nanoporous alumina for protein recognition and purification. J Colloid Interface Sci 2012;366(1):57–63.
[109] Li P-F et al. Thermo-responsive gating membranes with controllable length and density of poly(N-isopropylacrylamide) chains grafted by ATRP method. J Membr Sci 2009;337(1–2):310–7.
[110] Sun L et al. High-capacity, protein-binding membranes based on polymer brushes grown in porous substrates. Chem Mater 2006;18(17):4033–9.
[111] Jain P et al. High-capacity purification of his-tagged proteins by affinity membranes containing functionalized polymer brushes. Biomacromolecules 2007;8(10):3102–7.
[112] Wang W et al. Synthesis of metallic nanotube arrays in porous anodic aluminum oxide template through electroless deposition. Mater Res Bull 2006;41(8):1417–23.
[113] Sehayek T et al. Template synthesis of nanotubes by room-temperature coalescence of metal nanoparticles. Chem Mater 2005;17(14):3743–8.
[114] Lahav M et al. Nanoparticle nanotubes. Angew Chem 2003;115(45):5734–7.
[115] Grimm S et al. Nondestructive replication of self-ordered nanoporous alumina membranes via cross-linked polyacrylate nanofiber arrays. Nano Lett 2008;8(7):1954–9.
[116] Jani AMM et al. Nanoporous anodic aluminium oxide membranes with layered surface chemistry. Chem Commun 2009:3062–4.
[117] Jani AMM et al. Dressing in layers: layering surface functionalities in nanoporous aluminum oxide membranes. Angew Chem Int Ed 2010;49(43):7933–7.
[118] Allara DL, Nuzzo RG. Spontaneously organized molecular assemblies. 1. Formation, dynamics, and physical properties of n-alkanoic acids adsorbed from solution on an oxidized aluminum surface. Langmuir 1985;1(1):45–52.
[119] Allara DL, Nuzzo RG. Spontaneously organized molecular assemblies. 2. Quantitative infrared spectroscopic determination of equilibrium structures of solution-adsorbed n-alkanoic acids on an oxidized aluminum surface. Langmuir 1985;1(1):52–66.
[120] Chang C-S, Suen S-Y. Modification of porous alumina membranes with n-alkanoic acids and their application in protein adsorption. J Membr Sci 2006;275(1-2):70–81.
[121] Cheow P-S, Liu L, Toh C-S. Grafting of nanoporous alumina membranes and films with organic acids. Surface Interface Anal 2007;39(7):601–10.
[122] Karaman ME, Antelmi DA, Pashley RM. The production of stable hydrophobic surfaces by the adsorption of hydrocarbon and fluorocarbon carboxylic acids onto alumina substrates. Colloids Surfaces A: Physicochem Eng Aspects 2001;182(1–3):285–98.
[123] Öberg K et al. Comparison of monolayer films of stearic acid and methyl stearate on an Al_2O_3 surface. Thin Solid Films 2001;397(1-2):102–8.
[124] ter Maat J et al. Organic modification and subsequent biofunctionalization of porous anodic alumina using terminal alkynes. Langmuir 2011;27(22):13606–17.
[125] Janshoff A, Steinem C. Transport across artificial membranes—an analytical perspective. Anal Bioanal Chem 2006;385(3):433–51.
[126] Schmitt EK et al. Electrically insulating pore-suspending membranes on highly ordered porous alumina obtained from vesicle spreading. Soft Matter 2008;4(2):250–3.
[127] Chekmenev EY et al. Flow-through lipid nanotube arrays for structure-function studies of membrane proteins by solid-state NMR spectroscopy. Biophys J 2006;91(8):3076–84.
[128] Proux-Delrouyre V et al. Formation of tethered and streptavidin-supported lipid bilayers on a microporous electrode for the reconstitution of membranes of large surface area. Langmuir 2002;18(8):3263–72.
[129] Hennesthal C, Steinem C. Pore-spanning lipid bilayers visualized by scanning force microscopy. J Am Chem Soc 2000;122(33):8085–6.
[130] Hennesthal C, Drexler J, Steinem C. Membrane-suspended nanocompartments based on ordered pores in alumina. ChemPhysChem 2002;3(10):885–9.
[131] Drexler J, Steinem C. Pore-suspending lipid bilayers on porous alumina investigated by electrical impedance spectroscopy. J Phys Chem B 2003;107(40):11245–54.
[132] Schmitt EK, Weichbrodt C, Steinem C. Impedance analysis of gramicidin D in pore-suspending membranes. Soft Matter 2009;5(17):3347–53.
[133] Smirnov AI, Poluektov OG. Substrate-supported lipid nanotube arrays. J Am Chem Soc 2003;125(28):8434–5.
[134] Guo Y et al. Dimension control of glycolipid nanotubes by successive use of vesicle extrusion and porous template. Chem Mater 2006;18(6):1577–80.
[135] Li RQ et al. Polarization-dependent fluorescence of proteins bound to nanopore-confined lipid bilayers. J Chem Phys 2008;129(9):095102–8.
[136] Peyratout CS, Dähne L. Tailor-made polyelectrolyte microcapsules: from multilayers to smart containers. Angew Chem Int Ed 2004;43(29):3762–83.
[137] Balachandra AM, Dai J, Bruening ML. Enhancing the anion-transport selectivity of multilayer polyelectrolyte membranes by templating with Cu^{2+}. Macromolecules 2002;35(8):3171–8.
[138] Liu X, Bruening ML. Size-selective transport of uncharged solutes through multilayer polyelectrolyte membranes. Chem Mater 2003;16(2):351–7.
[139] Hong SU, Bruening ML. Separation of amino acid mixtures using multilayer polyelectrolyte nanofiltration membranes. J Membr Sci 2006;280(1–2):1–5.
[140] Hong SU, Malaisamy R, Bruening ML. Separation of fluoride from other monovalent anions using multilayer polyelectrolyte nanofiltration membranes. Langmuir 2007;23(4):1716–22.

[141] Hong SU, Ouyang L, Bruening ML. Recovery of phosphate using multilayer polyelectrolyte nanofiltration membranes. J Membr Sci 2009;327(1–2):2–5.
[142] Ouyang L, Malaisamy R, Bruening ML. Multilayer polyelectrolyte films as nanofiltration membranes for separating monovalent and divalent cations. J Membr Sci 2008;310(1–2):76–84.
[143] Dai J, Baker GL, Bruening ML. Use of porous membranes modified with polyelectrolyte multilayers as substrates for protein arrays with low nonspecific adsorption. Anal Chem 2005;78(1):135–40.
[144] Dotzauer DM et al. Catalytic membranes prepared using layer-by-layer adsorption of polyelectrolyte/metal nanoparticle films in porous supports. Nano Lett 2006;6(10):2268–72.
[145] He Q et al. Self-assembly of composite nanotubes and their applications. Current Opin Colloid Interface Sci 2009;14(2):115–25.
[146] Qi D et al. Optical emission of conjugated polymers adsorbed to nanoporous alumina. Nano Lett 2003;3(9):1265–8.
[147] Jain P, Baker GL, Bruening ML. Applications of polymer brushes in protein analysis and purification. Annu Rev Anal Chem 2009;2(1):387–408.
[148] Barbey R et al. Polymer brushes via surface-initiated controlled radical polymerization: synthesis, characterization, properties, and applications. Chem Rev 2009;109(11):5437–527.
[149] Nagale M, Kim BY, Bruening ML. Ultrathin, hyperbranched poly(acrylic acid) membranes on porous alumina supports. J Am Chem Soc 2000;122(47):11670–8.
[150] Balachandra AM, Baker GL, Bruening ML. Preparation of composite membranes by atom transfer radical polymerization initiated from a porous support. J Membr Sci 2003;227(1–2):1–14.
[151] Sun L, Baker GL, Bruening ML. Polymer brush membranes for pervaporation of organic solvents from water. Macromolecules 2005;38(6):2307–14.
[152] Grajales ST et al. Effects of monomer composition on CO_2—selective polymer brush membranes. Chem Mater. 2010;22(13):4026–33.
[153] Lee H-S, Penn LS. Polymer brushes make nanopore filter membranes size selective to dissolved polymers. Macromolecules 2009;43(1):565–7.
[154] Bruening ML et al. Creation of functional membranes using polyelectrolyte multilayers and polymer brushes. Langmuir 2008;24(15):7663–73.
[155] Stuart MAC et al. Emerging applications of stimuli-responsive polymer materials. Nat Mater 2010;9(2):101–13.
[156] Cui Y et al. Synthesis of PNIPAM-co-MBAA copolymer nanotubes with composite control. Langmuir 2006;22(19):8205–8.
[157] Cui Y et al. Synthesis of thermosensitive PNIPAM-co-MBAA nanotubes by atom transfer radical polymerization within a porous membrane. Macromol Rapid Commun 2005;26(19):1552–6.
[158] Fu Q et al. Reversible control of free energy and topography of nanostructured surfaces. J Am Chem Soc 2004;126(29):8904–5.
[159] Wang H-J et al. Template synthesized molecularly imprinted polymer nanotube membranes for chemical separations. J Am Chem Soc 2006;128(50):15954–5.
[160] Gorman CB, Petrie RJ, Genzer J. Effect of substrate geometry on polymer molecular weight and polydispersity during surface-initiated polymerization. Macromolecules 2008;41(13):4856–65.
[161] Lau KHA, Duran H, Knoll W. In situ characterization of n-carboxy anhydride polymerization in nanoporous anodic alumina. J Phys Chem B 2009;113(10):3179–89.
[162] Shi W et al. Functionalized anodic aluminum oxide (AAO) membranes for affinity protein separation. J Membr Sci 2008;325(2):801–8.
[163] Song C et al. pH-sensitive characteristics of poly(acrylic acid)-functionalized anodic aluminum oxide (AAO) membranes. J Membr Sci 2011;372(1–2):340–5.
[164] Oliveira GB et al. Enzyme immobilization on anodic aluminum oxide/polyethyleneimine or polyaniline composites. React Funct Polym 2008;68(1):27–32.
[165] Jeon G et al. Electrically actuatable smart nanoporous membrane for pulsatile drug release. Nano Lett 2011;11(3):1284–8.
[166] Hench LL, West JK. The sol–gel process. Chem Rev 1990;90(1):33–72.
[167] Kickelbick G. Formation of hexagonal mesoporous silica in submicrometer channels. Small 2005;1(2):168–70.
[168] Lakshmi BB, Patrissi CJ, Martin CR. Sol–gel template synthesis of semiconductor oxide micro- and nanostructures. Chem Mater 1997;9(11):2544–50.
[169] Hunks WJ, Ozin GA. Challenges and advances in the chemistry of periodic mesoporous organosilicas (PMOs). J Mater Chem 2005;15(35–36):3716–24.
[170] Yamaguchi A et al. Self-assembly of a silica-surfactant nanocomposite in a porous alumina membrane. Nat Mater 2004;3(5):337–41.
[171] Wang K et al. Synthesis and characterisation of ordered arrays of mesoporous carbon nanofibres. J Mater Chem 2009;19(9):1331–8.
[172] Ma B et al. Hierarchically structured anatase nanotubes and membranes. Micropor Mesopor Mater 2009;124(1–3):162–8.
[173] Rørvik PM et al. Template-assisted synthesis of $PbTiO_3$ nanotubes. J Eur Ceram Soc 2009;29(12):2575–9.
[174] Xin C et al. Formation of titania/silica hybrid nanowires containing linear mesocage arrays by evaporation-induced block-copolymer self-assembly and atomic layer deposition. Angew Chem Int Ed 2007;46(36):6829–32.
[175] Li X et al. Template-synthesized $LiCoO_2$, $LiMn_2O_4$, and $LiNi_{0.8}Co_{0.2}O_2$ nanotubes as the cathode materials of lithium ion batteries. J Phys Chem B 2005;109(29):14017–24.
[176] Wang Y et al. One-dimensional SnO_2 nanostructures: facile morphology tuning and lithium storage properties. Nanotechnology 2009;20(34):345704.
[177] Park M-H et al. Silicon nanotube battery anodes. Nano Lett 2009;9(11):3844–7.
[178] Shi C et al. NiO nanotubes assembled in pores of porous anodic alumina and their optical absorption properties. Chem Phys Lett 2008;454(1–3):75–9.
[179] Mikhail P et al. Polymer-derived SiOC nanotubes and nanorods via a template approach. Eur J Inorg Chem 2009;2009(23):3496–506.

[180] Lee SB et al. Antibody-based bio-nanotube membranes for enantiomeric drug separations. Science 2002;296(5576):2198–200.
[181] Platschek B et al. Vertical columnar block-copolymer-templated mesoporous silica via confined phase transformation. J Am Chem Soc 2008;130(51):17362–71.
[182] Platschek B, Petkov N, Bein T. Tuning the structure and orientation of hexagonally ordered mesoporous channels in anodic alumina membrane hosts: a 2D small-angle x-ray scattering study. Angew Chem 2006;118(7):1152–6.
[183] Wu Y et al. Composite mesostructures by nano-confinement. Nat Mater 2004;3(11):816–22.
[184] Lu Q et al. Ordered SBA-15 nanorod arrays inside a porous alumina membrane. J Am Chem Soc 2004;126(28):8650–1.
[185] Zhang A et al. Synthesis of silica nanotubes with orientation controlled mesopores in porous membranes via interfacial growth. Chem Mater 2012;24(6):1005–10.
[186] Cazacu A et al. Dynamic hybrid materials for constitutional self-instructed membranes. Proc Natl Acad Sci 2009;106(20):8117–22.
[187] Shi W et al. Lysine-attached anodic aluminum oxide (AAO)-silica affinity membrane for bilirubin removal. J Membr Sci 2010;349(1–2):333–40.
[188] Saumitra KV et al. SiO_2-coated porous anodic alumina membranes for high flow rate electroosmotic pumping. Nanotechnology 2007;18(27):275705.
[189] Berrigan JD et al. Protein-enabled layer-by-layer syntheses of aligned, porous-wall, high-aspect-ratio TiO_2 nanotube arrays. Adv Funct Mater 2011;21(9):1693–700.
[190] Wang K et al. Mesoporous titania nanotubes: their preparation and application as electrode materials for rechargeable lithium batteries. Adv Mater 2007;19(19):3016–20.
[191] Bae C et al. Template-directed synthesis of oxide nanotubes: fabrication, characterization, and applications. Chem Mater 2008;20(3):756–67.
[192] Hurst SJ et al. Multisegmented one-dimensional nanorods prepared by hard-template synthetic methods. Angew Chem Int Ed 2006;45(17):2672–92.
[193] Hong Jin F, Peter W, Margit Z. Semiconductor nanowires: from self-organization to patterned growth. Small 2006;2(6):700–17.
[194] Thompson GE et al. Nucleation and growth of porous anodic films on aluminium. Nature 1978;272(5652):433–5.
[195] Liu L et al. Fabrication and characterization of a flow-through nanoporous gold nanowire/AAO composite membrane. Nanotechnology 2008;19(33):335604.
[196] Lee HJ et al. Simple and rapid preparation of vertically aligned gold nanoparticle arrays and fused nanorods in pores of alumina membrane based on positive dielectrophoresis. Sensor Actuat B: Chem 2009;136(2):320–5.
[197] Qin Y et al. General assembly method for linear metal nanoparticle chains embedded in nanotubes. Nano Lett 2008;8(10):3221–5.
[198] Woo L et al. A template-based electrochemical method for the synthesis of multisegmented metallic nanotubes. Angew Chem Int Ed 2005;44(37):6050–4.
[199] Burdick J et al. High-throughput templated multisegment synthesis of gold nanowires and nanorods. Nanotechnology 2009;20(6):065306.
[200] Hoang NV, Kumar S, Kim G-H. Growth of segmented gold nanorods with nanogaps by the electrochemical wet etching technique for single-electron transistor applications. Nanotechnology 2009;20(12):125607.
[201] Kondo T, Nishio K, Masuda H. Surface enhanced Raman scattering in multilayered Au nanoparticles in anodic porous alumina. Appl Phys Exp 2009;2(3):0320001.
[202] Hassan A, Christine I. A review of electroless gold deposition processes. Gold Bull 1984;17(14).
[203] Niesen TP, De Guire MR. Review: deposition of ceramic thin films at low temperatures from aqueous solutions. Solid State Ionics 2002;151(1–4):61–8.
[204] Wirtz M, Yu S, Martin CR. Template synthesized gold nanotube membranes for chemical separations and sensing. Analyst 2002;127(7):871–9.
[205] Cheng M et al. Au nanoparticle arrays with tunable particle gaps by template-assisted electroless deposition for high performance surface-enhanced Raman scattering. Nanotechnology 2010;21(1):015604.
[206] Yu Y et al. Gold nanotube membranes have catalytic properties. Micropor Mesopor Mater 2012;153(0):131–6.
[207] Velleman L, Losic D, Shapter JG. The effects of surface functionality positioning on the transport properties of membranes. J Membr Sci 2012;411–412(0):211–8.
[208] Zhou JH et al. Ternary alloy Ni–W–P nanoparticles electroless deposited within alumina nanopores. Mater Sci Technol 2008;24:1250–3.
[209] Zhang S-H et al. Synthesis of silver nanotubes by electroless deposition in porous anodic aluminium oxide templates. Chem Commun 2004(9):1106–7.
[210] Wang G et al. Synthesis and characterization of Ag nanoparticles assembled in ordered array pores of porous anodic alumina by chemical deposition. Mater Lett 2007;61(18):3795–7.
[211] Piao Y et al. Nanostructured materials prepared by use of ordered porous alumina membranes. Electrochim Acta. 2005;50(15):2997–3013.
[212] Hou S et al. Layer-by-layer nanotube template synthesis. J Am Chem Soc 2004;126(18):5674–5.
[213] Nguyen BTT, Ting EZC, Toh C-S. Development of a biomimetic nanoporous membrane for the selective transport of charged proteins. Bioinspirat Biomim 2008;3(3):035008.
[214] Cheow P-S et al. Transport and separation of proteins across platinum-coated nanoporous alumina membranes. Electrochim Acta 2008;53(14):4669–73.
[215] Teng Q et al. Controlled assembly of highly Raman-enhancing silver nanocap arrays templated by porous anodic alumina membranes. Small 2009;5(20):2333–7.
[216] Zhang L, Fang Y, Zhang P. Laser-MBE of nickel nanowires using AAO template: a new active substrate of surface enhanced Raman scattering. Spectrochim Acta Part A: Mol Biomol Spectrosc 2008;69(1):91–5.
[217] Pereira A et al. Functionally modified macroporous membrane prepared by using pulsed laser deposition. Adv Funct Mater 2007;17(3):443–50.

[218] Wang S et al. Large-area uniform nanodot arrays embedded in porous anodic alumina. Nanotechnology 2007;18(1):015303.
[219] Siow KS et al. Plasma methods for the generation of chemically reactive surfaces for biomolecule immobilization and cell colonization – a review. Plasma Process Polym 2006;3(6-7):392–418.
[220] Brevnov DA et al. Fabrication of anisotropic super hydrophobic/hydrophilic nanoporous membranes by plasma polymerization of C4F8 on anodic aluminum oxide. J Electrochem Soc 2004;151(8):B484–9.
[221] Losic D et al. Surface modification of nanoporous alumina membranes by plasma polymerization. Nanotechnology 2008;19(24):245704.
[222] Knez M, Nielsch K, Niinistö L. Synthesis and surface engineering of complex nanostructures by atomic layer deposition. Adv Mater 2007;19(21):3425–38.
[223] Ott AW et al. Atomic layer controlled deposition of Al_2O_3 films using binary reaction sequence chemistry. Appl Surf Sci 1996;107:128–36.
[224] Berland BS et al. In situ monitoring of atomic layer controlled pore reduction in alumina tubular membranes using sequential surface reactions. Chem Mater 1998;10(12):3941–50.
[225] Elam JW et al. Conformal coating on ultrahigh-aspect-ratio nanopores of anodic alumina by atomic layer deposition. Chem Mater 2003;15(18):3507–17.
[226] Xiong G et al. Effect of atomic layer deposition coatings on the surface structure of anodic aluminum oxide membranes. J Phys Chem B 2005;109(29):14059–63.
[227] Banerjee P et al. Nanotubular metal–insulator–metal capacitor arrays for energy storage. Nat Nano 2009;4(5):292–6.
[228] Pitzschel K et al. Controlled introduction of diameter modulations in arrayed magnetic iron oxide nanotubes. ACS Nano 2009;3(11):3463–8.
[229] Liu CH et al. Electrical properties of zinc oxide nanowires and intramolecular p–n junctions. Appl Phys Lett 2003;83(15):3168–70.
[230] Soroka IL et al. Template-based multiwalled TiO_2/iron oxides nanotubes: structure and magnetic properties. J Appl Phys 2009;106(8):084313–7.
[231] Marianna K et al. Ta_2O_5- and TiO_2-based nanostructures made by atomic layer deposition. Nanotechnology 2009;21(3):035301.
[232] Bachmann J et al. Ordered iron oxide nanotube arrays of controlled geometry and tunable magnetism by atomic layer deposition. J Am Chem Soc 2007;129(31):9554–5.
[233] Martinson ABF et al. ZnO nanotube based dye-sensitized solar cells. Nano Lett 2007;7(8):2183–7.
[234] Martinson ABF et al. Radial electron collection in dye-sensitized solar cells. Nano Lett 2008;8(9):2862–6.
[235] Marianna K et al. Ta_2O_5- and TiO_2-based nanostructures made by atomic layer deposition. Nanotechnology 2010;21(3):035301.
[236] George SM. Atomic layer deposition: an overview. Chem Rev 2009;110(1):111–31.
[237] Marichy C, Bechelany M, Pinna N. Atomic layer deposition of nanostructured materials for energy and environmental applications. Adv Mater 2012;24(8):1017–32.
[238] Choy KL. Chemical vapour deposition of coatings. Prog Mater Sci 2003;48(2):57–170.
[239] Miranda LD et al. Direct coupling of a carbon nanotube membrane to a mass spectrometer: contrasting nanotube and capillary tube introduction systems. J Membr Sci 2009;344(1–2):26–31.
[240] Popp A, Engstler J, Schneider JJ. Porous carbon nanotube-reinforced metals and ceramics via a double templating approach. Carbon 2009;47(14):3208–14.
[241] Park S et al. Carbon nanosyringe array as a platform for intracellular delivery. Nano Lett 2009;9(4):1325–9.
[242] Che G et al. Chemical vapor deposition based synthesis of carbon nanotubes and nanofibers using a template method. Chem Mater 1998;10(1):260–7.
[243] Fan X et al. Sensitive optical biosensors for unlabeled targets: a review. Anal Chim Acta 2008;620(1–2):8–26.
[244] Altalhi T et al. Synthesis of carbon nanotube (CNT) composite membranes. Membranes 2010;1(1):37–47.
[245] Ansari SG et al. Glucose sensor based on nano-baskets of tin oxide templated in porous alumina by plasma enhanced CVD. Biosens Bioelectron 2008;23(12):1838–42.
[246] Khodin A et al. Nanomorph silicon grown on template alumina substrate by plasma-enhanced CVD. Mater Lett 2009;63(29):2552–5.
[247] Lai M, Riley DJ. Templated electrosynthesis of nanomaterials and porous structures. J Colloid Interface Sci 2008;323(2):203–12.
[248] Kuchibhatla SVNT et al. One dimensional nanostructured materials. Prog Mater Sci 2007;52(5):699–913.
[249] Barth S et al. Synthesis and applications of one-dimensional semiconductors. Prog Mater Sci 2010;55(6):563–627.
[250] Woo L, Jae-Cheon K. Highly ordered porous alumina with tailor-made pore structures fabricated by pulse anodization. Nanotechnology 2010;21(48):485304.
[251] Li L, Koshizaki N, Li G. Nanotube arrays in porous alumina membranes. J Mater Sci Technol 2008;24:550–62.
[252] Kolmakov A, Moskovits M. Chemical sensing and catalysis by one-dimensional metal-oxide nanostructures. Annu Rev Mater Res 2004;34(1):151–80.
[253] Taberna PL et al. High rate capabilities Fe_3O_4-based Cu nano-architectured electrodes for lithium-ion battery applications. Nat Mater 2006;5(7):567–73.
[254] Liu H et al. Synthesis of iron–palladium binary alloy nanotubes by template-assisted electrodeposition from metal-complex solution. J Electroanal Chem 2009;633(1):15–8.
[255] Yuan XY et al. Self-assembly synthesis and magnetic studies of Co–P alloy nanowire arrays. Nanotechnology 2004;15(1):59–61.
[256] Haberkorn N, Gutmann JS, Theato P. Template-assisted fabrication of free-standing nanorod arrays of a hole-conducting cross-linked triphenylamine derivative: toward ordered bulk-heterojunction solar cells. ACS Nano 2009;3(6):1415–22.
[257] Hong Jin F et al. Arrays of vertically aligned and hexagonally arranged ZnO nanowires: a new template-directed approach. Nanotechnology 2005;16(6):913.
[258] Chen J-T, Zhang M, Russell TP. Instabilities in nanoporous media. Nano Lett 2007;7(1):183–7.

[259] Lee HC et al. Synthesis of unidirectional alumina nanostructures without added organic solvents. J Am Chem Soc 2003;125(10):2882–3.
[260] Rabin O et al. Formation of thick porous anodic alumina films and nanowire arrays on silicon wafers and glass. Adv Funct Mater 2003;13(8):631–8.
[261] Yuan ZH, Huang H, Fan SS. Regular alumina nanopillar arrays. Adv Mater 2002;14(4):303–6.
[262] Chen D, Zhao W, Russell TP. P3HT nanopillars for organic photovoltaic devices nanoimprinted by AAO templates. ACS Nano 2012;6(2):1479–85.
[263] Choi MK et al. Simple fabrication of asymmetric high-aspect-ratio polymer nanopillars by reusable AAO templates. Langmuir 2011;27(6):2132–7.
[264] Lin P et al. Individual alumina nanotubes. Angew Chem Int Ed 2001;40(8):1490–3.
[265] Liu L, Park S. Direct formation of thin-walled palladium nanotubes in nanochannels under an electrical potential. Chem Mater 2011;23(6):1456–60.
[266] Xiao ZL et al. Fabrication of alumina nanotubes and nanowires by etching porous alumina membranes. Nano Lett 2002;2(11):1293–7.
[267] Steinhart M et al. Nanotubes by template wetting: a modular assembly system. Angew Chem Int Ed 2004;43(11):1334–44.
[268] Xia Y et al. One-dimensional nanostructures: synthesis, characterization, and applications. Adv Mater 2003;15(5):353–89.
[269] Cheng F et al. Template-directed materials for rechargeable lithium-ion batteries. Chem Mater 2007;20(3):667–81.
[270] Wang Y, Angelatos AS, Caruso F. Template synthesis of nanostructured materials via layer-by-layer assembly. Chem Mater 2007;20(3):848–58.
[271] Joshi RK, Schneider JJ. Assembly of one dimensional inorganic nanostructures into functional 2D and 3D architectures. Synthesis, arrangement and functionality. Chem Soc Rev 2012;41(15):5285–312.
[272] Kim D-K et al. Label-free optical detection of aptamer-protein interactions using gold-capped oxide nanostructures. Anal Biochem 2008;379(1):1–7.
[273] Alvarez SD et al. A label-free porous alumina interferometric immunosensor. ACS Nano 2009;3(10):3301–7.
[274] Pan S, Rothberg LJ. Interferometric sensing of biomolecular binding using nanoporous aluminum oxide templates. Nano Lett 2003;3(6):811–4.
[275] Dronov R et al. Nanoporous alumina-based interferometric transducers ennobled. Nanoscale 2011.
[276] Feng C-L et al. Graded-bandgap quantum- dot-modified nanotubes: a sensitive biosensor for enhanced detection of DNA hybridization. Adv Mater 2007;19(15):1933–6.
[277] Chang S et al. Nanoporous membranes with mixed nanoclusters for raman-based label-free monitoring of peroxide compounds. Anal Chem 2009;81(14):5740–8.
[278] Wang M et al. FITC-modified PPy nanotubes embedded in nanoporous AAO membrane can detect trace PCB20 via fluorescence ratiometric measurement. Chem Commun 2011;47(13):3808–10.
[279] Wang M et al. Fluorescence detection of trace PCB101 based on PITC immobilized on porous AAO membrane. Analyst 2011;136(2):278–81.
[280] Jia RP et al. Enhanced photoluminescence properties of morin and trypsin absorbed on porous alumina films with ordered pores array. Solid State Commun 2004;130(6):367–72.
[281] Run-Ping J et al. Photoluminescence spectra of human serum albumen and morin embedded in porous alumina membranes with ordered pore arrays. J Phys: Condens Matter 2003;15(49):8271.
[282] Kumeria T, Losic D. Controlling interferometric properties of nanoporous anodic aluminium oxide. Nanoscale Res Lett 2012;7(1):1–10.
[283] Kumeria T, Losic D. Reflective interferometric gas sensing using nanoporous anodic aluminium oxide (AAO). Phys Status Solidi (RRL) – Rapid Res Lett 2011;5(10-11):406–8.
[284] Kumeria T et al. Label-free reflectometric interference microchip biosensor based on nanoporous alumina for detection of circulating tumour cells. Biosens Bioelectron 2012;35(1):167–73.
[285] Kim D-K et al. Label-free DNA biosensor based on localized surface plasmon resonance coupled with interferometry. Anal Chem 2007;79(5):1855–64.
[286] Lazzara TD et al. Benefits and limitations of porous substrates as biosensors for protein adsorption. Anal Chem 2011;83(14):5624–30.
[287] Ko H, Chang S, Tsukruk VV. Porous substrates for label-free molecular level detection of nonresonant organic molecules. ACS Nano 2008;3(1):181–8.
[288] Ko H, Singamaneni S, Tsukruk VV. Nanostructured surfaces and assemblies as SERS media. Small 2008;4(10):1576–99.
[289] Ji N et al. Fabrication of silver decorated anodic aluminum oxide substrate and its optical properties on surface-enhanced raman scattering and thin film interference. Langmuir 2009;25(19):11869–73.
[290] Wada Y, Yanagishita T, Masuda H. Ordered porous alumina geometries and surface metals for surface-assisted laser desorption/ionization of biomolecules:â€‰ possible mechanistic implications of metal surface melting. Anal Chem 2007;79(23):9122–7.
[291] Grieshaber D et al. Electrochemical biosensors – sensor principles and architectures. Sensors 2008;8(3):1400–58.
[292] Stura E et al. Anodic porous alumina as mechanical stability enhancer for LDL-cholesterol sensitive electrodes. Biosens Bioelectron 2007;23(5):655–60.
[293] Shimomura T et al. Amperometric determination of choline with enzyme immobilized in a hybrid mesoporous membrane. Talanta 2009;78(1):217–20.
[294] Xian Y et al. Template synthesis of highly ordered Prussian blue array and its application to the glucose biosensing. Biosens Bioelectron 2007;22(12):2827–33.
[295] Darder M et al. Encapsulation of enzymes in alumina membranes of controlled pore size. Thin Solid Films 2006;495(1–2):321–6.
[296] González G et al. Mass transport effect of mesoscopic domains in the amperometric response of an electroactive species: modeling for its applications in biomolecule detection. Sensor Actuat B: Chem 2008;144(2):349–53.

[297] Maghsoodi S et al. A novel biosensor using entangled carbon nanotubes layer grown on an alumina substrate by CCVD of methane on FeOx–MgO. Sensor Actuat B: Chem 2009;141(2):526–31.
[298] Takmakov P, Vlassiouk I, Smirnov S. Hydrothermally shrunk alumina nanopores and their application to DNA sensing. The Analyst 2006;131(11):1248–53.
[299] Wang L et al. A novel electrochemical biosensor based on dynamic polymerase-extending hybridization for *E. coli* O157:H7 DNA detection. Talanta 2009;78(3):647–52.
[300] Yu J et al. A polyethylene glycol (PEG) microfluidic chip with nanostructures for bacteria rapid patterning and detection. Sensors Actuat A: Phys 2009;154(2):288–94.
[301] Koh G et al. Development of a membrane-based electrochemical immunosensor. Electrochim Acta 2007;53(2):803–10.
[302] Nguyen BTT et al. Membrane-based electrochemical nanobiosensor for the detection of virus. Anal Chem 2009;81(17):7226–34.
[303] Zhou Y-G et al. Gold nanoparticles integrated in a nanotube array for electrochemical detection of glucose. Electrochem Commun 2009;11(1):216–9.
[304] Jagminas A et al. Modification of alumina matrices through chemical etching and electroless deposition of nano-Au array for amperometric sensing. Nanoscale Res Lett 2007;2(3):130–4.
[305] de la Escosura-Muñiz A, Merkoçi A. A nanochannel/nanoparticle-based filtering and sensing platform for direct detection of a cancer biomarker in blood. Small 2011;7(5):675–82.
[306] Yang Z, Si S, Zhang C. Study on the activity and stability of urease immobilized onto nanoporous alumina membranes. Micropor Mesopor Mater 2008;111(1–3):359–66.
[307] Fu J, Mao P, Han J. Artificial molecular sieves and filters: a new paradigm for biomolecule separation. Trends Biotechnol 2008;26(6):311–20.
[308] Bohn PW. Nanoscale control and manipulation of molecular transport in chemical analysis. Annu Rev Anal Chem 2009;2(1):279–96.
[309] Punit Kohli MW, Charles RM. Nanotube membrane based biosensors. Electroanalysis 2004;16(1–2):9–18.
[310] Martin CR et al. Controlling ion-transport selectivity in gold nanotubule membranes. Adv Mater 2001;13(18):1351–62.
[311] Bluhm EA et al. Surface effects on cation transport across porous alumina membranes. Langmuir 1999;15(25):8668–72.
[312] McCleskey TM et al. Asymmetric membranes with modified gold films as selective gates for metal ion separations. J Membr Sci 2002;210(2):273–8.
[313] Le QTH et al. Ultra-thin gates for the transport of phenol from supported liquid membranes to permanent surface modified membranes. J Membr Sci 2002;205(1–2):213–22.
[314] Dai J et al. Controlling ion transport through multilayer polyelectrolyte membranes by derivatization with photolabile functional groups. Macromolecules 2002;35(8):3164–70.
[315] Yamaguchi A et al. Diffusion of metal complexes inside of silicaâ'surfactant nanochannels within a porous alumina membrane. J Phys Chem B 2008;112(7):2024–30.
[316] Steenkamp GC et al. Copper(II) removal from polluted water with alumina/chitosan composite membranes. J Membr Sci 2002;197(1–2):147–56.
[317] Yang Y et al. Preparation and assessment of fluorous supported liquid membranes based on porous alumina. J Membr Sci 2009;345(1–2):170–6.
[318] Yamaguchi A et al. Extraction mechanisms of charged organic dye molecules into silica-surfactant nanochannels in a porous alumina membrane. Anal Chim Acta 2006;556(1):157–63.
[319] Henrich VE. The surfaces of metal oxides. Rep Prog Phys 1985;48(11):1481.
[320] Brown GE et al. Metal oxide surfaces and their interactions with aqueous solutions and microbial organisms. Chem Rev 1998;99(1):77–174.
[321] Liu G, Dotzauer DM, Bruening ML. Ion-exchange membranes prepared using layer-by-layer polyelectrolyte deposition. J Membr Sci 2010;354(1–2):198–205.
[322] Dotzauer DM et al. Nanoparticle-containing membranes for the catalytic reduction of nitroaromatic compounds. Langmuir 2009;25(3):1865–71.
[323] Mitchell DT et al. Smart nanotubes for bioseparations and biocatalysis. J Am Chem Soc 2002;124(40):11864–5.
[324] Son SJ et al. Magnetic nanotubes for magnetic-field-assisted bioseparation, biointeraction, and drug delivery. J Am Chem Soc 2005;127(20):7316–7.
[325] Song J et al. Polyrhodanine modified anodic aluminum oxide membrane for heavy metal ions removal. J Hazard Mater 2011;187(1–3):311–7.
[326] Yamashita T et al. Separation of adenine, adenosine-5′-monophosphate and adenosine-5′-triphosphate by fluidic chip with nanometre-order diameter columns inside porous anodic alumina using an aqueous mobile phase. Lab Chip 2009;9(10):1337–9.
[327] Osmanbeyoglu HU, Hur TB, Kim HK. Thin alumina nanoporous membranes for similar size biomolecule separation. J Membr Sci 2009;343(1–2):1–6.
[328] Lee S et al. A polyethylene oxide-functionalized self-organized alumina nanochannel array for an immunoprotection biofilter. Lab Chip 2011;11(6):1049–53.
[329] Chen W et al. Entrapment of protein in nanotubes formed by a nanochannel and ion-channel hybrid structure of anodic alumina. Small 2012;8(7):1001–5.
[330] Napoli M, Eijkel JCT, Pennathur S. Nanofluidic technology for biomolecule applications: a critical review. Lab Chip 2010;10(8):957–85.
[331] Fredlake CP et al. Ultrafast DNA sequencing on a microchip by a hybrid separation mechanism that gives 600 bases in 6.5 minutes. Proc Natl Acad Sci 2008;105(2):476–81.
[332] Sano T et al. Size-exclusion chromatography using self-organized nanopores in anodic porous alumina. Appl Phys Lett 2003;83(21):4438–40.
[333] Chang C-S et al. Preparation of inorganic–organic anion-exchange membranes and their application in plasmid DNA and RNA separation. J Membr Sci 2008;311(1–2):336–48.

[334] Moon J-M et al. Capture and alignment of phi29 viral particles in sub-40 nanometer porous alumina membranes. Biomed Microdevice 2009;11(1):135–42.
[335] Stair P et al. Novel, uniform nanostructured catalytic membranes. Top Catal 2006;39(3):181–6.
[336] Wang Z, Haasch RT, Lee GU. Mesoporous membrane device for asymmetric biosensing. Langmuir 2005;21(4):1153–7.
[337] Williams DF. On the mechanisms of biocompatibility. Biomaterials 2008;29(20):2941–53.
[338] Popat KC et al. Influence of nanoporous alumina membranes on long-term osteoblast response. Biomaterials 2005;26(22):4516–22.
[339] Swan EEL et al. Fabrication and evaluation of nanoporous alumina membranes for osteoblast culture. J Biomed Mater Res Part A 2005;72A(3):288–95.
[340] Popat KC et al. Osteogenic differentiation of marrow stromal cells cultured on nanoporous alumina surfaces. J Biomed Mater Res Part A 2007;80A(4):955–64.
[341] Karlsson M et al. Initial in vitro interaction of osteoblasts with nano-porous alumina. Biomaterials 2003;24(18):3039–46.
[342] Karlsson M et al. Nanoporous aluminum oxide affects neutrophil behaviour. Microsc Res Techn 2004;63(5):259–65.
[343] Karlsson M, Tang L. Surface morphology and adsorbed proteins affect phagocyte responses to nano-porous alumina. J Mater Sci: Mater Med 2006;17(11):1101–11.
[344] Ferraz N et al. Influence of nanoporesize on platelet adhesion and activation. J Mater Sci: Mater Med 2008;19(9):3115–21.
[345] Popat KC et al. Poly (ethylene glycol) grafted nanoporous alumina membranes. J Membr Sci 2004;243(1–2):97–106.
[346] Wolfrum B et al. Suspended nanoporous membranes as interfaces for neuronal biohybrid systems. Nano Lett 2006;6(3):453–7.
[347] Prasad S, Quijano J. Development of nanostructured biomedical micro-drug testing device based on in situ cellular activity monitoring. Biosens Bioelectron 2006;21(7):1219–29.
[348] Hoess A et al. Cultivation of hepatoma cell line HepG2 on nanoporous aluminum oxide membranes. Acta Biomater 2007;3(1):43–50.
[349] Ishibashi T et al. A porous membrane-based culture substrate for localized in situ electroporation of adherent mammalian cells. Sensor Actuat B: Chem 2007;128(1):5–11.
[350] Graham A et al. Neuronal cell biocompatibility and adhesion to modified CMOS electrodes. Biomed Microdevice 2009;11(5):1091–101.
[351] Kant K et al. Nanopore gradients on porous aluminum oxide generated by nonuniform anodization of aluminum. ACS Appl Mater Interface 2010;2(12):3447–54.
[352] Sedel L. Evolution of alumina-on-alumina implants: a review. Clin Orthopaed Relat Res 2000;379:48–54.
[353] Klawitter JJ et al. An evaluation of porous alumina ceramic dental implants. J Dental Res 1977;56(7):768–76.
[354] Karageorgiou V, Kaplan D. Porosity of 3D biomaterial scaffolds and osteogenesis. Biomaterials 2005;26(27):5474–91.
[355] Mour M et al. Advances in porous biomaterials for dental and orthopaedic applications. Materials 2010;3(5):2947–74.
[356] Bose S et al. Processing and characterization of porous alumina scaffolds. J Mater Sci: Mater Med 2002;13(1):23–8.
[357] Briggs EP et al. Formation of highly adherent nano-porous alumina on Ti-based substrates: a novel bone implant coating. J Mater Sci: Mater Med 2004;15(9):1021–9.
[358] Mainardes RM, Silva LP. Drug delivery systems: past, present, and future. Current Drug Targets 2004;5:449–55.
[359] Vallet-Regí M, Balas F, Arcos D. Mesoporous materials for drug delivery. Angew Chem Int Ed 2007;46(40):7548–58.
[360] Jain KK. The role of nanobiotechnology in drug discovery. Drug Discov Today 2005;10(21):1435–42.
[361] Simovic S, Losic D, Vasilev K. Controlled drug release from porous materials by plasma polymer deposition. Chem Commun 2010;46(8):1317–9.
[362] Aw MS et al. Polymeric micelles in porous and nanotubular implants as a new system for extended delivery of poorly soluble drugs. J Mater Chem 2011.
[363] Jeon G, Yang SY, Kim JK. Functional nanoporous membranes for drug delivery. J Mater Chem 2012;22(30):14814–34.
[364] Wieneke H et al. Stent coating: a new approach in interventional cardiology. Herz 2002;27(6):518–26.
[365] Kang H-J et al. Controlled drug release using nanoporous anodic aluminum oxide on stent. Thin Solid Films 2007;515(12):5184–7.
[366] Wieneke H et al. Synergistic effects of a novel nanoporous stent coating and tacrolimus on intima proliferation in rabbits. Catheterizat Cardiovasc Intervent 2003;60(3):399–407.
[367] Tao SL, Desai TA. Microfabricated drug delivery systems: from particles to pores. Adv Drug Deliv Rev 2003;55(3):315–28.
[368] Desai TA et al. Nanoporous microsystems for islet cell replacement. Adv Drug Deliv Rev 2004;56(11):1661–73.
[369] Gong D et al. Controlled molecular release using nanoporous alumina capsules. Biomed Microdevice 2003;5(1):75–80.
[370] La Flamme KE et al. The effects of cell density and device arrangement on the behavior of macroencapsulated-cells. Cell Transplant 2007;16:765–74.
[371] Flamme KEL et al. Nanoporous alumina capsules for cellular macroencapsulation: transport and biocompatibility. Diabetes Technol Therapeut 2005;7(5):684–94.
[372] Liu R et al. Synthesis and characterization of RuO_2/poly(3,4-ethylenedioxythiophene) composite nanotubes for supercapacitors. Phys Chem Chem Phys 2010;12(17):4309–16.
[373] Nakayama K, Tanabe K, Atwater HA. Plasmonic nanoparticle enhanced light absorption in GaAs solar cells. Appl Phys Lett 2008;93(12):121903–4.
[374] Bachmann J et al. Size effects in ordered arrays of magnetic nanotubes: pick your reversal mode. J Appl Phys 2009;105(7). 07B521-3.
[375] Tsai W-C et al. Preparation of vertically-aligned nickel nanowires with anodic aluminum oxide templates and their application as field emitters. Electrochem Commun 2009;11(3):660–3.
[376] Fang Z et al. Structural and optical properties of ZnO films grown on the AAO templates. Mater Lett 2003;57(26–27):4187–90.
[377] Zong R-L et al. Optical properties of transparent copper nanorod and nanowire arrays embedded in anodic alumina oxide. J Chem Phys 2005;123(9):094710–5.
[378] Li Z et al. Large-area highly-oriented sic nanowire arrays: synthesis, raman, and photoluminescence properties. J Phys Chem B 2006;110(45):22382–6.

[379] Zhou Z-K et al. Tuning gold nanorod-nanoparticle hybrids into plasmonic fano resonance for dramatically enhanced light emission and transmission. Nano Lett 2011;11(1):49–55.
[380] Huang K et al. Photoluminescence oscillations in porous alumina films. Appl Phys Lett 2006;89(20):201113–8.
[381] Chen JH et al. The investigation of photoluminescence centers in porous alumina membranes. Appl Phys A: Mater Sci Process 2006;84(3):297–300.
[382] Wada Y, Yanagishita T, Masuda H. Ordered porous alumina geometries and surface metals for surface-assisted laser desorption/ionization of biomolecules: possible mechanistic implications of metal surface melting. Anal Chem 2007;79(23):9122–7.
[383] González G et al. Mass transport effect of mesoscopic domains in the amperometric response of an electroactive species: modeling for its applications in biomolecule detection. Sensor Actuat B: Chem 2010;144(2):349–53.
[384] Matsumoto F et al. Nanometer-scale patterning of DNA in controlled intervals on a gold-disk array fabricated using ideally ordered anodic porous alumina. Adv Mater 17(13) (2005) 1609-1612.
[385] Cheng MS et al. Development of an electrochemical membrane-based nanobiosensor for ultrasensitive detection of dengue virus. Anal Chim Acta 2012;725(0):74–80.
[386] Myler S et al. Ultra-thin-polysiloxane-film-composite membranes for the optimisation of amperometric oxidase enzyme electrodes. Biosens Bioelectron 2002;17(1–2):35–43.
[387] Chen D et al. A BOD biosensor based on a microorganism immobilized on an Al_2O_3 sol–gel matrix. Anal Bioanal Chem 2002;372(5):737–9.
[388] Bridge K et al. Polydivinylbenzene/ethylvinylbenzene composite membranes for the optimization of a whole blood glucose sensor. Electroanalysis 2006;18(1):95–102.